DISSERTATION

THE COMPACTION OF AGGREGATES OF NON-SPHERICAL VISCOPLASTIC PARTICLES

Submitted by

Yu-Ching Wu

Department of Civil Engineering

In partial fulfillment of the requirements for

the Degree of Doctor of Philosophy

Colorado State University

Fort Collins, Colorado

Summer 2002

ProQuest Information and Learning Company
300 North Zeeb Road
P.O. Box 1346
Ann Arbor, MI 48106-1346

COLORADO STATE UNIVERSITY

June 04, 2002

WE HEREBY RECOMMEND THAT THE DISSERTATION PREPARED UNDER OUR SUPERVISION BY YU-CHING WU ENTITLED THE COMPACTION OF AGGREGATES OF NON-SPHERICAL VISCOPLASTIC PARTICLES BE ACCEPTED AS FULFILLING IN PART REQUIREMENTS FOR THE DEGREE OF DOCTOR OF PHILOSOPHY.

Committee on Graduate Work

Committee Member: Dr. Frederick W. Smith

Dr. Kurt Georg

Dr. Paul DuChateau

Co-Advisor: Dr. Erik G. Thompson

Advisor: Dr. Paul R. Heyliger

Department Head: Dr. Sandra L. Woods

ABSTRACT OF DISSERTATION

THE COMPACTION OF AGGREGATES OF NON-SPHERICAL VISCOPLASTIC PARTICLES

This dissertation presents a study of the compaction of aggregates of non-spherical, viscoplastic particles under external load. A numerical model is developed in which each particle is treated individually, including the appropriate constitutive equations, kinematic conditions, and contact constraints, for every particle in the aggregate. The advantage of the model is that it can be applied to aggregates of particles that have a wide range of shape, size and properties.

A penalty iterative method has been derived to improve the efficiency of computing. Substitution of the proper value of the bulk modulus reduces the time of convergence and speeds up calculation. Also, the use of a sparse matrix approach saves a large amount of computer memory and increases the capability of the technique to handle large numbers of particles. A mesh update algorithm was generated based on a system of mixed triangular and quadrilateral elements. The algorithm is used to detect contact, generate meshes, modify concave elements and prevent locking. A general triangular mesh system is used to solve all problems at the same time, but the number of triangular elements need to be appropriately controlled due to their lower number of degrees of freedom. A series of numerical simulations for both single and multiple materials are presented to demonstrate the efficiency and accuracy of the model, and to visualize the process of compaction. The number of particles in

these simulations ranges from tens to thousands. This work presents the first viscoplastic simulation model using the discrete element method applied to non-spherical particles.

This model has been used to study the effects of particle size, shape, distribution, orientation, mechanical properties, and compaction. As expected, larger numbers of granular elements yield more precise solutions. However, the detailed behavior of a single element can have considerable effect on the response of the whole system. Several factors have significant impact on the behavior of granular systems including void ratio, void shape, distance between voids, and void pattern. The algorithms presented here are useful for a wide variety of problems involving granular media that can be characterized as visco plastic in this behavior. The results presented here provide significant insight into the fundamental behavior of granular media under compaction conditions, including prediction of the overall aggregate stress-strain response.

Wu, Yu-Ching
Civil Engineering Department
Colorado State University
Fort Collins, CO 80523
Summer 2002

ACKNOWLEDGEMENTS

I wish to express my appreciation to Dr. Paul R. Heyliger and Dr. Erik G. Thompson, my dissertation directors, for the guidance and helpful suggestions provided throughout the course of graduate studies. Gratitude is extended to the members of the thesis committee, Dr. Frederick W. Smith, Dr. Kurt Georg, and Dr. Paul DuChateau, for their time and constructive criticism.

This dissertation is dedicated to my parents for their encouragement and unending support throughout my career as a student.

CONTENTS

LIST OF TABLES

LIST OF FIGURES

CHAPTER 1

INTRODUCTION

The behavior of granular media is complex and often non-intuitive. Small changes in individual particle shape or material properties can result in large changes in overall aggregate response. The mechanics of granular media is important to many fields of application, such as powder processing, snow mechanics, soil consolidation, food processing, bitumen technology and sintering. Yet many aspects of the fundamental mechanical behavior of granular aggregates are not well understood.

There have been many empirical and theoretical attempts to predict the basic behavior of particle aggregates. These studies have led to significant insight into the fundamental behavior of these materials. Among the theoretical models for granular media, the most powerful and versatile are those that represent each particle individually. These techniques are often labeled discrete-element methods(DEM), distinct element methods, particle models or network models. A large number of such studies have been made using two-dimensional representations while three dimensional studies have been fewer in number and mostly limited to spherical particles.

Perhaps more important than particle shape, most numerical studies of particle aggregates have been limited to either assumptions of rigid particles or small-strain micro-constitutive theories. Whereas these limitations are appropriate for some

applications and materials such as sands, there are many other materials where they may not appropriate such as polymers, lead, food products, aluminum, thermoplastics, bitumen, and some soils. For applications associated with these materials, it may be more appropriate to assume the particles as visco-plastic materials which, during compaction, undergo plastic strain-rates that are large in comparison to the corresponding rate at which elastic strains are changing. Under such an assumption, it is possible to follow the compaction process through large strains without mathematical complications.

The purpose of this research is to investigate the use of a particle model to study the fundamental behavior of aggregates made up of visco-plastic particles, during and after compaction. Finite element formulations of visco-plastic materials have been derived to solve several types of two-dimensional problems, such as plain strain with a constraint of incompressibility, a viscous approximation for steady creeping flow, and steady-state radial flow (Thompson (1975), Dawson and Thompson (1978), Shimazaki and Thompson(1981)). In this work, a discrete element model is developed in which each particle is treated individually, using appropriated constitutive relations, kinematic conditions, and contact constraints, for every particle in the aggregate. It is the first time for visco-plastic application to discrete element method on non-spherical particles. The advantage of the model is that it can be used in every different particle shape, size and mechanical properties of particle assembly. However, the detailed behavior of a single element can have considerable influence on the behavior of the whole system. The current research is for the first phase of a two phase investigation of this topic, and it is limited to two dimensional simulations. The second phase will be to extend the results

and techniques developed for two-dimensional simulations to three dimensions and that will be the subject of a later project.

The difference between spherical and non-spherical particles is the contact condition. For a sphere, there is always only one contact point no mater what size of particle and what direction two particles are touched. But it is not true for non-spherical particles. Infinite types of contacts might appear in a non-spherical particle assembly. The first issue is how to use a general mesh system to quantify and qualify all possible situations. The current project focuses on development of suitable elements to model individual particles for the simulation of aggregate behavior during and after compaction, and use of this model to investigate macroscopic stress as a function of relative density and the effect of random size, shape and orientation of particles at the beginning of compaction on the compaction process and the final compacted solid. A triangular mesh system has been generated to offer effective solutions for several problems such as contact detection, concave element modification, and mesh generation. To detect contact and concave element, we calculate the area of every element. When any element turns to be zero or negative area, mesh generation is installed. Mesh generation is a simple process of adding one node and one triangular element into the whole mesh system. Although the triangular element has terrific characteristic that it is easy to be organized and systematized, locking is a possible drawback for viscoplastic material. However, the limitation of quantity of adjacent three-node elements reduces the possibility to the least. Therefore, the mesh update algorithm includes a subroutine which mixes any two connected triangular elements together. The similar generation method is used for multiple-material granular systems. However, the composite aggregate is more

complicated due to variety of materials. A special algorithm is developed to deal with two adjacent triangular elements with two different materials. A series of computer simulations are created to visualize the process of compaction, and to test the efficiency and accuracy of the numerical model. The relation of stress and void ratio is studied for several various granular systems. The systems with more degrees of freedom got smoother curve than those with less degrees of freedom. It indicates that the larger granular systems yield the more precise and stable solutions. Although the systems with less number of particle are less accurate, all experiments show that stresses dramatically increase when the density is high.

The cost of computation is another important issue concerned in the current study. The storage of sparse matrix increases the size of assembly from one thousand particles to about four thousand particles. We developed a penalty iterative method which improved the efficiency of computation by substituting a proper value of bulk modulus. An analysis of matrix and development of iterative procedure make the iteration converge at once. It reduces the cost of computation in some cases.

Various numerical experiments have been made to study the effects of particle size, particle shape, density, distribution, orientation, property, and compaction. Several particle assemblies of different quantity ranged from tens to thousands of particles are experimented. Density has been proved to have a significant effect to macroscopic conditions. The low-density aggregates have less stiffness. It slightly increases when density increases. It has dramatic change when the density is close to one. As expected, the system with the larger average particle size is stiffer. Also, the small granular systems are unstable. Void shape and distribution of voids have considerable impact on the

macroscopic behavior of the global system. Generally, uniform distribution and similarity of shape increase the stiffness. Triangular and concave quadrilateral elements are stiffer than normal polygons. After hundred of cases have been tested, all have close stress components in x and y directions, it is demonstrated that orientation does not affect the macroscopic behavior too much. Two different types of compactions, isostatic and close-die compactions have been tested. With high density, when the incompressibility has been almost achieved, stress components in x and y direction are almost the same for both cases.

The final stage of research focuses on the considerable difference of overall aggregate response among hundred of cases which have the same density and random particle distribution. In addition to void ratio, there are some factors that significantly affect the macroscopic behavior of granular systems, including void shape, distance between voids, and void pattern. According the analyses presented here, it is not accurate to use a single element to represent a single particle. The alternative method is to use four elements to represent one particle. Void shape has a significant impact on global behaviors. The result of void shape test demonstrates that there is approximately 29 percent difference between the disk with a circular void and the one with a square hole. Nearness of voids is another parameter. When two voids are getting closer to each other, the stress components drop dramatically. Void pattern is a minor factor compared with other variables, but its effect is noticeable.

CHAPTER 2

LITERATURE REVIEW

The fundamental characteristic behind the physics of granular materials have been well-developed during the last decade (Jaeger and Nagel (1992), Jaeger, Nagel, and Behinger (1996), Herrmann and Luding (1998)). One of the most interesting features in granular media is the transfer of force. Unlike a continuum, for which the stress and displacement components are continuous quantities that result in fairly smooth distributions of elastic fields throughout most regions, the discrete nature of granular materials gives rise to force chains that are non-uniform and that depend significantly on local density and orientation of individual particles. These have been many studies of these force distributions in two-dimensional packing including those of Liu et a. (1995), Radjai et al. (1996), Coppersmith el al. (1996), Hong (1993), Liffman et al. (1994), Wittmer et al. (1997), Luding (1997), and Matuttis (1998). These studies used several different shapes for the particles, including the relatively simple idealization of a circle up to the more complex polygon.

2.1 FORCE DISTRIBUTIONS AND GLOBAL AGGREGATE STRESS

One of the key features of force distributions and the simultaneous development of global aggregate stress under static or quasi-static conditions is the strong dependence on boundary restraint. A particle aggregate in a constrained structure such as a silo does

not exhibit a linear increase with height such as that found for a fluid, but instead reaches a critical value (Janssen (1895)) because of friction and arching within the aggregate. In unrestrained aggregates such as sandpiles, there are no walls available to take part of the weight and hence the bottom of the pile must bear all the weight. It is at this stage that force chains are observed to act, distributed throughout the aggregate and dependent on history. One of the reasons for renewed interest in force distributions is that experimental evidence (Jotaki and Moriyama (1979) and Trollope and Burman (1980)) indicates the existence of pressure minima in granular cones. Under more general loading conditions, force chains can develop in a manner that depends strongly on particle shape, size, and density, and as the aggregate compacts and individual contacts spread from a point to adjoining edges, the evolution of these force chains develops in a manner that is still not well understood.

2.2 YIELD BEHAVIOR

Another key feature of particle aggregates is yield behavior. This is perhaps best described through the traditional mechanics concept of a yield or creep dissipation surfaces. However, it is first necessary to treat the aggregate as a macroscopic continuum and develop a means of transitioning from particle force to aggregate stress. One of the most complete sequences of treatments of yield surfaces in powder aggregates are those of Fleck and co-workers (Fleck (1995), Fleck, Kuhn, and McMeeking (1992), Fleck, Storakers, and McMeeking (1997)) and Storakers et al. (1999). These studies considered an analytic treatment of powder aggregates of spheres under a variety of material behaviors. Although the assumptions used in these studies did not consider the behavior

of individual particles, they showed for the first time the basic behavior of precompacted powder aggregate yield surfaces for plastic and viscoplastic material response. Yield surfaces were found that agreed very well the experimental results of Akisanya, Cocks, and Fleck (1997) and showed yield surfaces for aggregates precompacted under cold isostatic and closed-die compaction. However, this study used the assumption of affine motion for the particle aggregate and also did not consider the behavior of each individual particle, but instead used average or effective properties of the particles.

2.3 THE DISCRETE ELEMENT METHOD

The discrete-element method (DEM) has been used far more than alternative approaches in modeling particle aggregates. The phrase "discrete-element" was originally used by Cundall and Strack (1979) in what has become perhaps the most-cited paper in particle mechanics. The acronym DEM can at times be misleading because a wide variety of assumptions can be used to model granular assemblies, and in fact other names have been used for similar models of particle behavior. Yet the basic mechanics of treating individual particles rather than smearing the behavior out over a continuum has seen significant extension, modification and application (Bathurst and Rethenburg (1988) , Thorton (1988,1997), Bashir and Goddard (1991), Dobry and Ng (1992)). Many of the key features of particle aggregates can be captured using spheres or, in two-dimensions, circles; yet other shapes such as ellipses (Ting 1992), superquadrics (Williams and Pentland 1992), continuously connected circular segments (Potapov and Campbell (1998), and polygons (Issa and Nelson 1992) have been used. In terms of constitutive models for the particles, it is common to represent only the kinematic

relations between particles or use only linear elastic constitutive relations. Although simple to model and useful for tracking stress in an aggregate, these are not as useful to model a packing that compresses and generates contacts that evolve from point to line or surface.

The characteristics of the discrete element method as they have been applied to date in particle mechanics are to model the kinematics and kinetics associated with the constant change in position and force balance from contacts between adjoining particles. It is somewhat intuitive that spheres, with normal contact forces that always act through the particle centers, a lack of sharp corners, and the associated difficulties (Krishnasamg and Jakiela (1995)) would be the easiest to analyze. This is in fact the case. However, it is also often the case that although the word "sphere" is used to described a problem, it is actually a long cylinder in two-dimensional analysis. Three-dimensional applications, even for spheres, are rare. Jagota and co-workers have made several three-dimensional studies of spherical particle aggregates for sintering applications (Jagota et al. (1988, 1990, 1995)). Parahami and McMeeking (2000) have studied the overall constitutive and yield surface behavior for aggregates of perfectly plastic spheres.

2.4 ELASTO VISCO-PLASTIC FLOW

In addition to granular system, elasto visco-plastic flow has also been investigated in the past two decades. Zero mean strain rate leads to the Euler equation specifying material incompressibility. Through the use of a Lagrange multiplier, which indicates the physical meaning of mean normal stress or pressure, the finite element formulations incorporates the constraint of incompressibility into the potential energy

functional. Complete incompressibility has been defined as the constraint condition can be satisfied everywhere within an element, whereas average incompressibility means that the constraint is satisfied only in an average sense for the entire element. Such finite element formulations have been established to solve several types of two-dimensional problems, such as a plain strain with constraint of incompressibility, a viscous approximation for steady creeping flow, a non-trivial steady-state radial flow (Thompson (1975), Dawson and Thompson (1978), Shimazaki and Thompson(1981)). However, no paper focus on granular systems made of incompressible materials.

2.5 THE CONTACT PROBLEM

The contact problem is another important issue of granular system under large deformations. Solutions of the contact problem include equation derivation and mesh update. Geometric compatibility is an important condition need to be considered. Planar contact cases for elastic materials involving sticking, frictional sliding and separation have been well developed. The incremental potential of the contact forces is added to the Euler equation while contact is occurring. Various frictional resistance for sticking and sliding conditions are substituted into the incremental potential (Chan and Tuba (1971), Goodman, Taylor and Brekke (1968), Wilson and Parsons (1970), Francavilla and Zienkiewicz (1975), Herrmann (1978), Okamoto and Nakazawa (1979), Kalker, Allaert and Mul (1981), Bathe and Chaudhary (1985)). However, according to our knowledge, the contact problem of visco-plastic granular system with non-spherical particles has never been investigated. For non-spherical particles, the point of contact does not have to be only one. It is very different from spherical objects. Also, the goal of the current study

is not only focus on one step. In other words, we want to simulate the whole process of the compaction. So one of the challenges is to update the mesh system and keep running the next step. For that, we need a good mesh generation algorithm.

2.6 MESH GENERATION

At a discrete model level, mesh generation is critical for finite element methods. One of the key points is to build up mesh automatically no matter what shape the object is. Numerous research have focused on the development of automatic mesh generation techniques. One of the most interesting methods is called Intelligent Local Approach (ILA), in which size and aspect ratio of meshes are well controlled (Yagawa, Yoshioka, Yoshimura and Soneda (1993), Yagawa, Shioya (1993), Yoshimura, Wada, Yagawa (1999)). Potentially, the similar method can be generated for automatic mesh update of discrete element model. Triangular elements have been well developed for mesh generation(L.L. Schumaker (1987) and R. Sibson (1978)). One of the most useful method is called delaunay triangulation. Delaunay triangulation is to produce the triangular-element mesh system for given nodes, in which those elements have most proper size and shape for finite element calculation. Also, voronoi diagrams, in which the Denaulay triangulation can be developed, have been investigated(F. Aurenhammer(1991)). In the present research, although the triangular mesh system is used, how to prevent locking is another issue particularly for visco-plastic material.

2.7 THE PRESENT STUDY

In the present study, particle aggregates made of high temperature aluminum or asphalt using a particle (or DEM) model of each individual particle are studied. The particles are non-spherical, two-dimensional, viscoplastic elements. Each particle is modeled to determine the global response of the entire aggregate. The overall particle aggregate stress-strain behavior for non-spherical particles in two-dimensions is studied to determine the relationship between aggregate density and applied stress, and the nature of how the several factors such as void shape, distance between voids, and void pattern in particle aggregates, affect and eventually transform into the macroscopic constitutive behavior of the aggregate. One of the fundamental questions is the effect of particle size and shape in terms of aggregate response. Our research objectives are based on the hypothesis that particle shape, and the history of the deformation process, both strongly influence the aggregate response, and that models using only spheres and limited to small strains, while extremely useful, prevent the investigation of many of the phenomenon important to powder and granular media technology. The results of study provide a fundamental and new foundation from which to launch future studies. Application areas are broad, and extensions to include a variety of constitutive models, composite aggregates, and stochastic processes are numerous.

CHAPTER 3

PROBLEM FORMULATION

In this chapter, the equation of equilibrium, the constitutive equation, the Euler equation, the stress-strain rate relation and the corresponding matrices form are presented. Through the use of a Lagrange multiplier, which indicates the physical meaning of mean normal stress or pressure, the finite element formulations incorporate the constraint of incompressibility into the potential energy functional. Complete and average incompressibility have been defined. Two numerical methods, the mixed method and the penalty iterative method, are generated.

3.1 GOVERNING EQUATIONS

The equation of equilibrium for an incompressible material in a region V bounded by a surface S is given as

$$\sigma_{ij,J} + \rho X_i = 0 \quad \text{in V} \tag{3.1}$$

where $\sigma_{ij,J}$ is stress rate tensor, and ρ is the density of the material. The incompressibility is achieved while $u_{i,i}=0$ in V. The constitutive equation for the incompressible material is given as

$$\sigma_{ij} = -p\,\delta_{ij} + 2G\,\varepsilon_{ij} \tag{3.2}$$

where ε_{ij} is strain rate tensor, G is modulus of viscosity, and p is pressure given as

$$p = -\frac{\sigma_{ii}}{3} = -\bar{\sigma} \tag{3.3}$$

where $\bar{\sigma}$ is mean stress. The bulk-modulus-stress relationship is

$$\bar{\sigma} = K \varepsilon_{kk} \tag{3.4}$$

where K is viscous bulk modulus. The stress-strain rate relation can be written as

$$\varepsilon_{ij} = \frac{1}{2}(u_{i,j} + u_{j,i}) \tag{3.5}$$

where u_i is velocity vector. The boundary conditions are given as

$$\sigma_{ij} \nu_j = \bar{T}_i \quad \text{on } S_\sigma \tag{3.6}$$

$$u_i = \bar{u}_i \qquad \text{on } S_u \tag{3.7}$$

where ν_j is unit normal vector to an element on S, $\bar{T}_i$ and $\bar{u}_i$ equal the specified surface tractions and velocities respectively. Lamb has shown equations (1) and (5) to be the Euler equations for the functional

$$J = \int_V G\varepsilon'_{ij}\varepsilon_{ij} dV - \int_{S_\sigma} \bar{T}_i u_i ds - \int_V \rho X_i u_i dV \tag{3.8}$$

When minimized with respect to all incompressible flow fields satisfying the prescribed boundary values $\bar{u}_i$ on S_u. The Lagrange multiplier p for the constant condition can be incorporated to include compressible and incompressible fields.

$$J = \int_V G\varepsilon'_{ij}\varepsilon_{ij} dV - \int_V p\varepsilon_{ii} dV - \int_{S_\sigma} \bar{T}_i u_i ds - \int_V \rho X_i u_i dV \tag{3.9}$$

The corresponding weak form is

$$\delta J = \int_V \delta\varepsilon_{ij} 2G\varepsilon_{ij} dV - \int_V \delta\varepsilon_{ij} p\delta_{ij} dV - \int_V \delta p\varepsilon_{ii} dV - \int_{S_\sigma} \bar{T}_i \delta u_i dS$$

$$- \int_V \rho X_i \delta u_i dV \tag{3.10}$$

Variation of J^* with respect to p gives

$$\delta J^* = -\int_V \delta p \varepsilon_{ii} dV = 0 \tag{3.11}$$

The following finite element approximations within an element e are now defined as

$$\{ u(x,y) \} = \lfloor N_u \rfloor_e \{ U \}_e \tag{3.12}$$

$$\{ \bar{\sigma}(x,y) \} = \lfloor N_\sigma \rfloor_e \{ \bar{\sigma} \}_e \tag{3.13}$$

The strain rate can be given in according to differentiation of equation (3.11) and equation (3.5) as

$$\{ \varepsilon(x,y) \} = \lfloor N'_u \rfloor_e \{ U \}_e \tag{3.14}$$

We also define

$$\varepsilon_{ii} = \lfloor h \rfloor \{ \varepsilon \} \tag{3.15}$$

$$\{ \sigma' \} = [M] \{ \varepsilon \} \tag{3.16}$$

The virtual work expression in matrices from can now be written as

$$\delta J_e = \{\delta U\}_e [K]_e \{U\}_e - \{\delta U\}_e [G]_e \{p\}_e - \{\delta p\}_e^T [G]_e \{U\}_e - \{\delta U\}_e^T \{F\}_e \tag{3.17}$$

where

$$[K]_e = \int_e [N']_e^T [M] [N']_e dV$$

$$[G]_e = \int_e [N_p]_e^T \lfloor h \rfloor [N']_e dV$$

$$\{ F \}_e = \int_{S_e} [N]_e^T \{ \bar{T} \} dS + \int_e [N]_e^T \{X\} dV$$

Summation of all element matrices provides the governing finite element equation

$$\begin{bmatrix} [K] & [G]^T \\ [G] & [0] \end{bmatrix} \begin{Bmatrix} \{U\} \\ \{p\} \end{Bmatrix} = \begin{Bmatrix} \{F\} \\ \{0\} \end{Bmatrix} \tag{3.18}$$

3.2 NUMERICAL METHODS

There are two numerical methods introduced in this section. In the first division, the mixed method is derived. The internal energy is presented in terms of the strain rate. The variational internal energy in terms of the components of strain is given. In the second division, the penalty iterative method is introduced. Both complete incompressibility and average incompressibility are defined and presented.

3.2.1 The Mixed Method

From equations (3.2), (3.3), (3.4), the constitutive law can be modified as

$$\sigma_{ij} = 2G\,\dot{\varepsilon}'_{ij} + 3K\,\dot{\varepsilon}_{kk}\,\delta_{ij} \tag{3.19}$$

The approach of the mixed method is to let the viscous bulk modulus K much larger than the modulus of viscosity G. Then it leads to material incompressibility, $\dot{\varepsilon}_{kk}=0$. Then the constitutive equation can be rewritten as

$$\sigma_i = C_{ij}\,\dot{\varepsilon}_j \qquad i,j=1,\ldots,3 \tag{3.20}$$

where C_{ij} is the tensor of modulus of viscosity. The single subscript for the stress components represents the double subscript notation such as $11=1$, $22=2$, $12=3$. The viscosity constants are given by C_{11}, C_{12}, C_{22} and C_{33}. The matrices form is given as

$$\begin{Bmatrix}\sigma_1\\ \sigma_2\\ \sigma_3\end{Bmatrix} = \begin{bmatrix}C_{11} & C_{12} & 0\\ C_{21} & C_{22} & 0\\ 0 & 0 & C_{33}\end{bmatrix}\begin{Bmatrix}\dot{\varepsilon}_1\\ \dot{\varepsilon}_2\\ \dot{\varepsilon}_3\end{Bmatrix} \tag{3.21}$$

where $C_{11}=C_{22}=2G+K$, $C_{33}=G$, and $C_{12}=C_{21}=K$.

H is the internal energy per volume, and can be expressed in terms of the strain rate

$$H(S_i)=\frac{1}{2}C_{ij}\varepsilon_i\varepsilon_j \tag{3.22}$$

The variational internal energy in terms of the components of strain is given as

$$\delta H = C_{ijkl}\,\varepsilon_{ij}\,\delta\varepsilon_{kl}$$

$$= C_{11}\varepsilon_1\delta\varepsilon_1 + C_{12}\varepsilon_1\delta\varepsilon_2 + C_{21}\varepsilon_2\delta\varepsilon_1 + C_{22}\varepsilon_2\delta\varepsilon_2 + C_{33}\varepsilon_3\delta\varepsilon_3 \tag{3.23}$$

Using the first variation of internal energy, the stress-strain rate relations are substituted into the Euler equation. The corresponding form is given by

$$0 = \int \{ C_{11}\frac{\partial u}{\partial x}\frac{\partial \delta u}{\partial x} + C_{12}\frac{\partial u}{\partial x}\frac{\partial \delta v}{\partial y} + C_{21}\frac{\partial v}{\partial y}\frac{\partial \delta u}{\partial x} + C_{22}\frac{\partial v}{\partial y}\frac{\partial \delta v}{\partial y} +$$

$$+ C_{33}\left(\frac{\partial u}{\partial y}+\frac{\partial v}{\partial x}\right)\left(\frac{\partial \delta u}{\partial y}+\frac{\partial \delta v}{\partial x}\right)\}\,dxdy \tag{3.24}$$

A four-node element, Figure 3.1, and a three-node element, Figure 3.2, are used in the finite element model. The shape functions are given as

$N_1(u,v)=(1-u)(1-v)$

$N_2(u,v)= u(1-v)$

$N_3(u,v)= uv$

$N_4(u,v)= v(1-u)$

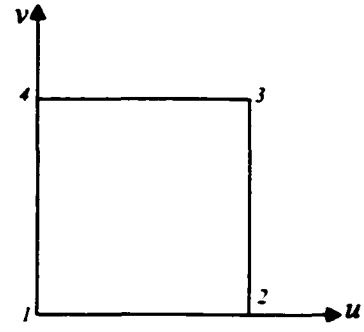

Figure 3.1: A four-node element

$N_1(u,v)=1-u-v$

$N_2(u,v)=u$

$N_3(u,v)=v$

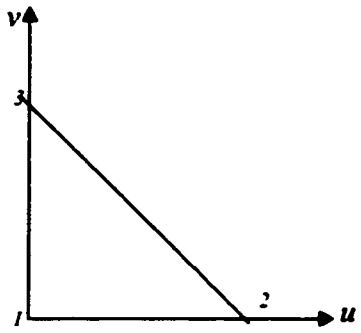

Figure 3.2: A three-node element

Substitution of the approximate velocity variations into the weak forms and collecting terms allows for writing the final equation in matrices form as

$$\begin{bmatrix} [K^{11}] & [K^{12}] \\ [K^{21}] & [K^{22}] \end{bmatrix} \begin{Bmatrix} \{u\} \\ \{v\} \end{Bmatrix} = \begin{Bmatrix} \{F^1\} \\ \{F^2\} \end{Bmatrix} \tag{3.25}$$

The disadvantage of the penalty method is that it is easy to get ill condition matrices during calculation.

3.2.2 The Penalty Iterative Method

In this division, there are two parts, complete incompressibility and average incompressibility. In the first part, the relation of the bulk modulus and the mean stress is introduced. The constitutive equation is substituted into the virtual expression. The iterative process is written in terms of matrices forms. The iterative method for average incompressibility is presented.

3.2.2.1 Complete Incompressibility

In order to develop the iterative method, it is first necessary to factor the bulk-modulus-mean-stress relationship as follows

$$\bar{\sigma} = (K_0 + \Delta K)\varepsilon_{kk} \tag{3.26}$$

where K_0 is reference bulk modulus, ΔK is difference between reference and actual bulk moduli. Rewrite as

$$\varepsilon_{kk} = \frac{\bar{\sigma}}{K_0 + \Delta K} = \left(\frac{1}{K_0} - \frac{\Delta K}{K_0(K_0 + \Delta K)} \right) \bar{\sigma}$$

to obtain

$$\varepsilon_{kk} = \frac{1}{K_0}\bar{\sigma} - \frac{\Delta K}{K_0(K_0 + \Delta K)}\bar{\sigma}$$

Hence

$$\bar{\sigma} = K_0 \varepsilon_{kk} + \left(\frac{\Delta K}{K_0 + \Delta K} \right) \bar{\sigma} \tag{3.27}$$

Substituted the constitutive equation (3.27) into the virtual expression, equation (3.10), this form allows us to use the factored form of the bulk-modulus-mean-stress relationship to obtain

$$\int \delta\varepsilon_{ij}[2G\varepsilon'_{ij} + K_0\varepsilon_{kk}\delta_{ij}]dV + \int \delta\varepsilon_{ij}[(\frac{\Delta K}{K_0 + \Delta K})\delta_{ij}\bar{\sigma}]dV - \int \delta u_i X_i dV$$

$$- \int_S \delta u_i \bar{T}_i dS = 0 \tag{3.28}$$

Let n be the current iterative number, then solve the following equation for displacements based on the current value for the mean stress $\bar{\sigma}_{(n)}$

$$\int \delta\varepsilon_{ij}[2G\varepsilon'_{ij} + K_0\varepsilon_{kk}\delta_{ij}]dV = - \int \delta\varepsilon_{ij}[(\frac{\Delta K}{K_0 + \Delta K})\delta_{ij}\bar{\sigma}]dV + \int \delta u_i X_i dV$$

$$+ \int_S \delta u_i \bar{T}_i dS = 0 \tag{3.29}$$

After the displacement field is obtained, update the mean stress using

$$\int_V \delta\bar{\sigma}[\bar{\sigma}_{(n+1)}]dV = \int_V \delta\bar{\sigma}[(\frac{\Delta K}{K_0 + \Delta K})\bar{\sigma}_{(n)}]dV - \int_V \delta\bar{\sigma}K_0\varepsilon_{kk}dV \tag{3.30}$$

where the weak form is used to be consistent with the weak form of the equation of motion. These two equations are solved iteratively until there are only insignificant changes in the mean stress rates or velocities.

The matrices form of the weak formula can be written as

$$[K]\{U\} = -\{F_{\bar{\sigma}}\} + \{F\} \tag{3.31}$$

where

$$[K] = \sum_1^n \int_V [N']^T [M][N']dV$$

$$[F_{\bar{\sigma}}] = \sum_1^n \int_V [N']^T \{\delta\}(\frac{\Delta K}{K_0 + \Delta K})[S][N_{\bar{\sigma}}]\{\bar{\sigma}\}dV$$

$$\{F\} = \sum_1^n \int_V \{N_u\}\{X\}dV + \sum_1^n \{N_u\}\{T\}dS$$

The mean stress is determined using

$$\{\bar{\sigma}\}_{i+1} = (\frac{\Delta K}{K_0 + \Delta K})\{\bar{\sigma}\}_i + \int_V \{N_{\bar{\sigma}}\}K_0[S][N']\{U\}dV \tag{3.32}$$

To know why it is convergent and how fast it is converged, the following analysis is made. Let us define

$$[K_0] = \int_V \{N_{\bar{\sigma}}\}K_0[S][N']dV \tag{3.33}$$

where

$$[S]=\begin{bmatrix}1 & 1 & 0\\ 1 & 1 & 0\\ 0 & 0 & 0\end{bmatrix}$$

The iterative process can be written in terms of matrices forms as

(1) $i=1$, $[K]\{u\}_1=\{F\}$; $\{u\}_1=[K]^{-1}\{F\}$;

(2) $i=2$, $[K]\{u\}_2=\{F\}-\{F_{\bar{\sigma}}\}_1=\{F\}-[K_0]\{u\}_1=\{F\}-[K_0][K]^{-1}\{F\}=([I]-[K_0][K]^{-1})\{F\}$;

$\{u\}_2=[K_0]^{-1}([I]-[K_0][K]^{-1})\{F\}$;

$\{F_{\bar{\sigma}}\}_1-\{F_{\bar{\sigma}}\}_0=[K_0][K]^{-1}\{F\}$;

(3) $i=3$, $[K]\{u\}_3=\{F\}-\{F_{\bar{\sigma}}\}_2=\{F\}-[K_0]\{u\}_1-[K_0]\{u\}_2$

$=\{F\}-[K_0][K]^{-1}\{F\}-[K_0][K]^{-1}([I]-[K_0][K]^{-1})\{F\}$

$\{u\}_3=[K]^{-1}([I]-[K_0][K]^{-1}-[K_0][K]^{-1}([I]-[K_0][K]^{-1}))\{F\}$

$\{F_{\bar{\sigma}}\}_2-\{F_{\bar{\sigma}}\}_1=[K_0]\{u\}_2=[K_0][K]^{-1}([I]-[K_0][K]^{-1})\{F\}$

(4) $i=4$, $[K]\{u\}_4=\{F\}-\{F_{\bar{\sigma}}\}_3=\{F\}-[K_0]\{u\}_1-[K_0]\{u\}_2-[K_0]\{u\}_3$

$=\{F\}-[K_0][K]^{-1}\{F\}-[K_0][K]^{-1}([I]-[K_0][K]^{-1})\{F\}-$

$[K_0][K]^{-1}([I]-[K_0][K]^{-1}-[K_0][K]([I]-[K_0][K]^{-1}))\{F\}$

$\{F_{\bar{\sigma}}\}_3-\{F_{\bar{\sigma}}\}_2=[K_0]\{u\}_3=[K_0][K]^{-1}([I]-[K_0][K]^{-1}-[K_0][K]^{-1}([I]-[K_0][K]^{-1}))\{F\}$

$=[K_0][K]^{-1}([I]-[K_0][K]^{-1})^2\{F\}$ .....

$i=n$, $\{F_{\bar{\sigma}}\}_{n-1}-\{F_{\bar{\sigma}}\}_{n-2}=[K_0][K]^{-1}([I]-[K_0][K]^{-1})^{n-2}\{F\}$

When the value of K_0 is large, $[K_0] \cong [K]$, and the value of $[I]-[K_0][K]^{-1}$ is small. Hence, it would be converged very fast and save computation cost.

3.2.2.2 Average Incompressibility

Equation (3.18) can be modified as

$$\begin{bmatrix} [K] & [G]^T \\ [G] & \left[\frac{1}{\xi}\right] \end{bmatrix} \begin{Bmatrix} \{U\} \\ \{p\} \end{Bmatrix} = \begin{Bmatrix} \{F\} \\ \{0\} \end{Bmatrix} \tag{3.34}$$

Here ξ is a large positive number which can be increased sufficiently to make equations (3.18). (3.22) nearly equivalent. Let's define ξ as

$$\xi = \xi_0 + \Delta\xi \tag{3.35}$$

Hence,

$$\frac{1}{\xi} = \frac{1}{\xi_0 + \Delta\xi} = \frac{1}{\xi_0} - \frac{\Delta\xi}{\xi_0(\xi_0 + \Delta\xi)} \tag{3.36}$$

Substitution into equation (3.22) leads

$$[G]\{U\} + \left(\frac{1}{\xi_0} - \frac{\Delta\xi}{\xi_0(\xi_0 + \Delta\xi)}\right)\{p\} = \{0\} \tag{3.37}$$

We then derive the following pressure updating equation as

$$\{P\}_{i+1} = [G]\xi_0\{U\}_i + \{P\}_i \tag{3.38}$$

The main iterative equation of average incompressibility is

$$[K]\{U\} = \{F\} - [G]^T\{P\} \tag{3.39}$$

To be convergent, ξ has to satisfy the following condition.

$$0 < \xi_0 < \frac{1}{\beta^2}$$

$\frac{1}{\beta^2}$ is the maximum eigenvalue of the matrices [K].

CHAPTER 4

NUMERICAL EXPERIMENTS

There are two sections in this chapter. In the first section, numerical experiments on void ratio of granular systems are presented. A couple of comparison among various cases with different particles, compaction types, and stress components are made. The second section focuses on a series of numerical experiments and tests for assembly with the same void ratio. If the solutions of randomly distributed granular systems are converged or not while the number of particle increases is the main issue of these experiments. The factors which might affect convergence include void ratio, void shape, degree of freedom, particle number and so on.

4.1 NUMERICAL EXPERIMENTS ON VOID RATIO

The purpose of this section is to demonstrate that void ratio is a significant variable which significantly affect behavior of granular systems, no matter what size they are, which type of compaction is loaded, and which direction of the stress component is. There are three divisions in this section. In the first division, a comparison among cases of different particle number is made. The second division introduces a comparison among cases loaded different types of compaction. In the third division, a comparison of stress components in two different directions is given.

4.1.1 A Comparison among Cases of Different Particle Numbers

In this division, several granular systems of different size are compared with one another. In Figure 4.1, comparison of stress-density relation of isostatic compaction for several single-material granular systems containing different number of elements is given. In Figure 4.2, similar comparison is made for a few multiple-material aggregates.

Figure 4.1 gives the comparison of stress-density relation of isostatic compaction for 10-element, 75-element, 296-element and 1076-element single-material system. It indicates that the stress component on 75-element, 296-element and 1076-element aggregate is less than one on 10-element system after density is more than 0.87, the most likely because the systems have more degrees of freedom. Also, the 10-element system is unstable when the density is 0.98. As expected, as more elements are used to describe the system, the results stop changing.

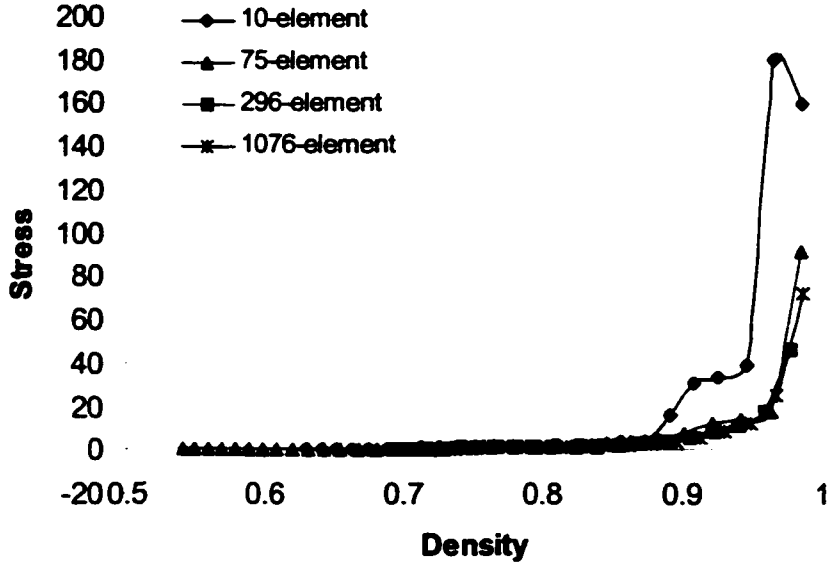

Figure 4.1: Comparison of stress-density relation of isostatic compaction for several granular systems containing different numbers of elements.

Figure 4.2 gives the comparison of stress-density relation of isostatic compaction for 10-element, 75-element, and 296-element multiple-material system. It indicates that the stress component on 75-element and 296-element is less than one on 10-element system after density is more than 0.85, the most likely because the systems have more degrees of freedom. Also, the 10-element system has an unstable curve. As expected, as more elements are used to describe the system, the results are nearly converged.

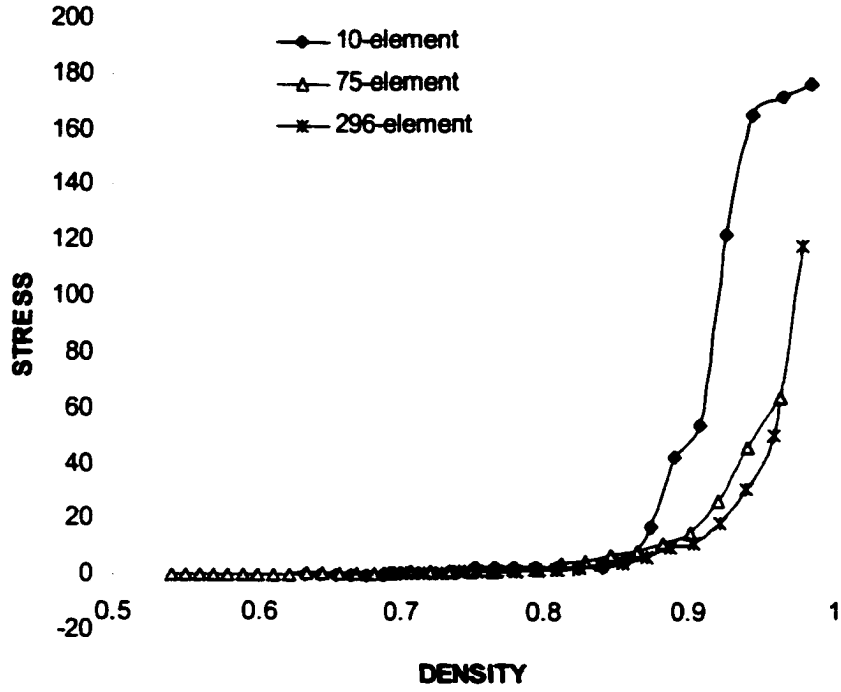

Figure 4.2: Comparison of stress-density relation of isostatic compaction for several granular systems containing different number of elements.

4.1.2 A Comparison among Cases with Various Compaction Types

In this division, the cases of two different compaction types are compared with one another. In Figure 4.3, a comparison of stress-density relation among different types

of compaction for the 296-element single-material granular system is presented. In Figure 4.4, a similar comparison for multiple material assembly is introduced.

Figure 4.3 shows a comparison of the stress-density relation between isotropic and close-die compaction for the 296-element granular system. The results of three compaction are quite different at the beginning. However, when incompressibility is almost achieved at the end, the results of three different compactions are pretty close in behavior, because incompressibility indicates that stress or strain component in x direction on x face should be equal to one in y direction on y face.

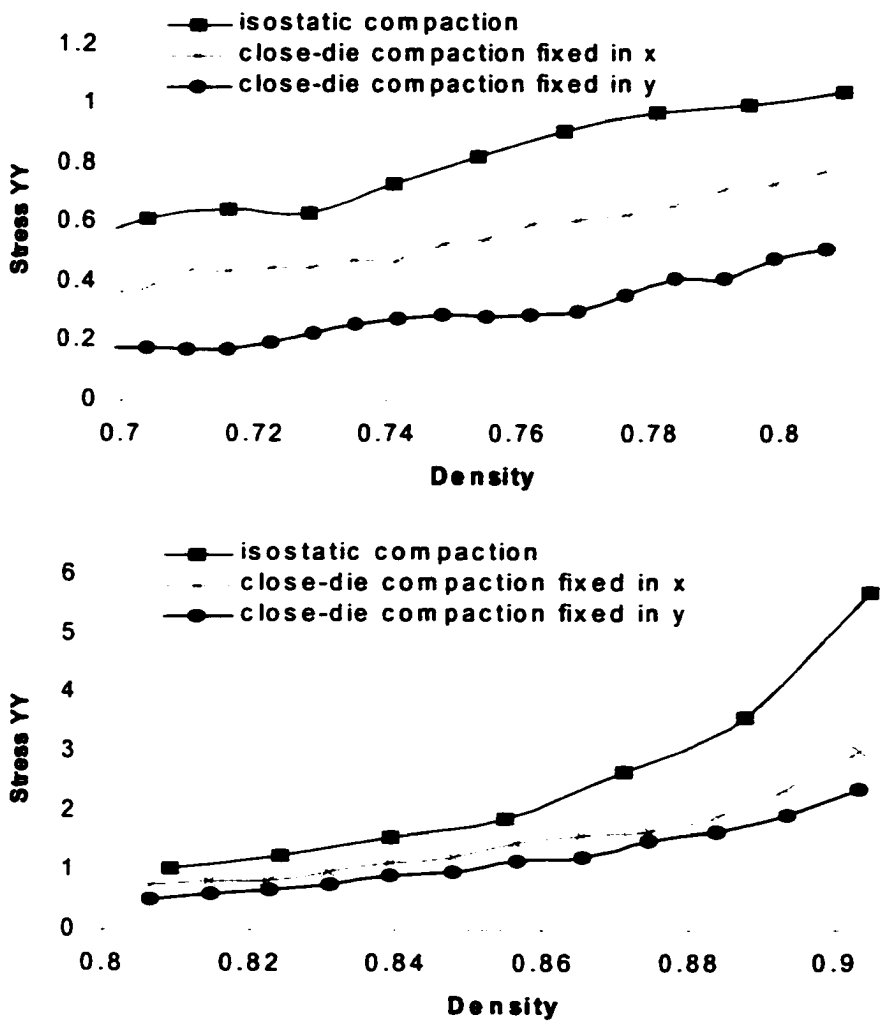

Figure 4.3: Comparison of stress-density relation among different types of compaction for the 296-element granular system.

Figure 4.4 shows a comparison of the stress-density relation between isotropic and close-die compaction for the 296-element granular system with multiple materials. The results of three compaction are quite different at first. Similar to the previous experiment, when incompressibility is almost achieved at the end, the results of three different compactions are pretty close in behavior, because incompressibility has almost been achieved.

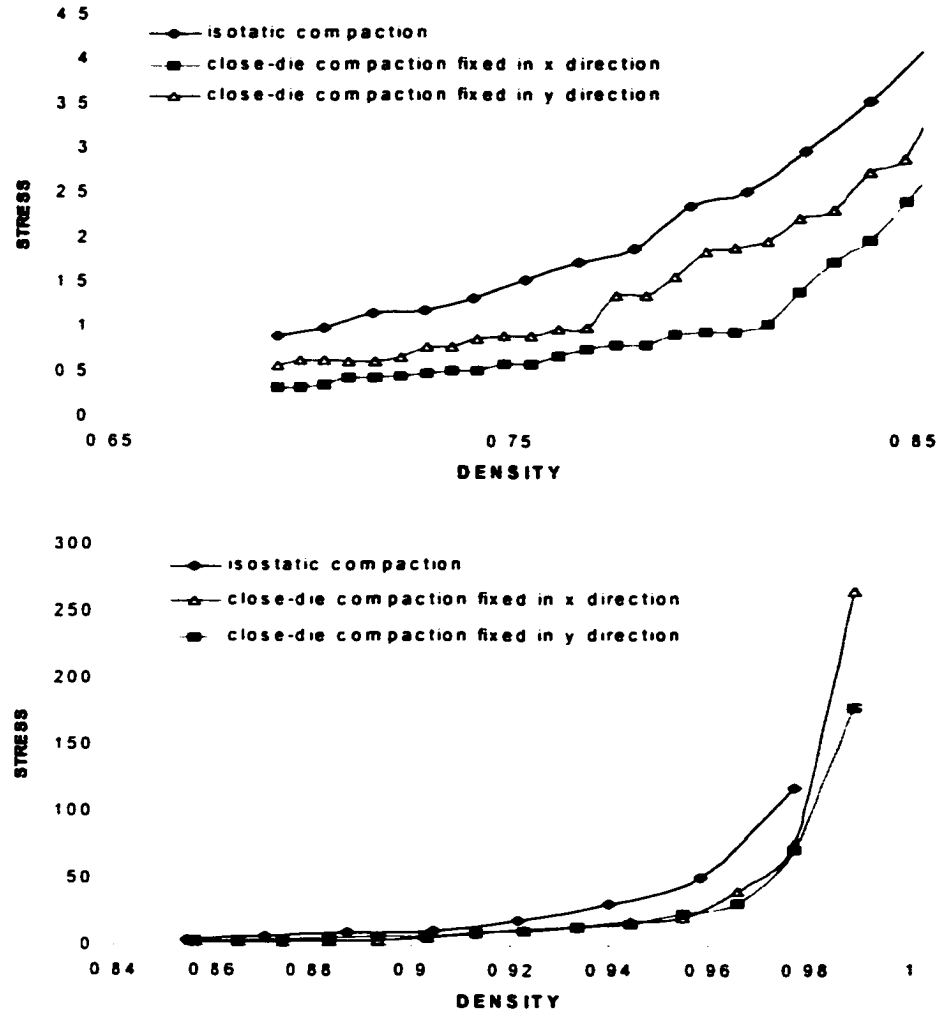

Figure 4.4: Comparison of stress-density relation between isotropic and close-die compaction for the 296-element granular system with multiple materials.

4.1.3 Comparison of Stress Components

The main purpose of this division is to compare the stress component in x direction with the one in y direction. There are two figures given in this division. Each figure has three diagrams which represent the response of three different cases of void ratios.

Figure 4.5 shows a comparison of stress in the two directions for close-die compaction with $u=0$ on the boundaries of the 1076-element case. There are three diagrams in Figure 4.5. The first diagram demonstrates the stress components of the density from 0.71 to 0.8. At the beginning, the stress component in the x direction is approximately 60 percent of the one in y direction. In the second diagram, the stress components of the density from 0.81 to 0.9. These two stress components are getting closer. In the third diagram, that the two stress components have highly closeness indicates that incompressibility has nearly been achieved.

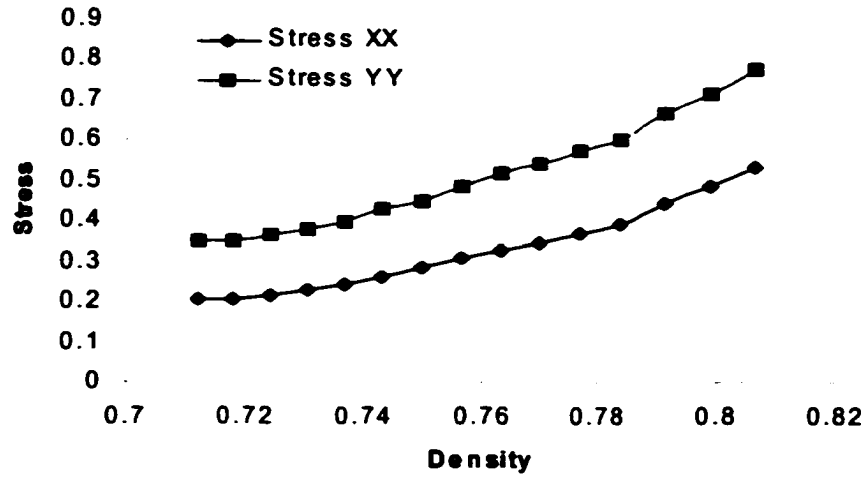

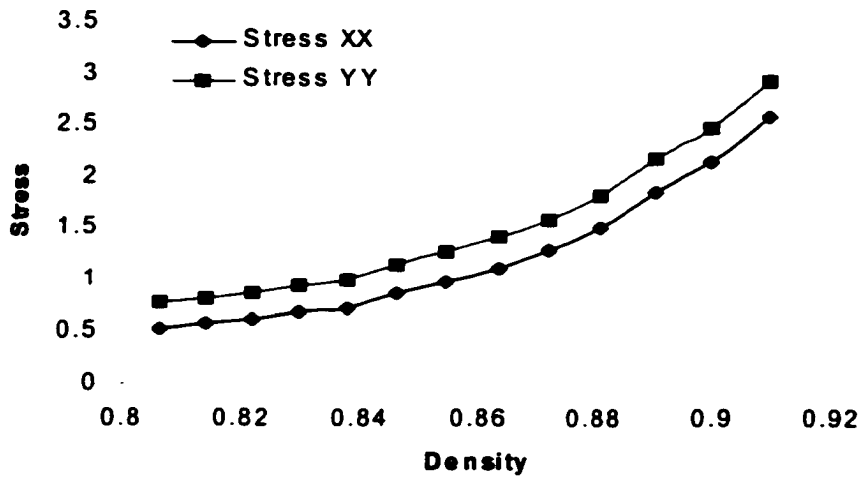

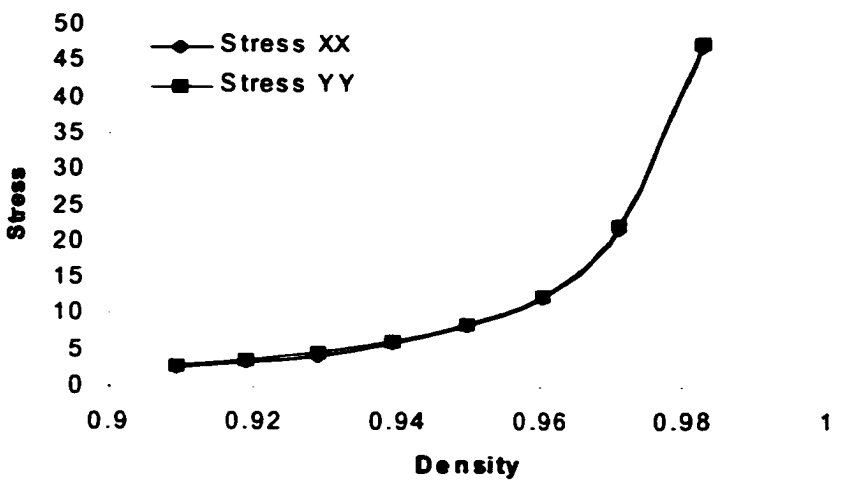

Figure 4.5: Comparison of stress in x and y direction for close-die compaction fixed in x direction of the 1076-element assembly.

Figure 4.6 shows a comparison of stress components in the two directions for close-die compaction with $u=0$ on the boundaries of the 1076-element multiple-material case. There are three diagrams in Figure 4.6. The first diagram demonstrates the stress components in two directions of the density from 0.69 to 0.81. At the beginning, the stress component on the moving face is about 20 percent higher than the one in the other direction. The second diagram shows stresses of the density from 0.81 to 0.91. The two stress components are much closer than the one shown in the preceding diagram. In the third diagram, the two stress components are very nearly equal indicating that incompressibility has nearly been achieved.

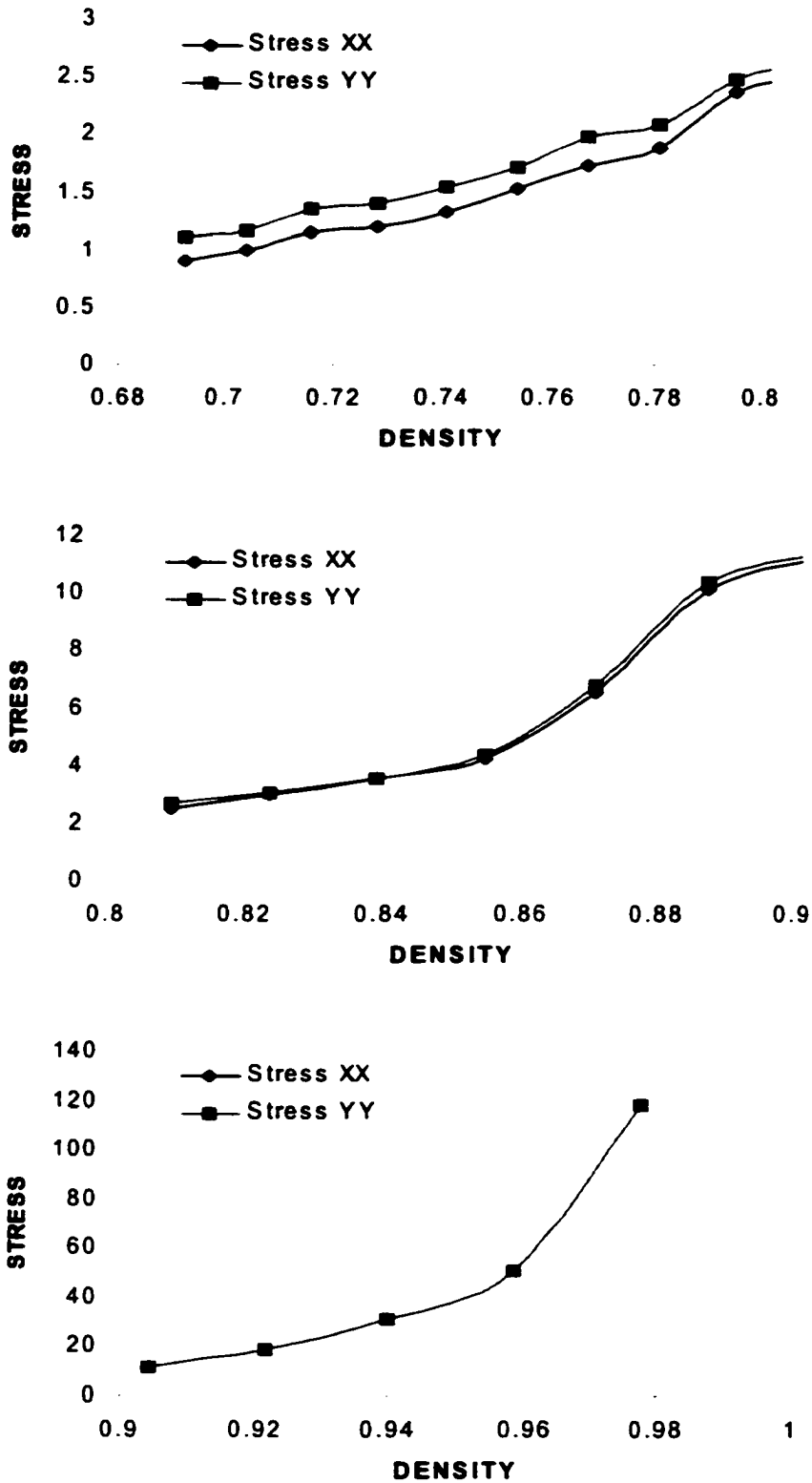

Figure 4.6: Comparison of stress in x and y direction for close-die compaction of the 1076-element assembly.

4.2 THE OTHER NUMERICAL EXPERIMENTS

In this section, the objective is to search what the other parameters are. The first hypothesis is that distribution of particles is one of other important variables which have some degree of impact on macroscopic behavior of the entire granular system. The experiment method used here is to keep density constant, and let particle be randomly distributed. Results demonstrate distribution of particle surely has an important effect on the granular system. However, results surprisingly show that random distribution of more than 2000 particles still has approximately 15 percent difference among tens of granular systems with the same void ratio. So the second conjecture is granular systems are affected by some other variables, such as the number of degrees of freedom, void position, distance between voids, and void shape. Using the same experiment method, the factors are tested one by one separately to determine if any of them has considerable influence on the response of the whole system. The details are reported in the following divisions.

In this section, there are seven numerical experiments made and reported in detail. The first division introduces the experiment on particle number, including bulk modulus and shear modulus tests. In the second division, numerical experiments on element shape are given. In the third division, the experiment on the number of degrees of freedom is introduced. The purpose of the experiments shown in the second and the third division is to eliminate numerical miscalculation. In the fourth division, the experiment on void position is presented. The fifth division demonstrates experiments on nearness of voids. In the sixth division, the void shape test is reported. Finally, the seventh division shows the experiment on fixed void ratio, void shape and nearness of

voids to verify the three variables create considerable difference among the previous tests.

4.2.1 The Experiment on Number of Particles

The purpose of this experiment is to figure out if particle distribution affects the response of the whole granular system or not. From the previous section, it is validated that void ratio is one variable which indeed has some degree of effect on aggregates behavior. In this experiment, the density is fixed in 0.8125. In several cases in which numbers of particles from 81 to 2031 are randomly spread in a square area. Then stresses are calculated in one time increment. The procedures are repeated 30 times for 30 different randomly disseminated cases. Appendix A shows 30 cases of 1300-element granular systems and their local density analysis. The contour diagrams demonstrate random distribution of particles. Figure 4.7 shows the numerical results of the experiment. There are nine cases with different particle numbers, which are 81, 183, 325, 508, 731, 995, 1300, 1645, and 2031. In the figure, the numbers following the particle numbers are the degrees of freedom. For instance, the 81-particle system has 281 degrees of freedom. Among 30 different 81-element systems, approximately 50 percent gap of difference is found. In contrast with these 81-element aggregates, the 2031-element systems have about 13 percent range of difference. It obviously proves that particle scattering is the other variable which has significant impact on behavior of granular systems in addition to void ratio.

However, the range of difference among 2031-particle systems is surprisingly big. It is assumed that random spread of a huge number of particles would pale the difference of solutions and make them converge to one single value. The huge range of

difference indicates that there are some other variables which have influence on the results.

In Figure 4.7, there are two gaps of interest. One is between the dash line 1 and the dash line 2. The gap represent the difference of bulk moduli among various granular systems. The other is between the dash line 3 and the dash line 4. This gap indicates difference between the stress component in x direction and the one in y direction. Figure 4.8 shows that standard deviation of stress components for 9 different size of granular systems. In Figure 4.9, standard deviation of difference between the stress component in the x direction and the one in the y direction is demonstrated. Both figures of standard deviation show some fluctuation, because, in the point of view of statistics, 30 cases for each type of granular systems is not big enough to be an ideal sample. However, as more particles are used, the results are closer.

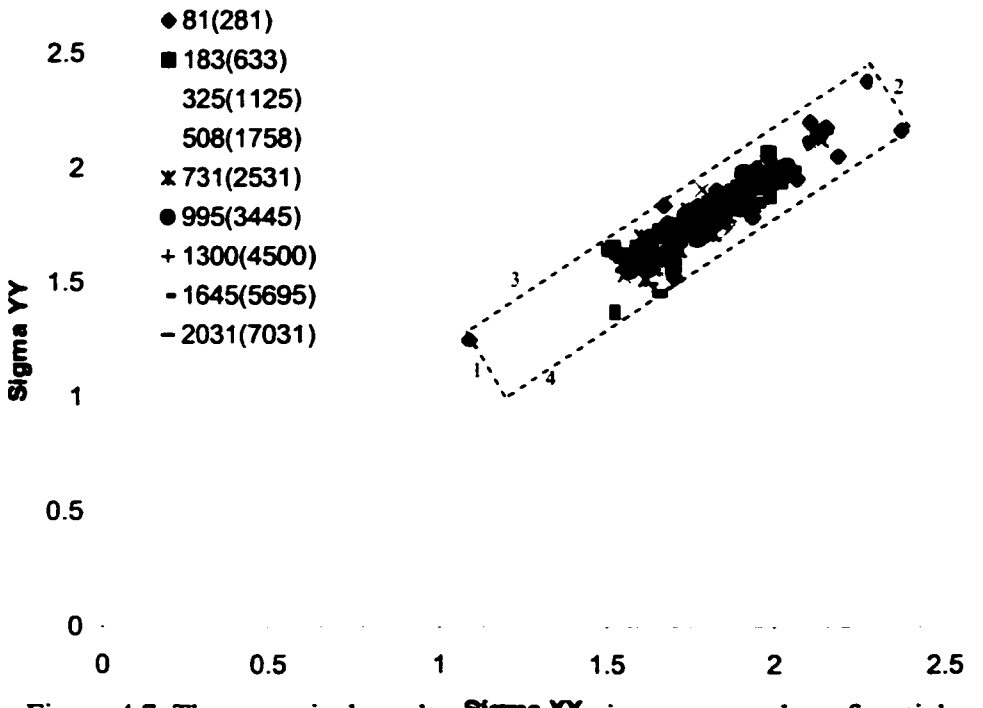

Figure 4.7: The numerical results of the experiment on number of particles

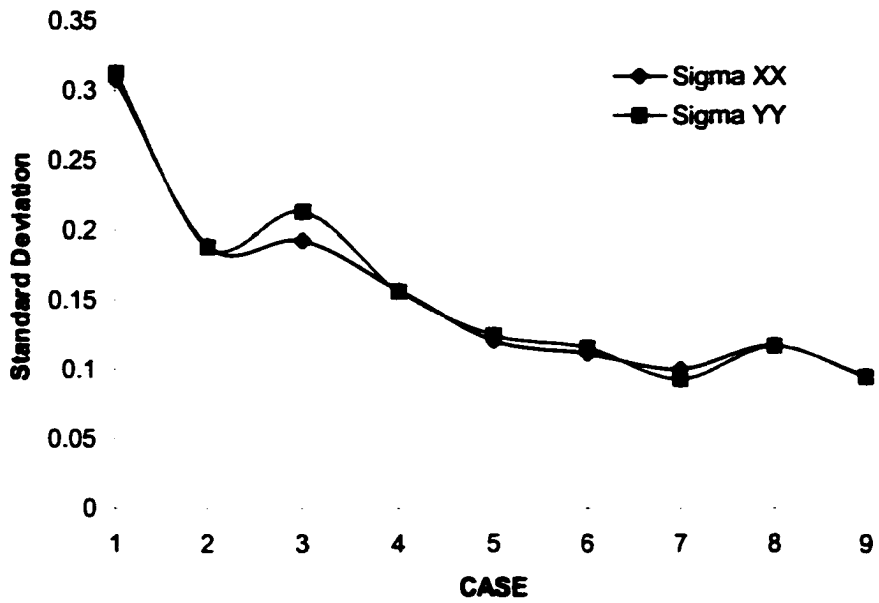

Figure 4.8: Standard deviation of stress components for nine different sizes of granular systems

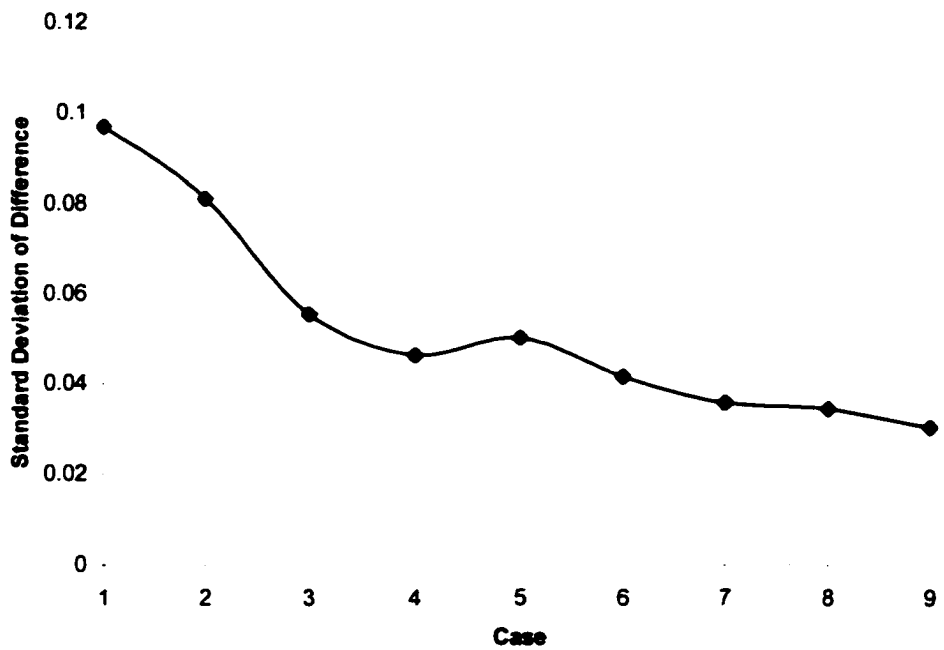

Figure 4.9: Standard deviation of difference between the stress component in x direction and the one in y direction

In addition to compaction tests, simple and pure shear tests are made to examine the granular system. Figures 4.10, 4.11 show that the solutions of shear stresses of 30 1000-particle granular systems with random particle size and position and the same density under shear load. The range of variation among the 30 cases is around 20 percent. The next goal is to find the variables to which the granular systems are so sensitive.

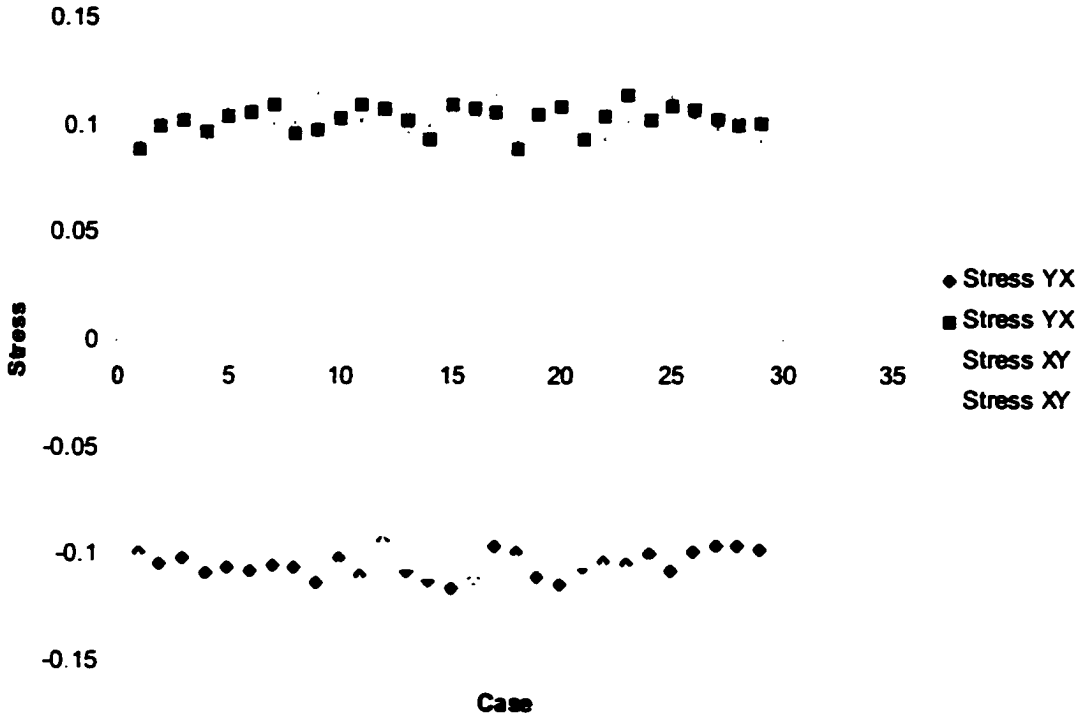

Figure 4.10: The results of the simple shear tests

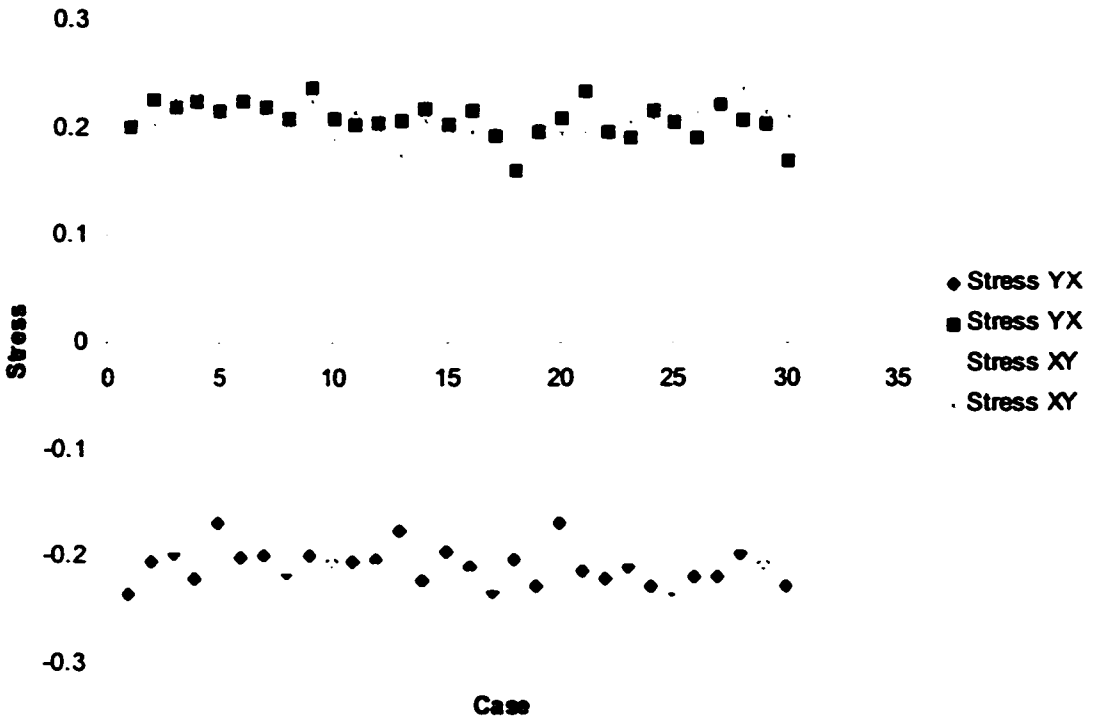

Figure 4.11: The results of the pure shear tests

4.2.2 Experiments on Mesh Element Shape

The hypothesis from the foregoing division is there are some other factors which considerably affect the macroscopic behavior. The first thing to do is to tune up the numerical model to eliminate all numerical flaws. The numerical experiment on mesh shape is made to test if mesh shape makes miscalculation or not. In a square hollow disk with a square hole on the center shown in Figure 6.1, tens of different styles of mesh systems are generated, and these meshes are used to run the finite element model. Results shown in Figure 4.12 demonstrate the difference of 30 cases is less than 2 percent. One of the most important reasons to create the numerical error is that the pressure for each mesh element is not constant. Because the numerical error is little, the results eliminate mesh shape as the main reason to cause problems.

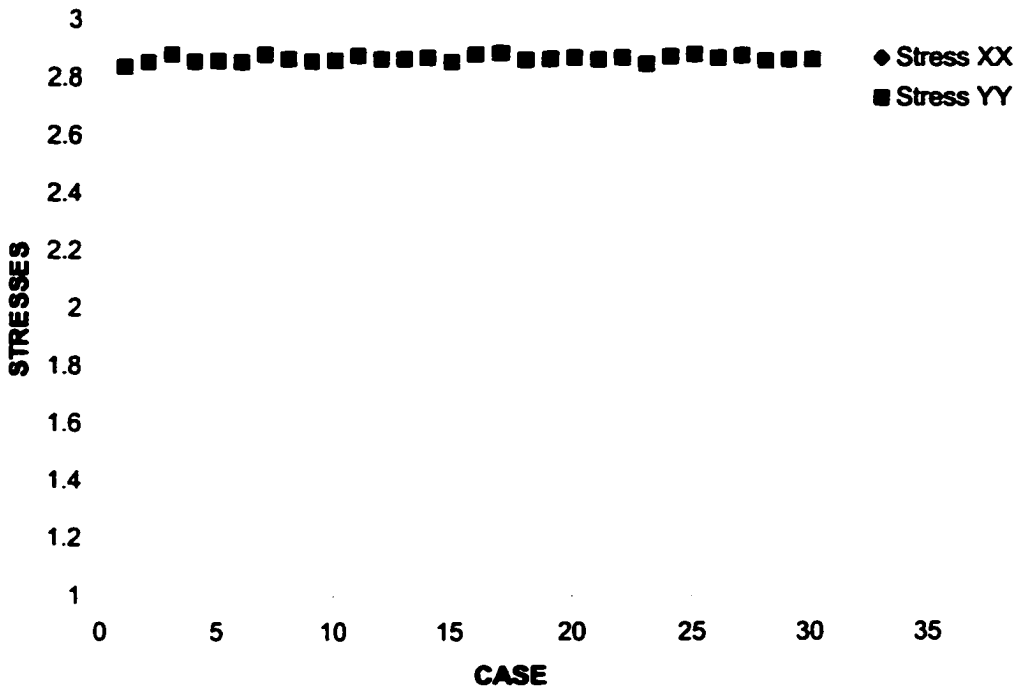

Figure 4.12: The results of the mesh shape test

4.2.3 Experiments on Number of Degrees of Freedom

One assumption to use the discrete element method, in which each particle is treated as an element individually, is that the random distribution of a huge number of particles will diminish the influence of individual behavior. However, the around 15 percent of difference range demonstrates that it is necessary to examine the original idea.

In contrast with the mesh shape test, the experiment on numbers of degrees of freedom is made to determine if numbers of degrees of freedom make macroscopic behavior different or not. The experiment is made as following. Stress components of two square disk with a square area of void on the center are calculated using the finite element program with different degrees of freedom from 16 to 6400 shown in Figure

4.13. The results presented in Figure 4.14 show that as a single element represents a single particle the stress component is about 6.8, around 100 percent different from the converged solution, which is approximately 3.0. However, using four elements reduces the error to approximately 10 percent. It indicates that a single element can not represent a single particle in the finite element model because it makes particles too stiff.

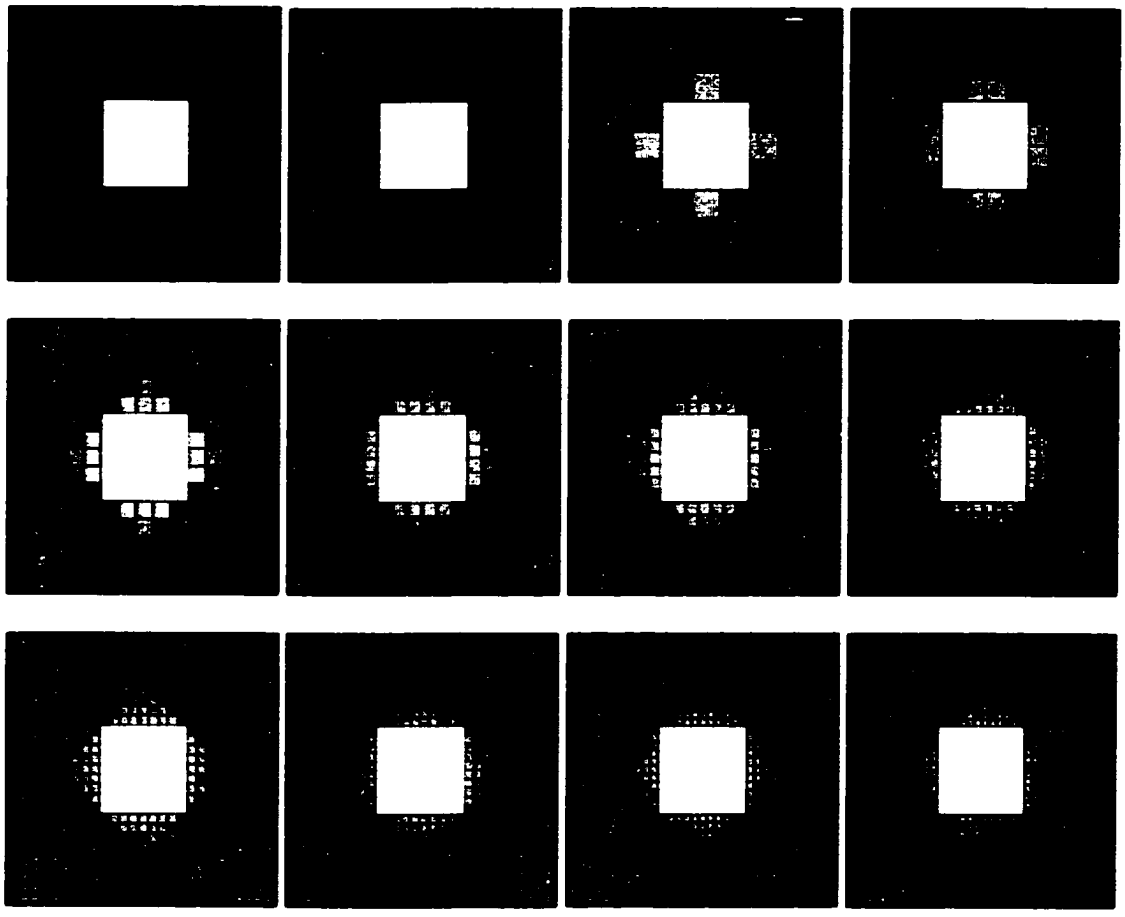

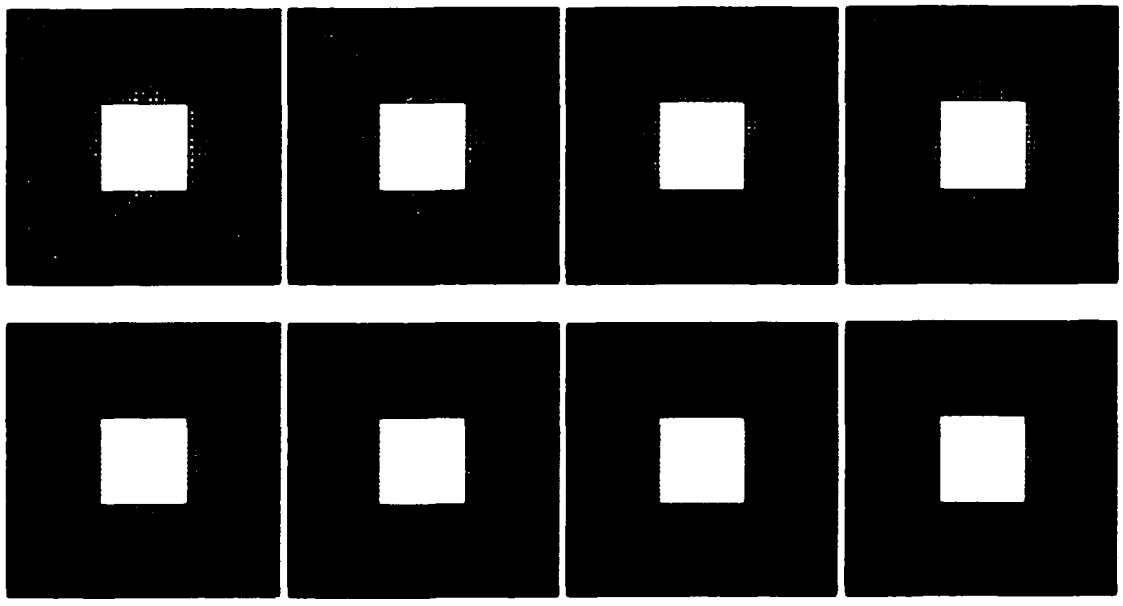

Figure 4.13: The 20 cases of the experiment on numbers of degrees of freedom

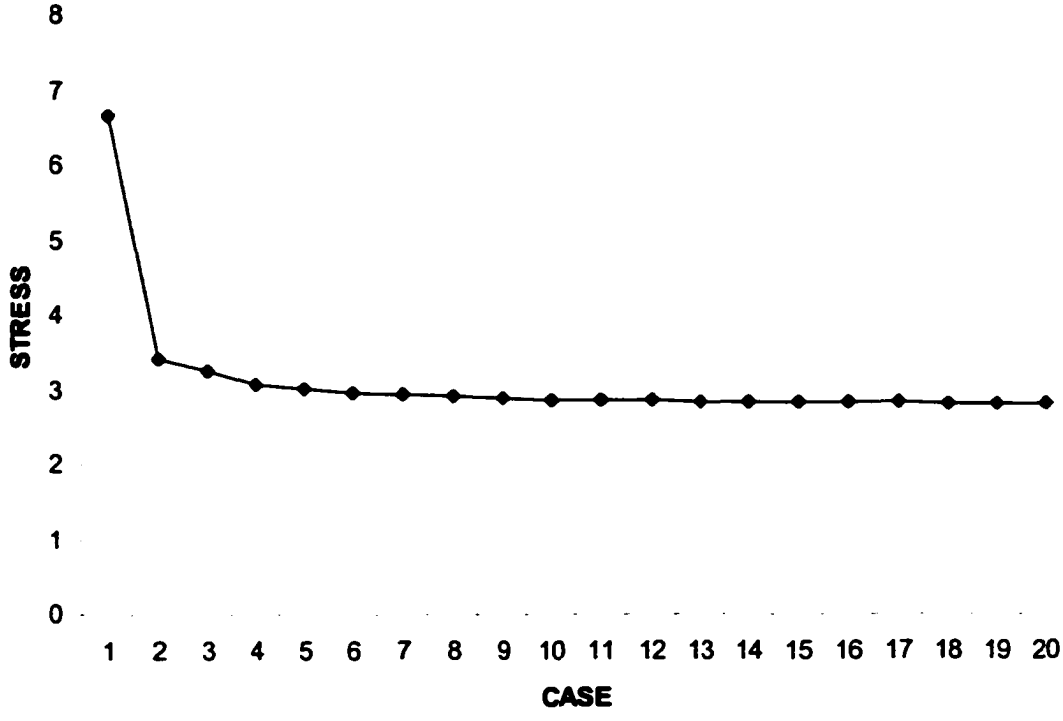

Figure 4.14: The results of the experiment on numbers of degrees of freedom

It is assumed that the increase of degree of freedom would decrease the range of stress differences and make them converge to one value. However, the following experiment disprove this hypothesis. The purpose of the following experiment is to show what happen if the degree of freedom increases. Figure 4.15 shows that the increase of degree of freedom shift the solution to about a half and the range of difference is decreased. However, the variation is not converged to a single value. In other words, the considerable difference still exists among the random spread granular systems.

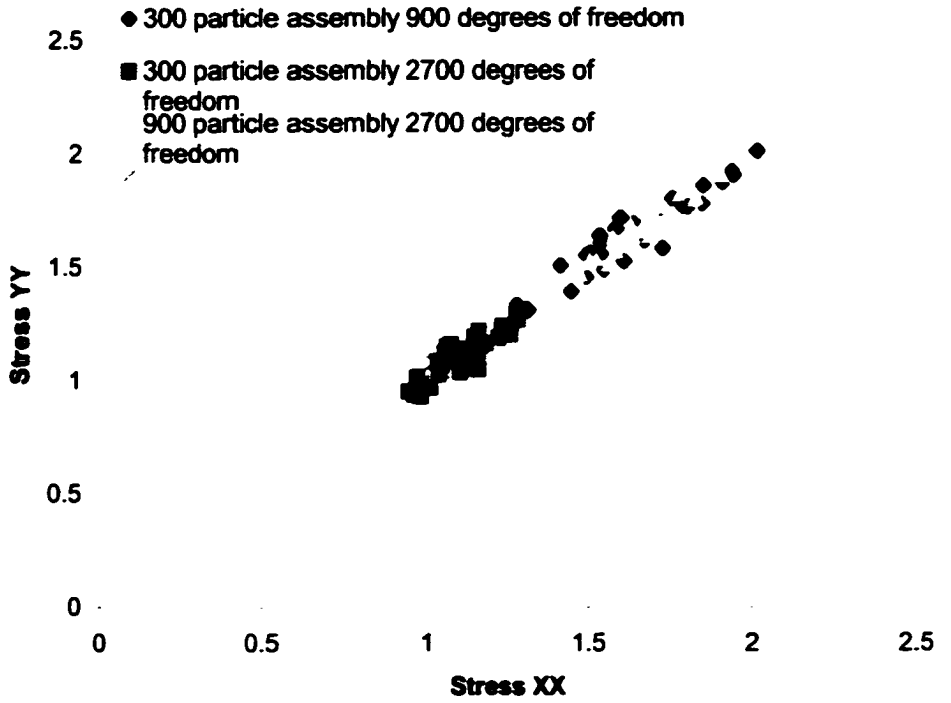

Figure 4.15: The increase of degrees of freedom shifts the solution to about a half.

Two significant conclusions can be drawn in this division. One is that the solutions of the discrete model in which each particle is treated as a single element individually need to be modified in some degree. Using four elements to represent one particle is

suggested due to its accuracy and efficiency. The other is that there are some variables which have noticeable impact on the macroscopic behavior of granular systems. The suspicious factors include void position, distance between voids, and void shape. The relevant numerical experiments on all factors are made individually and discussed in the following divisions.

4.2.4 The Experiment on Void Position

The experiment on void position is made to investigate if the void position is a factor having noticeable effect on global stresses. There are nine granular systems. Only one square void is put in each system. These voids are put in different positions of these systems. Stress components of all of systems are calculated and compared with one another. Figure 4.16 shows the nine experimented systems and their results. The closeness of these stress components disqualifies void position as one of main variables which have greatly influence on macroscopic behaviors.

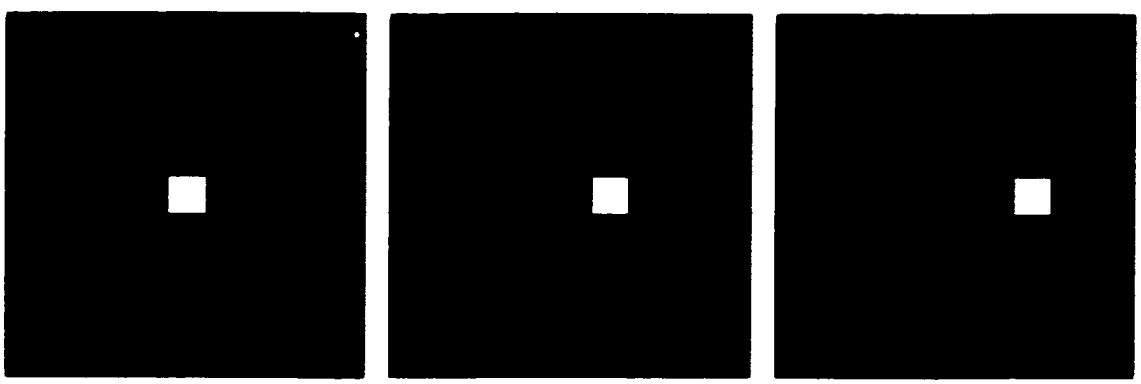

σ_{xx}=35.145, σ_{yy}=35.145 σ_{xx}35.090, σ_{yy}=35.091 σ_{xx}=34.837, σ_{yy}34.836

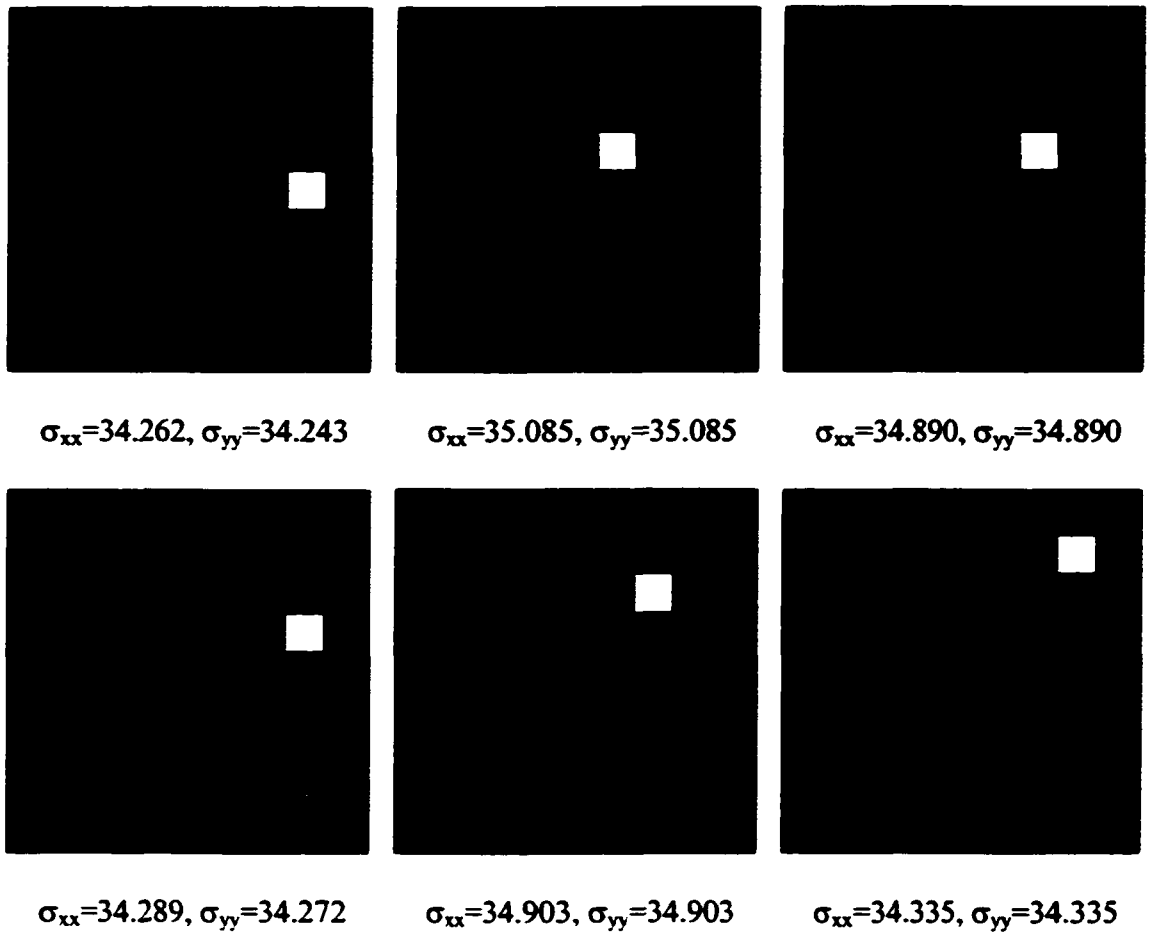

Figure 4.16: The nine tested cases of experiments on void position and their results

4.2.5 Experiments on Nearness of Voids

The objective of the experiments of void inter-distance is to examine if nearness of voids has substantial effect on global behavior or not. Several granular systems with two square voids are picked and tested. The two square voids in different systems have different distance between each other. If the distance between any two particles is one of significant factors, it will result in some considerable change.

In Figure 4.17, the results of the numerical experiment is presented. There are twelve diagrams in this figure. The first eight diagrams prove that when two voids keep some appropriate distance away from each other, the stress components are pretty close. The last four diagrams validate that when two voids do not keep a suitable distance, the stress components are dramatically changed.

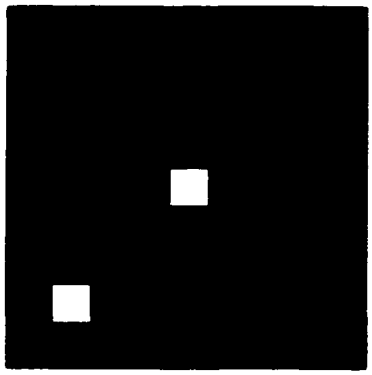

σ_{xx}=17.373, σ_{yy}=17.373

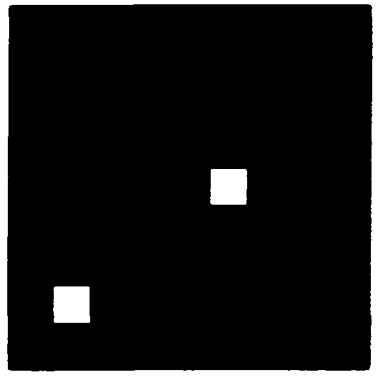

σ_{xx}=17.303, σ_{yy}=17.292

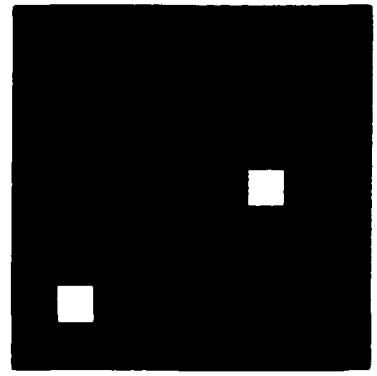

σ_{xx}=17.184, σ_{yy}=17.170

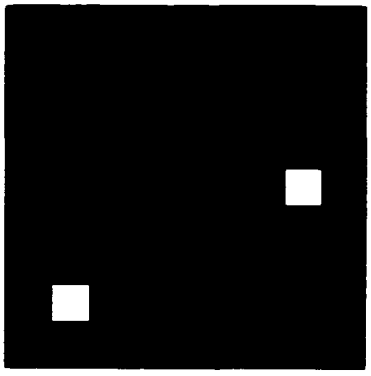

σ_{xx}=17.008, σ_{yy}=16.984

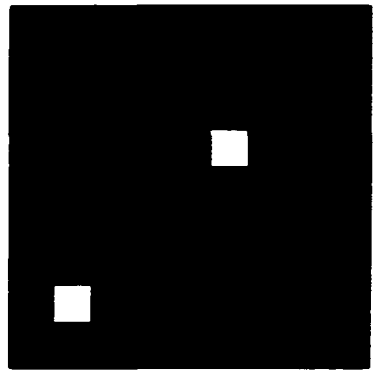

σ_{xx}=17.347, σ_{yy}=17.347

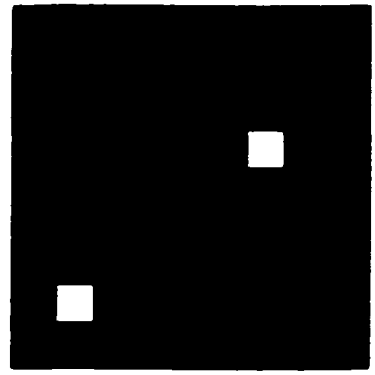

σ_{xx}=17.292, σ_{yy}=17.285

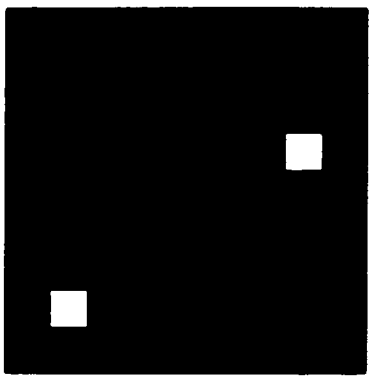

σ_{xx}=17.128, σ_{yy}=17.109

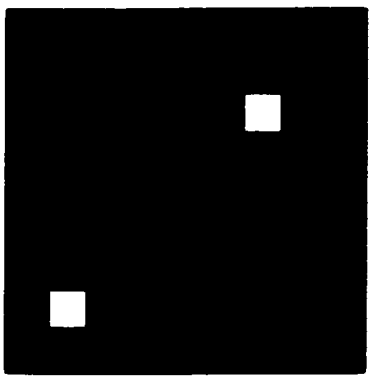

σ_{xx}=17.343, σ_{yy}=17.343

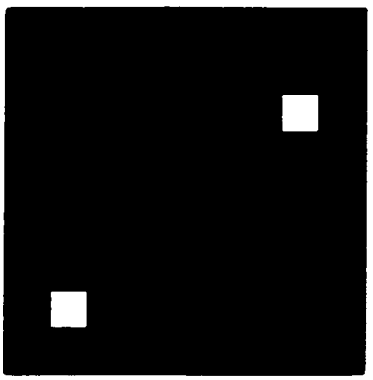

σ_{xx}=17.225, σ_{yy}=17.215

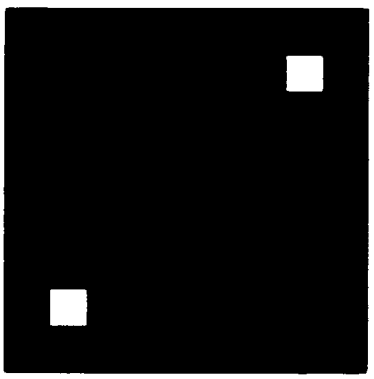

σ_{xx}=17.277, σ_{yy}=17.277

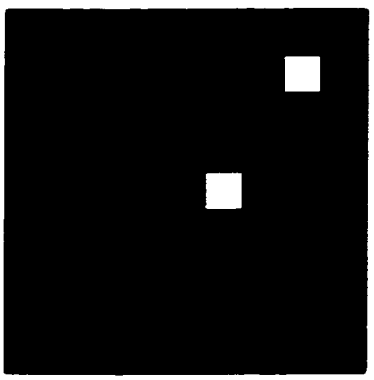

σ_{xx}=17.234, σ_{yy}=17.256

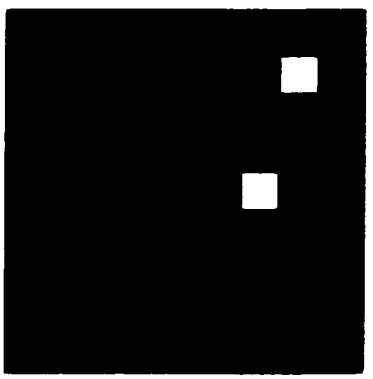

σ_{xx}=16.901, σ_{yy}=16.930

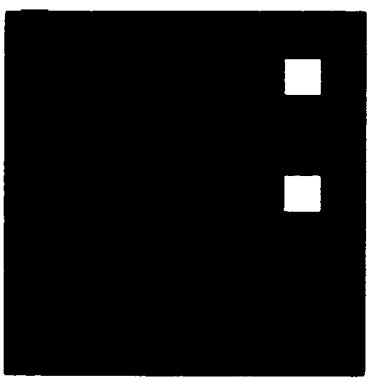

σ_{xx}=16.684, σ_{yy}=16.713

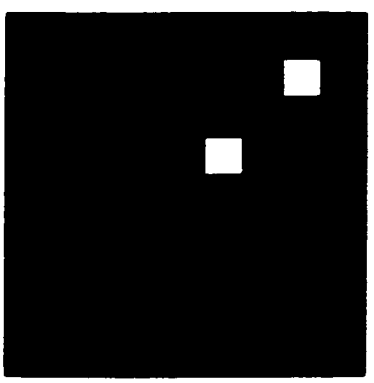

σ_{xx}=17.358, σ_{yy}=17.358

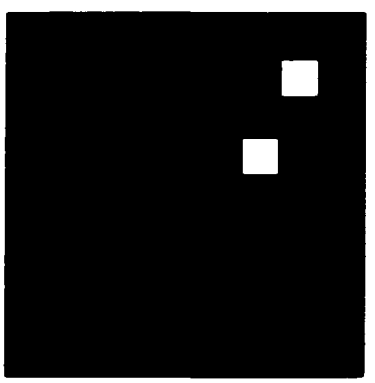

σ_{xx}=16.843, σ_{yy}=16.892

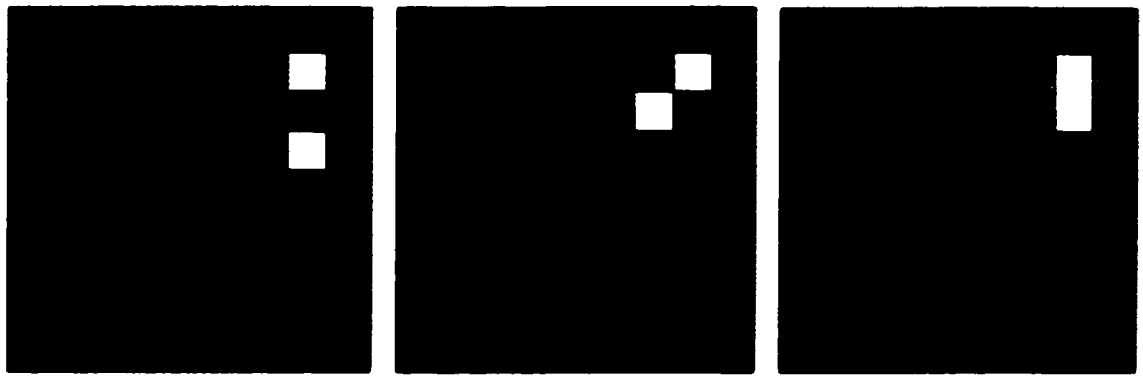

σ_{xx}=16.208, σ_{yy}=16.258 σ_{xx}=16.084, σ_{yy}=16.084 σ_{xx}=13.537, σ_{yy}=13.820

Figure 4.17: The results of the experiments on nearness of voids

In Figure 4.18, the results of the other experiment on nearness of voids are presented. There are fifteen diagrams in this figure. There are two different sizes of voids in each system. The first six diagrams demonstrate the effect of the distance in one direction. The next five diagrams prove the influence of the distance in the other direction. The last four diagrams show the impact of the distance in another direction. Similar to the preceding experiment, when the two voids keep some proper distance away from each other, the stress components are not very different. When two voids are getting closer, the stress components are greatly changed.

The conclusion drawn from these two numerical experiments is that nearness of voids has significant impact on the response of the whole system.

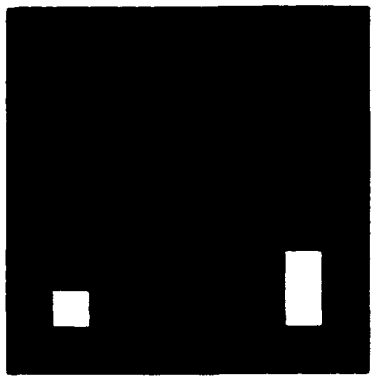

σ_{xx}=9.4278, σ_{yy}=9.5985

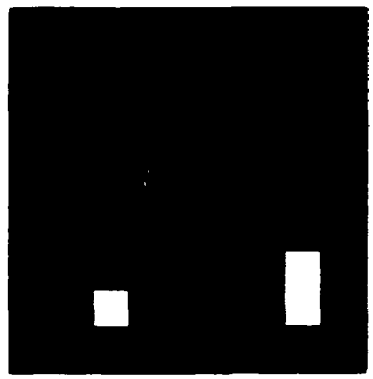

σ_{xx}=9.4653, σ_{yy}=9.6339

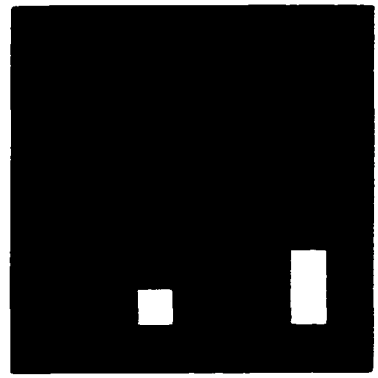

σ_{xx}=9.5100, σ_{yy}=9.6760

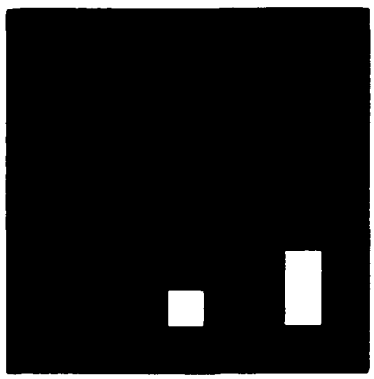

σ_{xx}=9.5167, σ_{yy}=9.6748

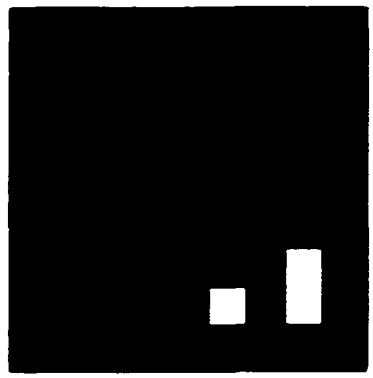

σ_{xx}=9.4905, σ_{yy}=9.6186

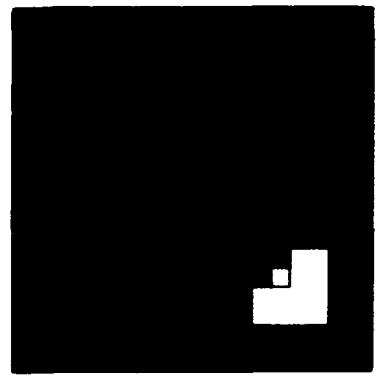

σ_{xx}=9.0873, σ_{yy}=9.0873

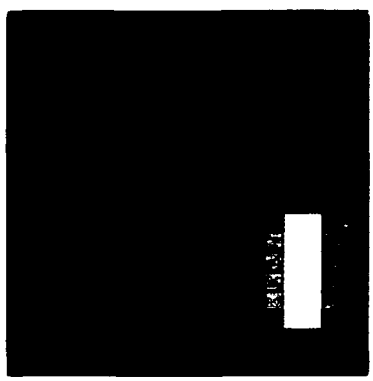

σ_{xx}=7.1200, σ_{yy}=7.5050

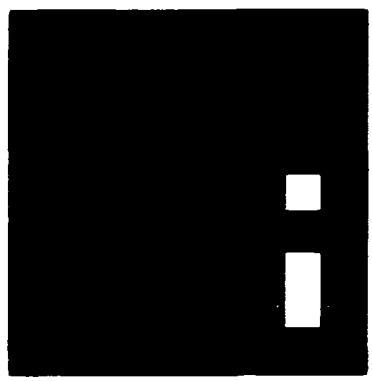

σ_{xx}=8.8505, σ_{yy}=9.0924

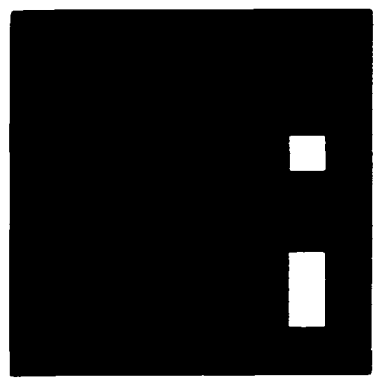

σ_{xx}=9.1191, σ_{yy}=9.3501

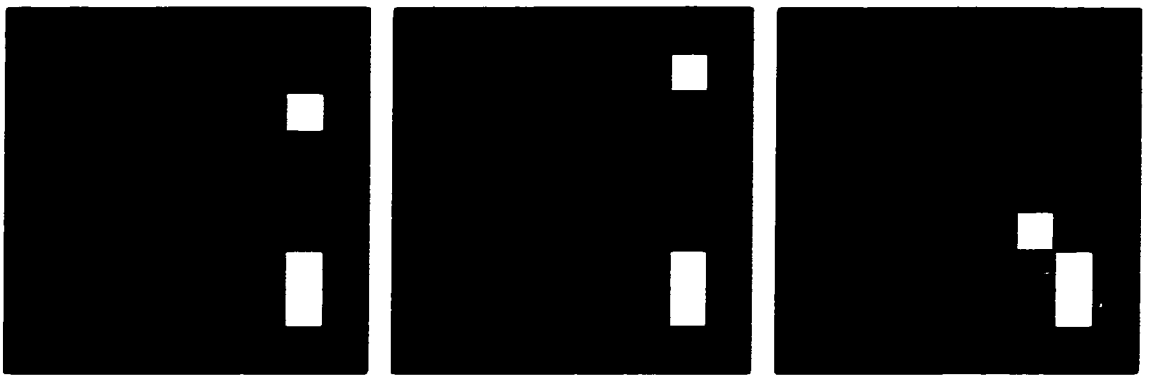

σ_{xx}=9.1511, σ_{yy}=9.3776 σ_{xx}=9.1626, σ_{yy}=9.3842 σ_{xx}=8.6793, σ_{yy}=8.9106

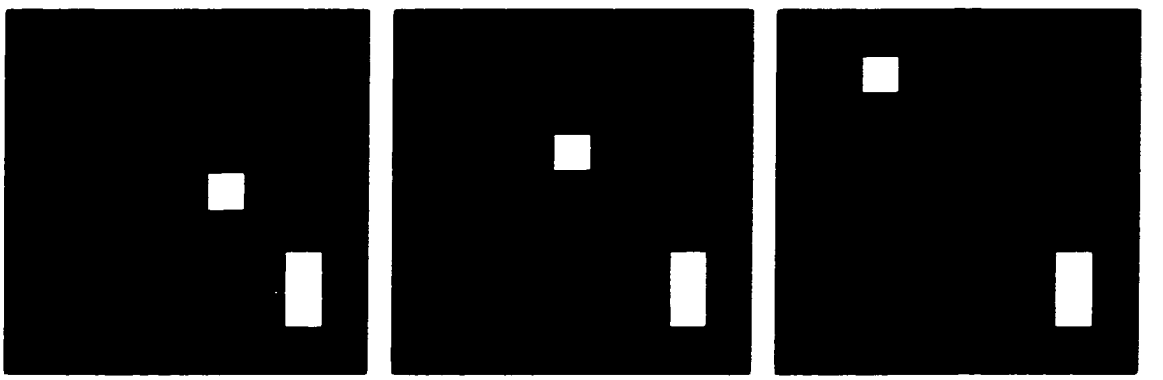

σ_{xx}=9.5431, σ_{yy}=9.7641 σ_{xx}=9.6371, σ_{yy}=9.8511 σ_{xx}=9.6913, σ_{yy}=9.9045

Figure 4.18: The results of the other experiment on nearness of voids

4.2.6 Experiments on Void Shape

The objective of the void shape test is to investigate if void shape is one of the main factors which largely affect macroscopic behaviors of assemblies. There are two experiments in this division. Figure 4.19 shows the first experiment on void shape and its results. A square disk with a square hole on the center is picked and its stress components are calculated. Then the void pattern is repeated several times. The cases and their stress components are shown in the first and second diagrams in Figure 4.19. The stress components of two disks are very close due to the symmetry of the disks.

Then the same experiment is repeated in the other rectangular disk with a circular hole on the center. The results are significantly different from the ones from the foregoing experiment. It is proved that void shape does make different.

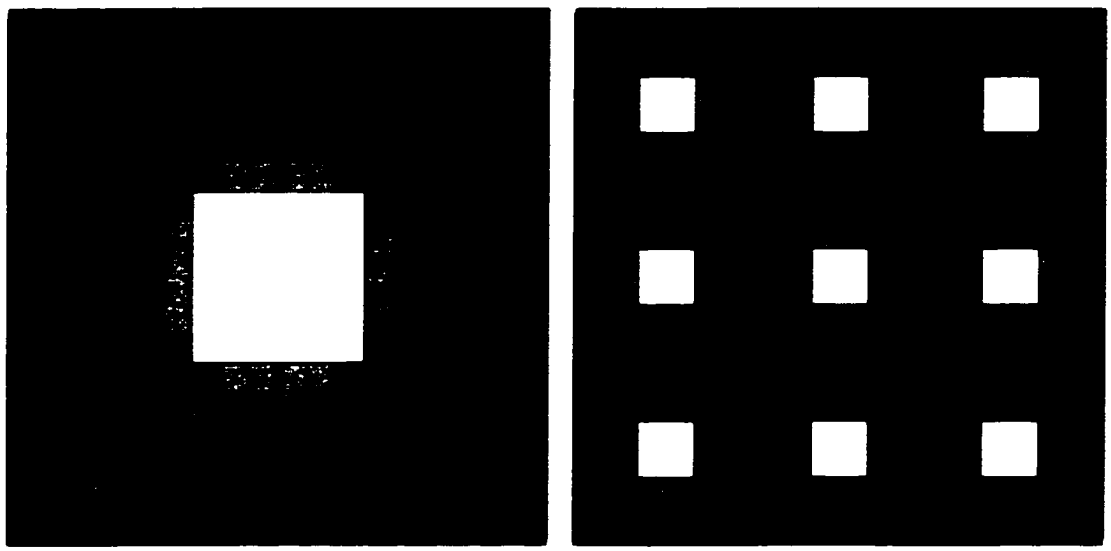

σ_{xx}=2.9523, σ_{yy}=2.9523 σ_{xx}=2.9487, σ_{yy}=2.9487

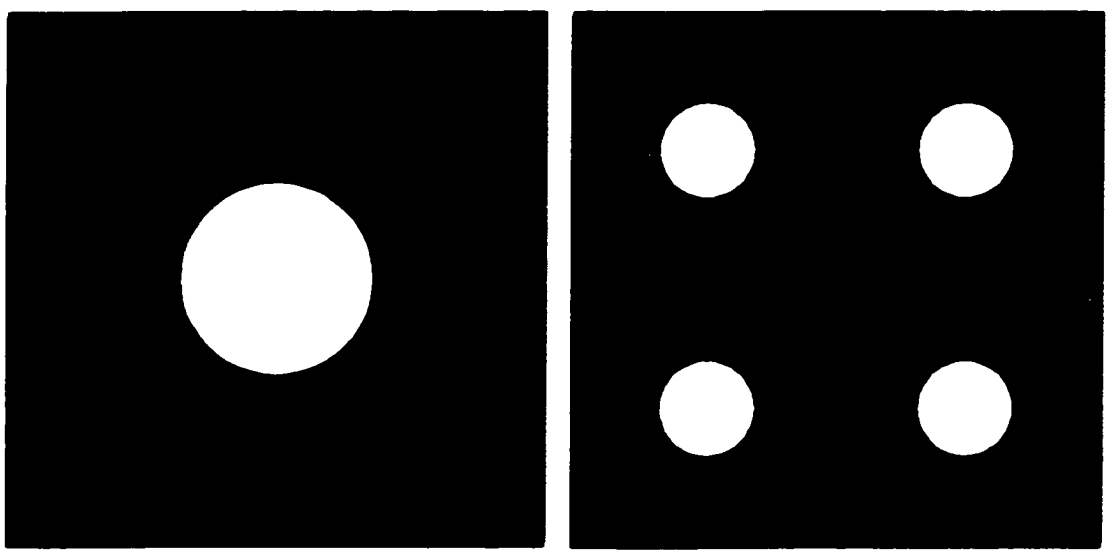

σ_{xx}=3.7399, σ_{yy}=3.7399 σ_{xx}=3.7394, σ_{yy}=3.7394

Figure 4.19: The first numerical experiment on void shape and its results

The purpose of the second numerical experiment is to examine if the ratio of length to width of each void will affect stresses or not. A granular system with a few randomly scattered rectangular voids is picked. As the length width ratio of every void is changed(shown in Figure 4.20), stress components are changed. Figure 4.21 demonstrates that when the length-width ratio is equal to one, the system is the stiffest. It is verified that void shape is one of the major variables affecting the global behavior.

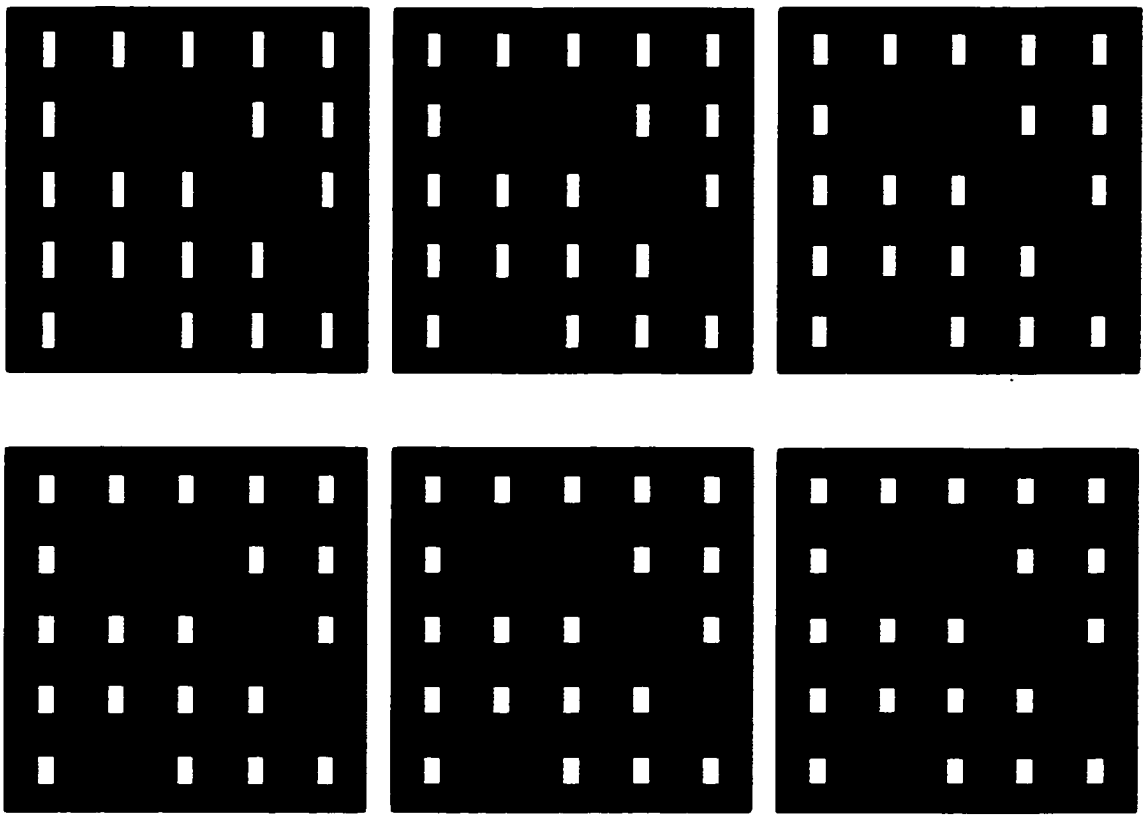

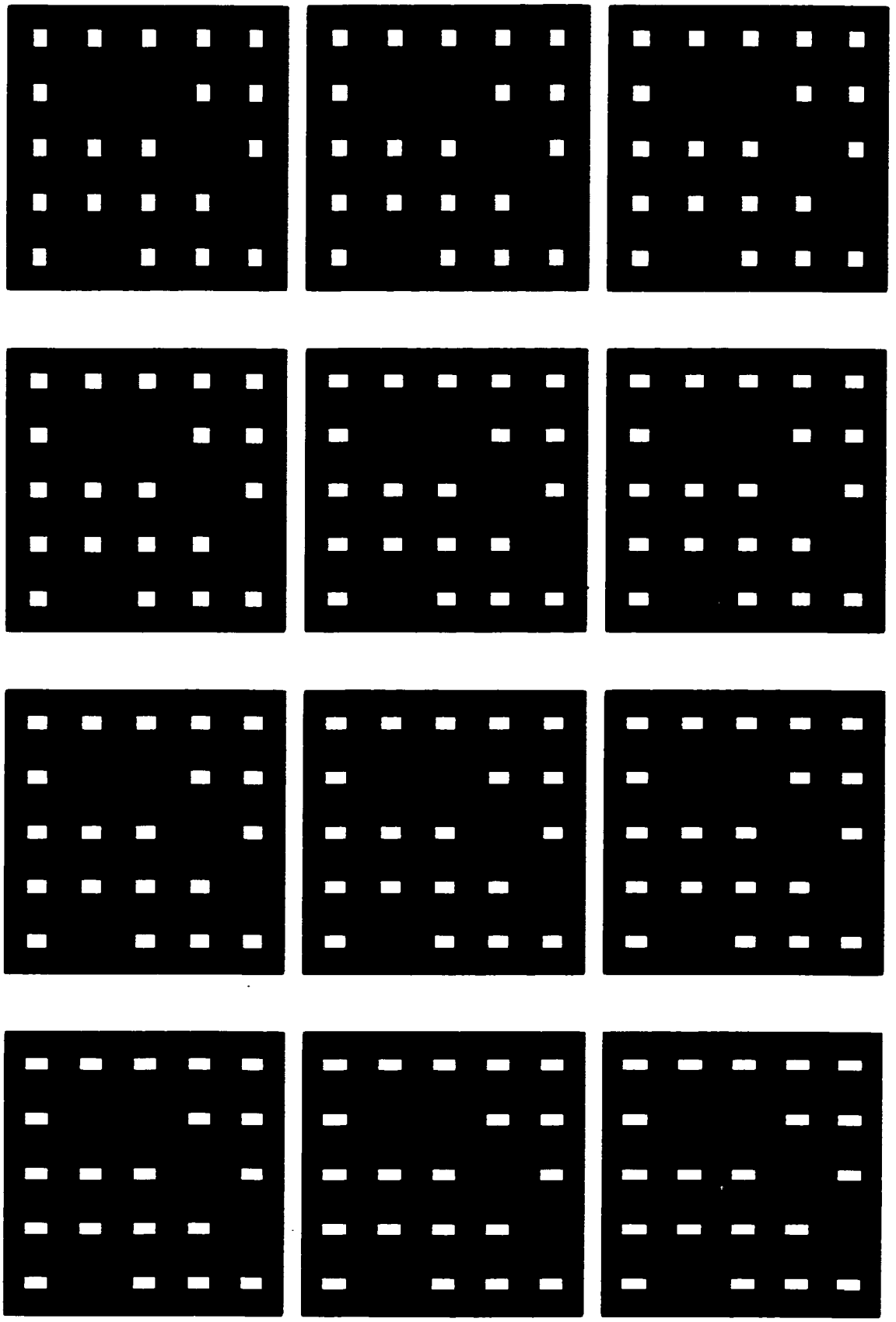

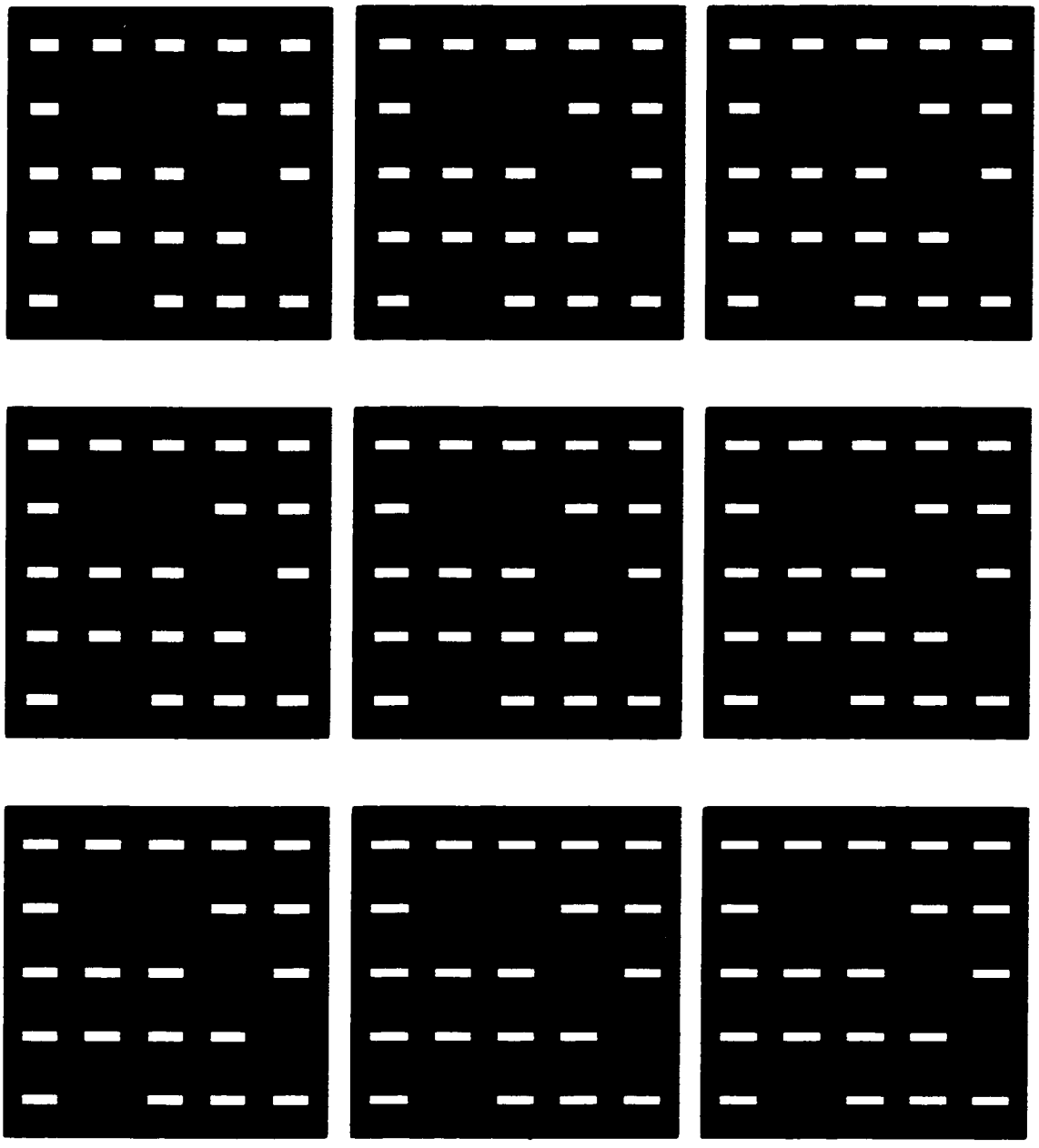

Figure 4.20: The cases of the second numerical experiment on void shape

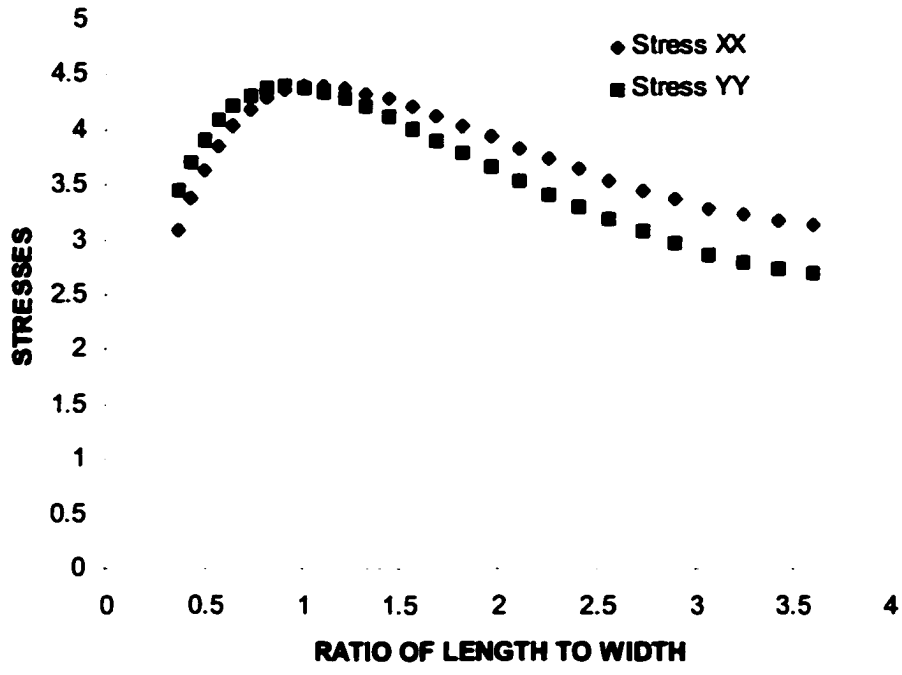

Figure 4.21: The results of the second experiment on void shape

4.2.7 Experiments on Void Pattern

The purpose of the void test is to figure out if void pattern is one of the main variables which greatly affect global behaviors of assemblies. There are two experiments presented in this division. Figure 4.22 shows the first experiment on void pattern and its results. The square disk which has square void on the center is compared with the one which has a diamond void. The two cases represent two different void patterns. The results reveal that void pattern does make the behavior different. It is proved that void pattern is one of the major parameters.

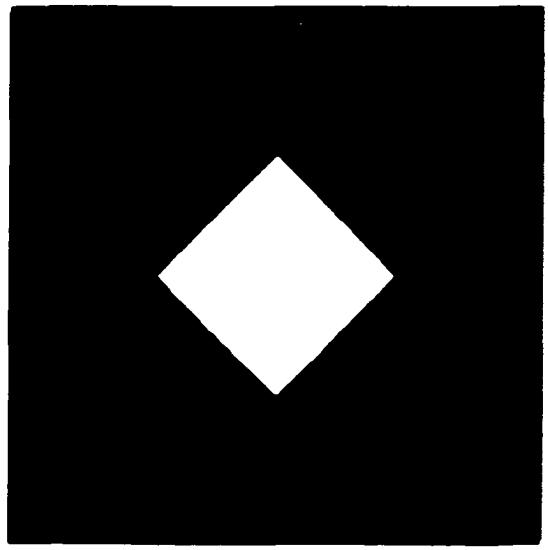

σ_{xx}=3.3164, σ_{yy}=3.3164

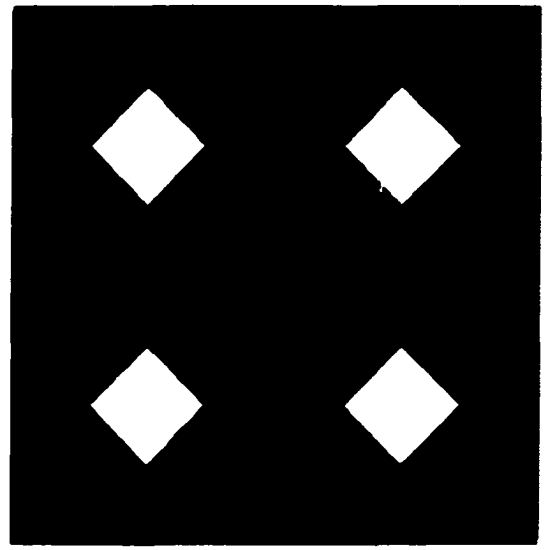

σ_{xx}=3.3153, σ_{yy}=3.3153

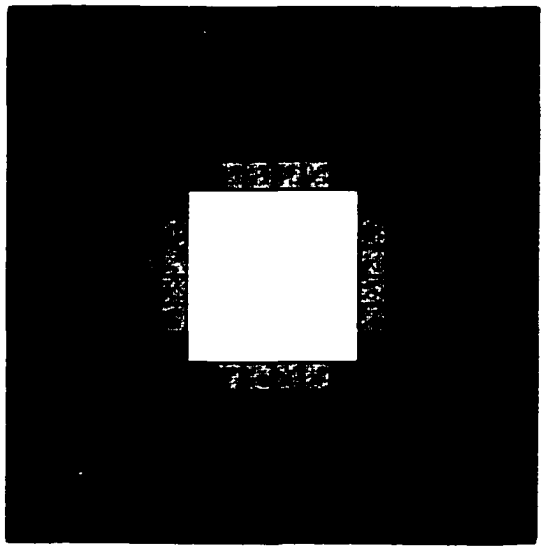

σ_{xx}=2.9523, σ_{yy}=2.9523

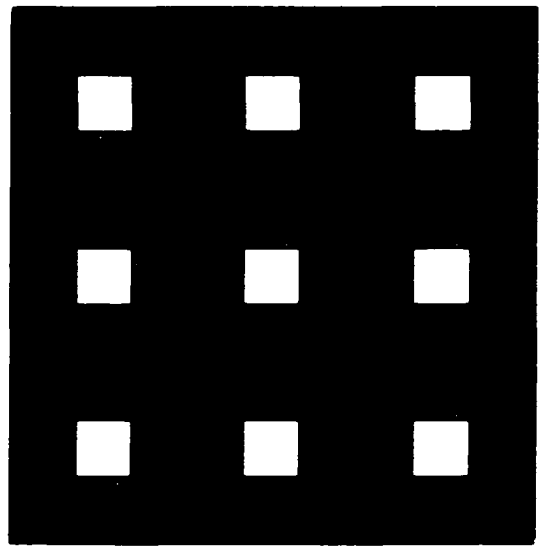

σ_{xx}=2.9487, σ_{yy}=2.9487

Figure 4.22: The first numerical experiment on void pattern and its results

In the second numerical experiment, a granular system with tens of square voids is picked and these voids are rotated to change the pattern(shown in Figure 4.23), and then the stress components are calculated. Figure 4.24 demonstrates that the results are

significantly different. It is verified that void pattern is one of the major variables affecting macroscopic behaviors.

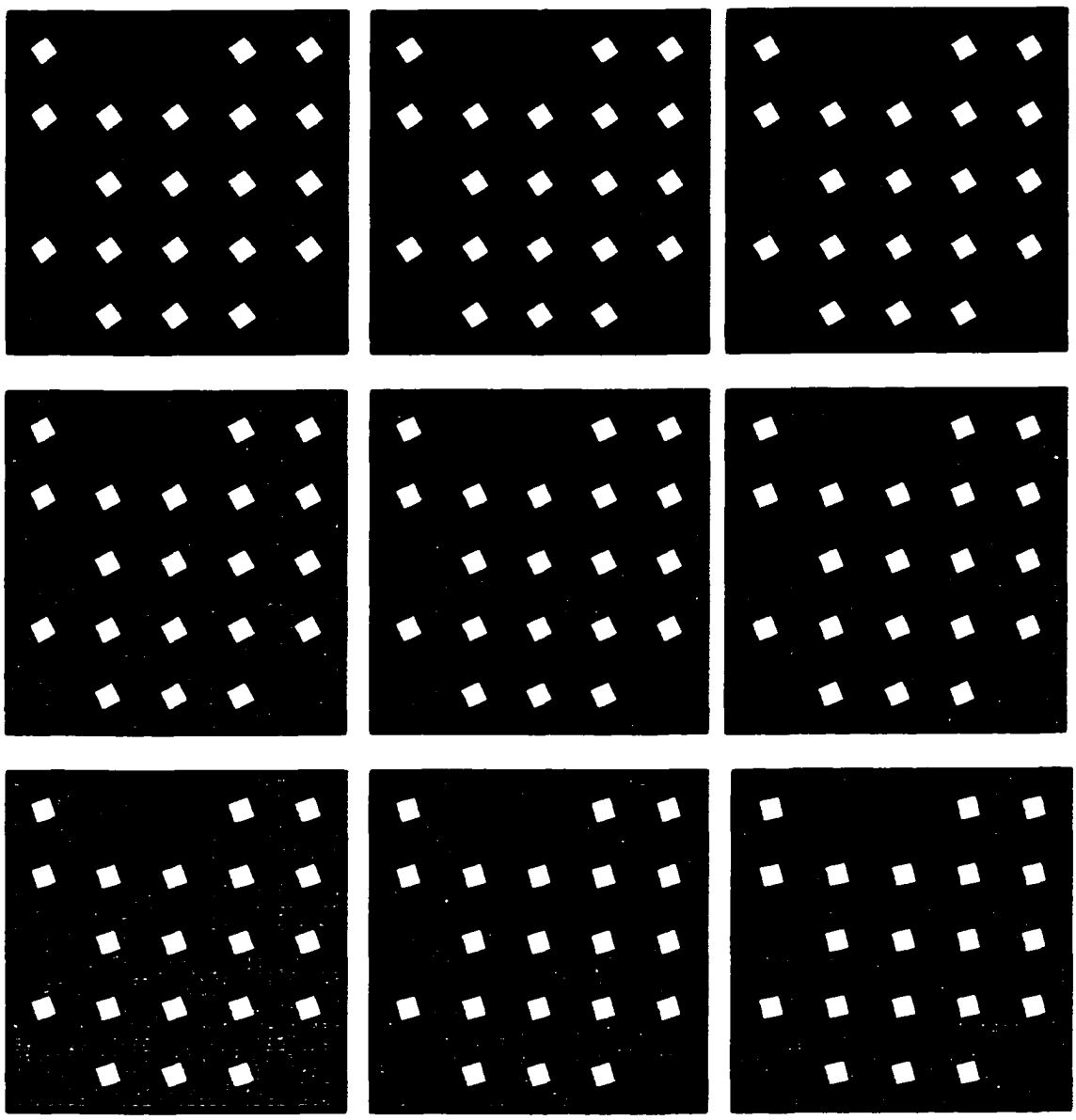

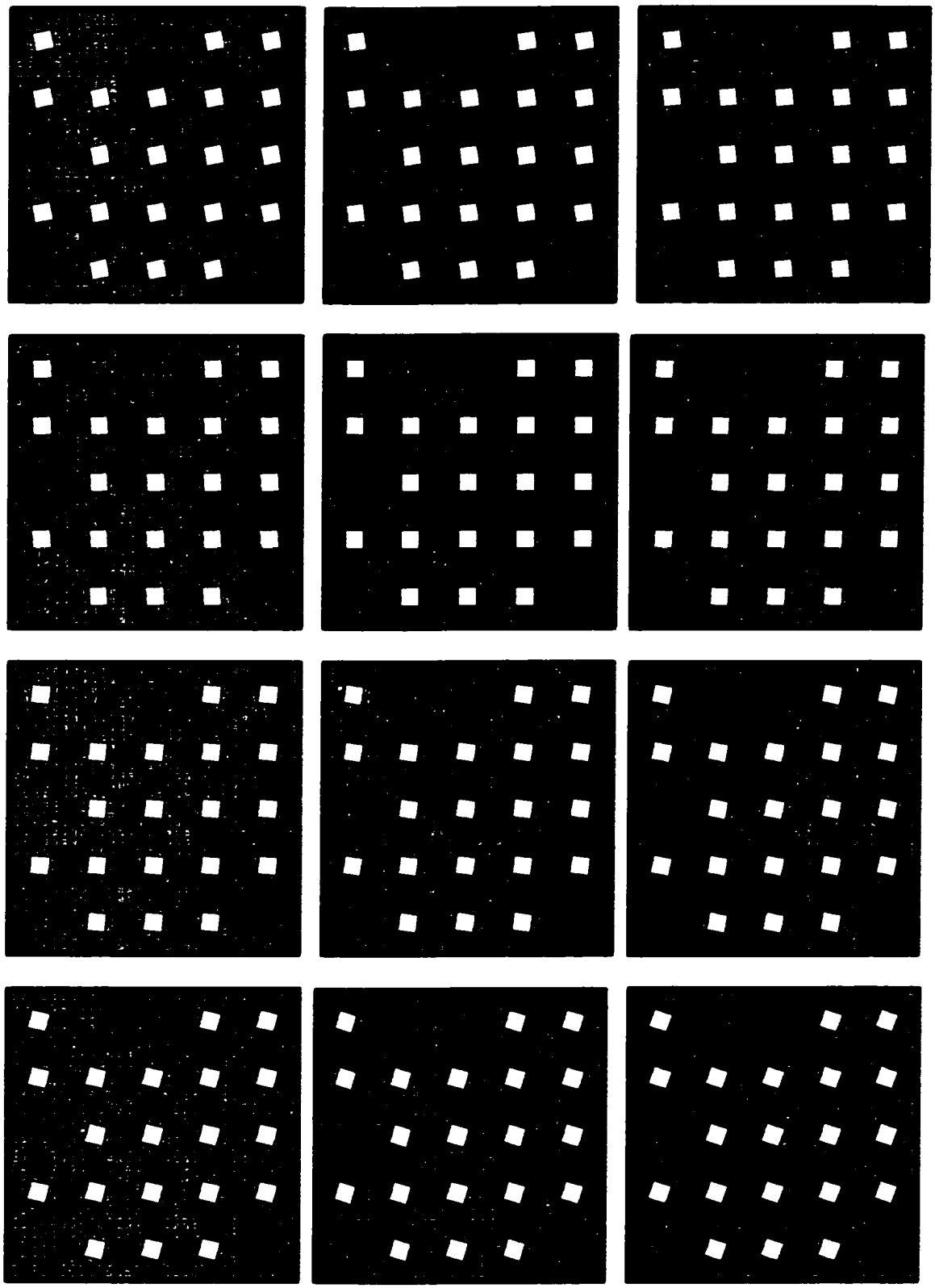

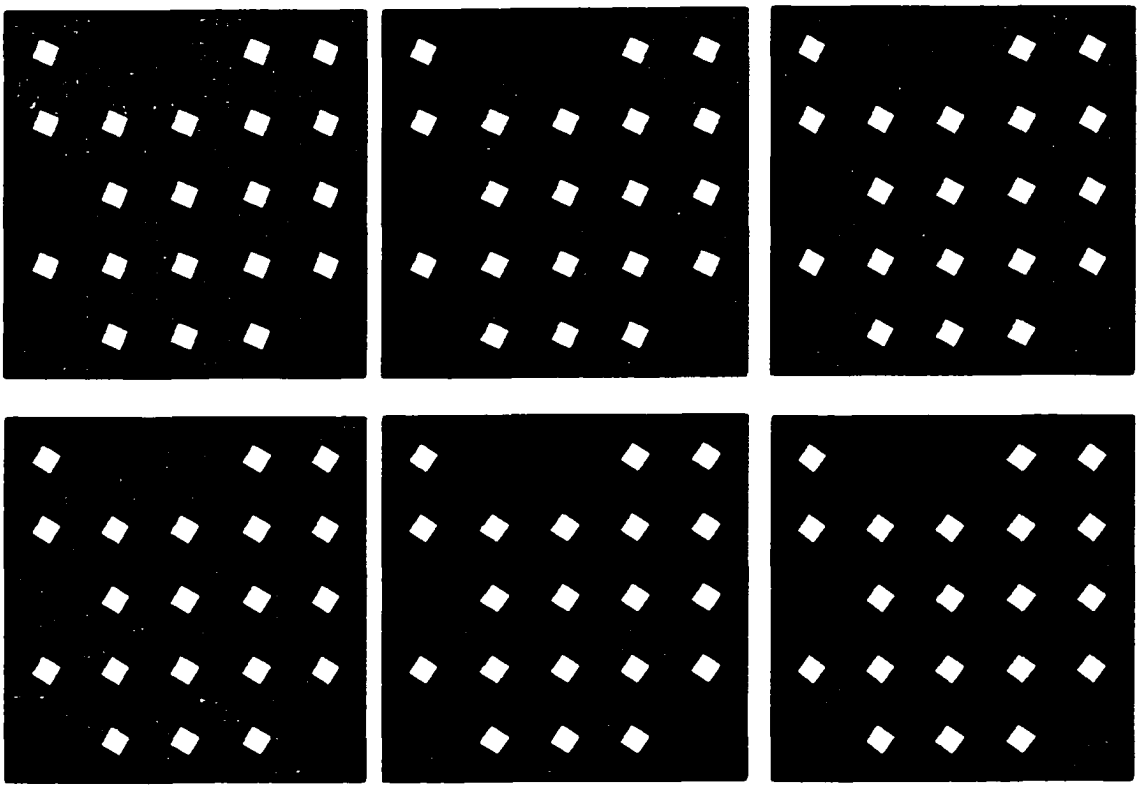

Figure 4.23: The cases of the second numerical experiment on void pattern

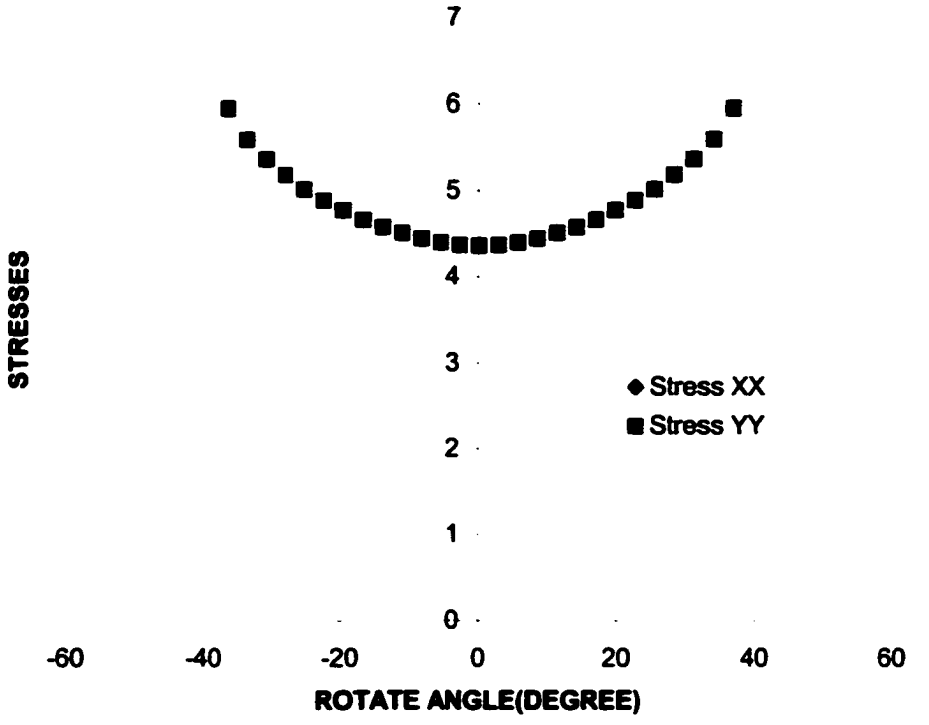

Figure 4.24: The results of the second experiment on void pattern

4.2.8 Experiments on Fixed Void Shape, Nearness of Voids, And Void Pattern

The aspiration of the experiment is to confirm that, in addition to void ratio, void shape, nearness of voids and void pattern are three main factors which create noticeable variation of stress components among tens of randomly distributed granular systems. In the numerical test, void ratio, void shape, nearness of voids, and void pattern are fixed to be constant, while the other factors, such as void position, local density, are let to be random, and stress components are computed.

Figure 4.25 demonstrates that when void ratio is fixed as 0.9111, void shape is square, voids are kept some appropriate distance away from one another, and void orientation is not changeable, the solutions of all cases are very close. The dash line

indicates the range of difference if we do not control void shape, distance between voids, and pattern. In Figure 4.26, the results of the pure shear test for the same group of systems are presented. The results have great closeness. Finally, it is confirmed that void shape, nearness of voids, and void pattern are three major factors to which the granular systems are very sensitive.

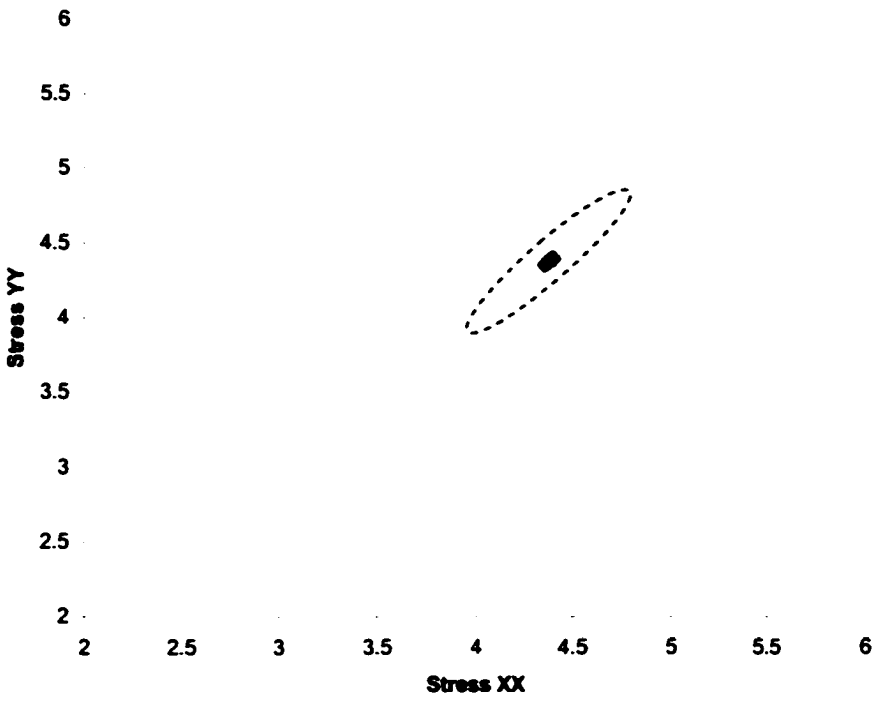

Figure 4.25: The results show the convergence of solutions while void ratio, void shape, nearness of voids, and void pattern are fixed

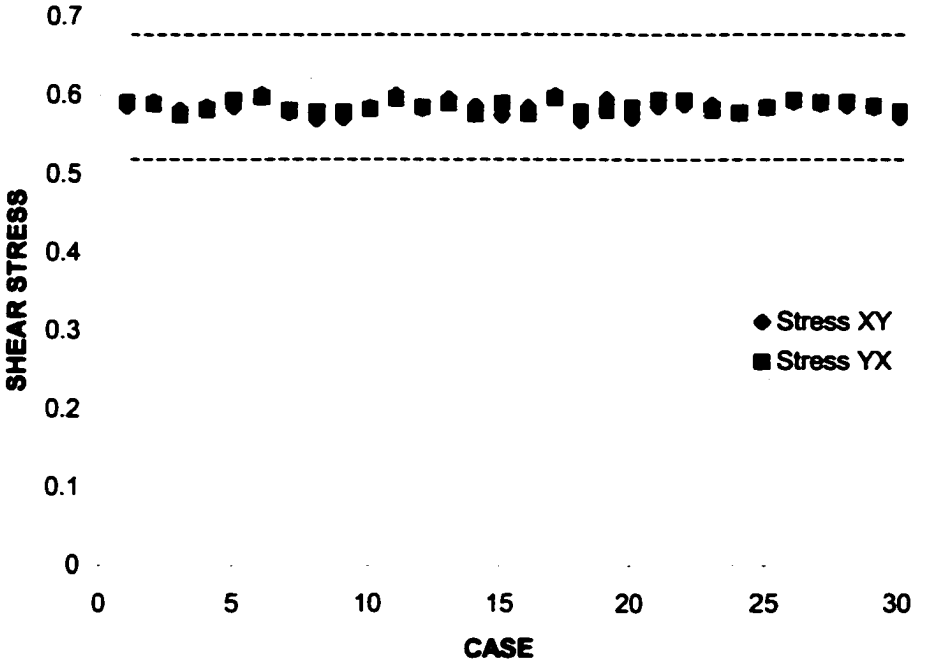

Figure 4.26: The results of pure shear test for these cases of fixed void ratio, void shape, nearness of voids, and void pattern

CHAPTER 5

ALGORITHMS

The main algorithm of the finite element penalty iterative procedures has been introduced in this chapter. The mesh update algorithm has been developed. The triangular mesh system has been developed and presented. The algorithms about contact detection, mesh generation, concave element modification, and locking prevention have been introduced in details.

5.1 MAIN ALGORITHM

The behavior of the incompressible flow in the granular system is studied following these procedures. After the components of the velocity are computed, all positions of nodes are updated by substituting a time step in and calculating displacements. Having got new positions of nodes, we check if any contact among elements is occurring. If so, an automatic mesh update is installed. The re-meshing processes includes overlapping detection and mesh generation. Details of the mesh update algorithms are discussed in the next section. Based on the new mesh, the components of velocity is computed using the finite element iterative penalty method. Figure 5.1 shows the flowchart of iterative method for the current research.

Two critical issues for the algorithm are how to save the computer cost and how to get most accurate solutions. Usually, these two issues are not compatible. In other

words, when we reduce the expense of computer, we lose the accuracy. However, to develop the current method to the cases with thousands of elements and three-dimensional cases in the future, it is necessary to find balance between two controversial issues.

5.2 MESH UPDATE ALGORITHMS

The mesh update algorithm includes four procedures: contact prediction and classification, mesh generation, locking prevention and concave modification. How to reduce computer cost and maintain the accuracy is the most important issue in the mesh update algorithm. There are three contact types considered in the study (Figure 5.2). The first type is the edge of one element hit the side of the other element. The second one is two sides of two different elements contact each other, and the lengths of these two sides are different. In the third case, two sides with same length hit each other.

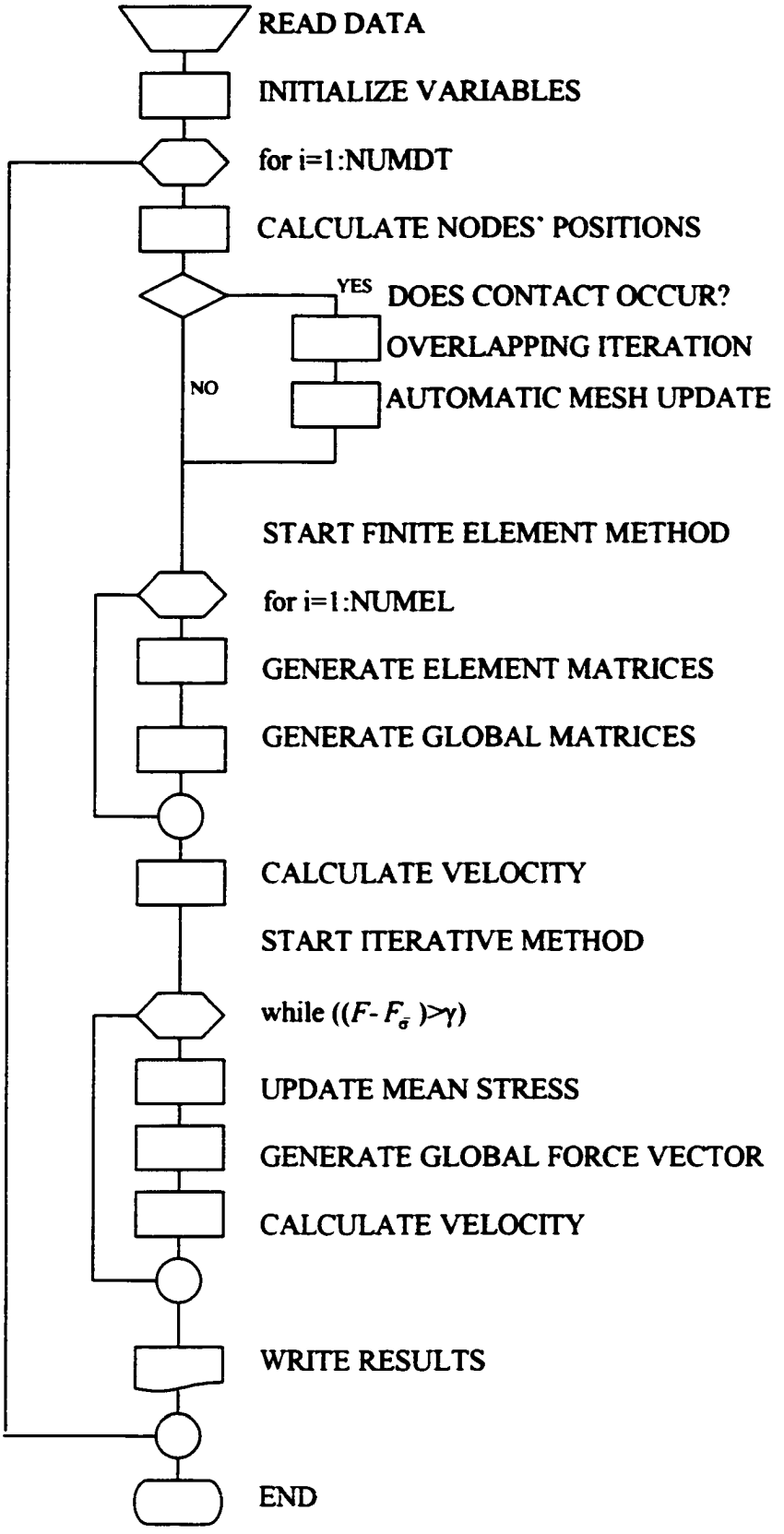

Figure 5.1: The flowchart of the finite element iterative penalty method

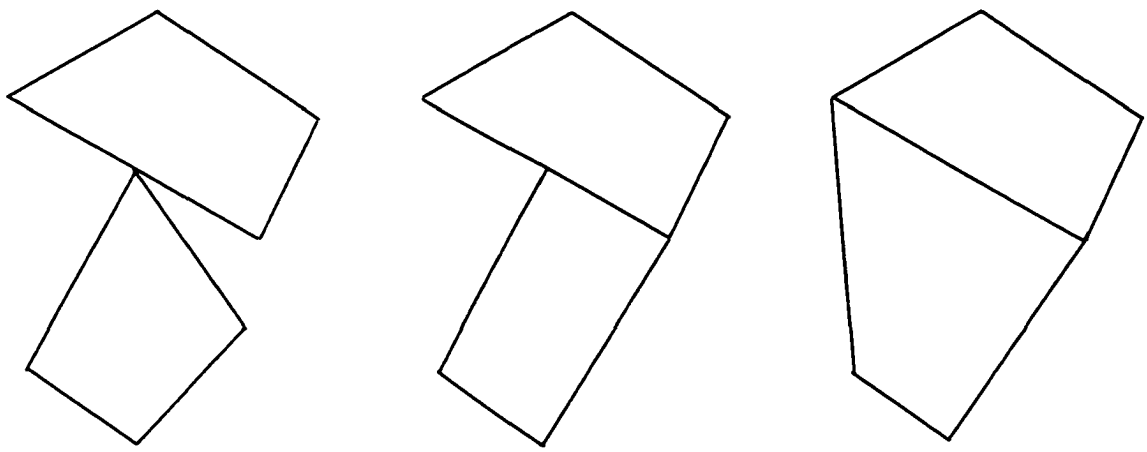

Figure 5.2: Three basic contact situations between two four-node elements

5.2.1 Contact Detection Algorithm

The contact detection algorithm is used to detect when and where contacts occur. At first, the triangular element mesh was generated on both void and solid area shown on Figure 5.3. Any negative or zero area of these triangular elements indicates contacts occur somewhere. For example, on Figure 5.4(1), if the node A hits line BC, the area of triangular ABC will be zero or negative. We calculate the area of every triangular element to detect contacts in each time increment. When any negative area was found, the following bisection iterative algorithm is to determine when exactly contacts occur. For instance, on Figure 5.4(1), if node A goes to A' in one time increment and we notice the negative area of triangular ABC, we divide the time increment by two. In the new

time increment node A goes to A", then we divide the time increment between A' and A" by two. Keep doing the bisection iterative procedure until the area of triangular ABC is close to zero. Then we can observe when and where two particles hit each other.

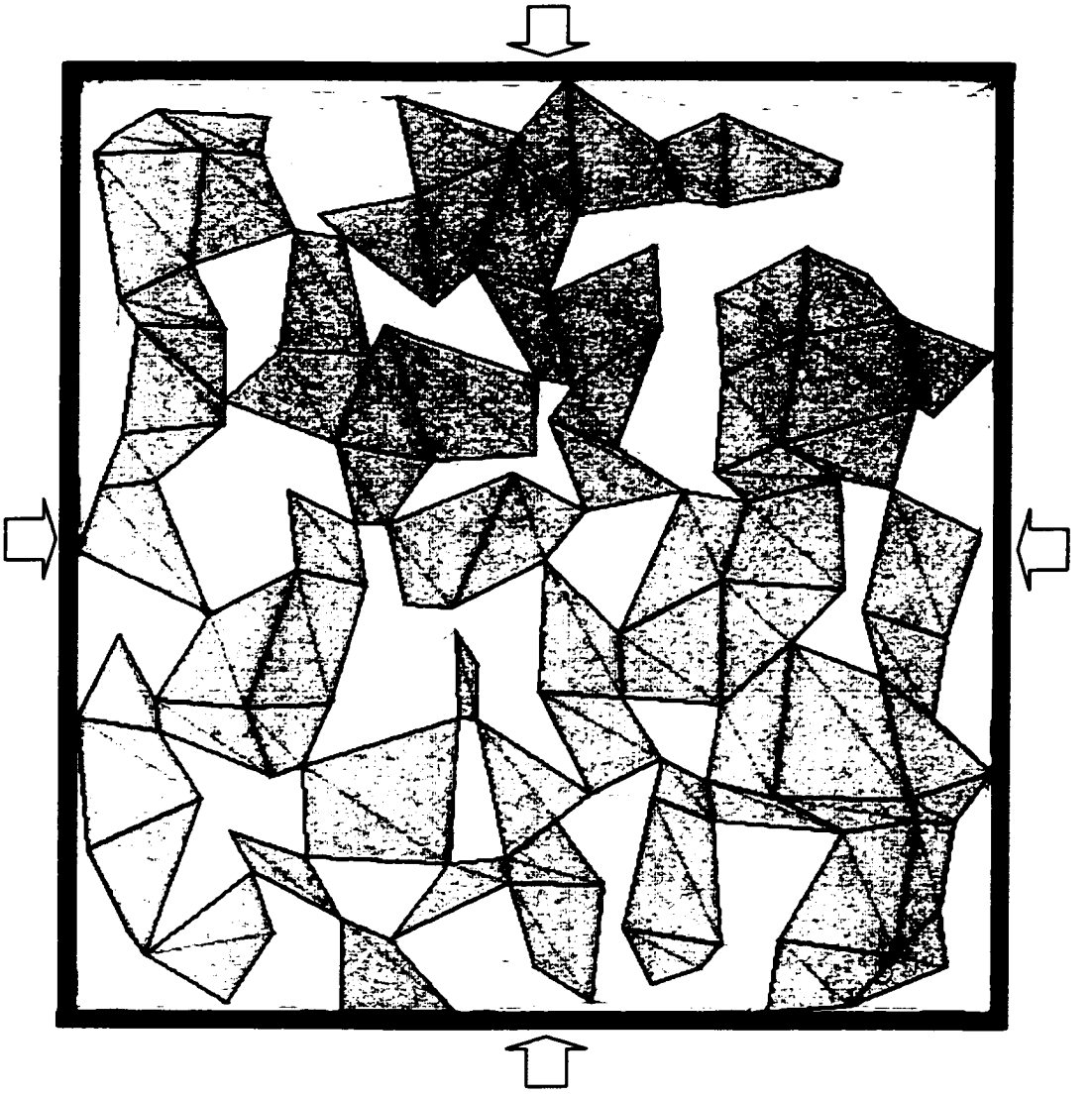

Figure 5.3: An aggregate of non-spherical particles, with the light regions representing air and dark regions the solid. Both void and solid areas are meshed using triangular elements.

(1)

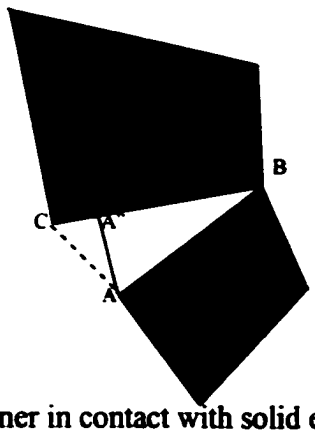

Corner in contact with solid element edge.

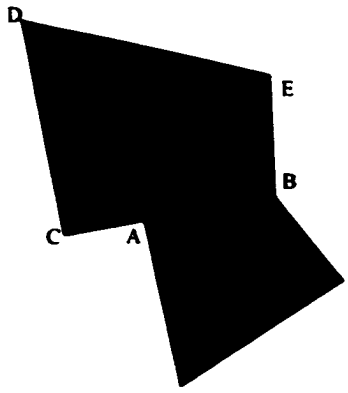

Formulation of new solid elements.

(2)

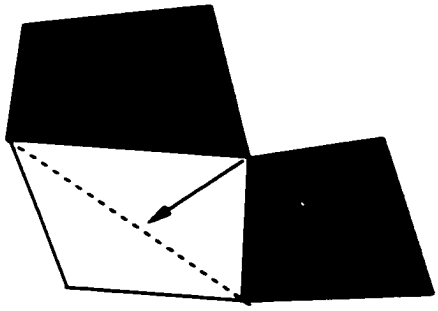

Corner in new contact with void element.

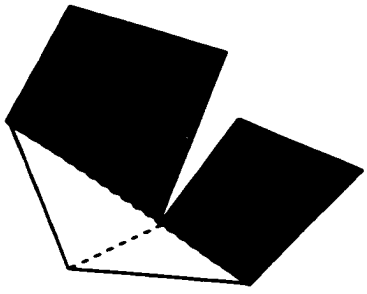

Formulation of new void elements.

(3)

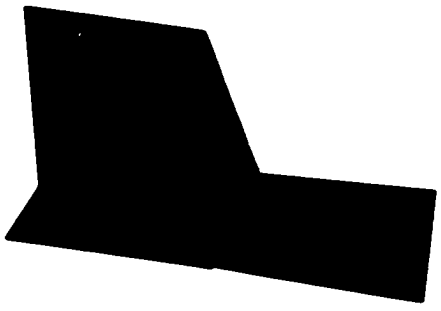

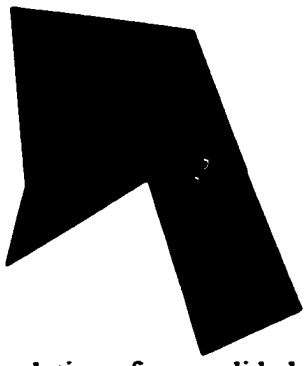

Solid element corner in contact with element edge. Formulation of new solid elements.

Figure 5.4: Three basic types of contacts and their mesh generation.

The other method used to distinguish which type of contact happens is to store the nodes around each void individually. In each time step, the dot and cross products of two possible contact vectors are calculated to check if any contact is occurring or not. If there is any contact appearing, then the bisection iterative method is utilized to compute exactly when the two elements are hitting each other. Sometimes there is no contact in a time step, but sometimes there might be a couple of hits occurring. For that situation, we divide the time step into several parts and install finite element method to calculate velocity step by step.

5.2.2 Mesh Generation Algorithm

To reduce computer cost and to maintain the accuracy are two critical issues in the mesh update algorithm. Figure 5.5 shows that one more node is created on the boundary when each contact occurs. With these boundary nodes, we need to generate mesh for the whole system more efficiently. Usually, constant searching in the algorithm dramatically increases computer cost and waste a lot of time, because whenever one more do loop is added, the cost is increased by power. (e.g. For a n-step loop, when we add one loop, the cost is n^2. When we add the other, the cost is n^3...etc.) The less number of elements has been affected, the less searching steps are used. The method introduced above will interfere too many elements. The best concept to update mesh is to limit the processes in only one element whenever contact is occurring.

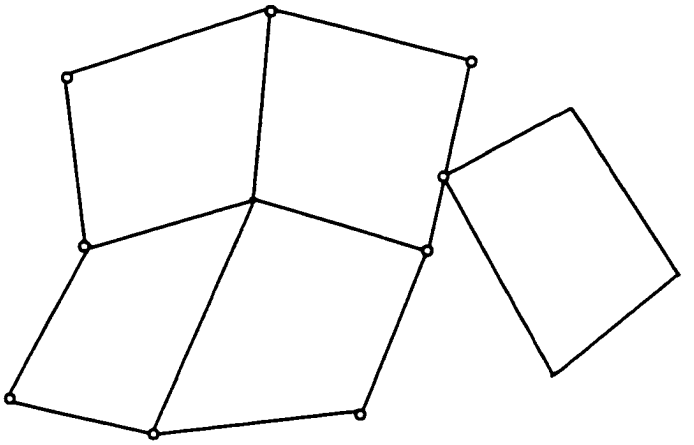

Figure 5.5: The system needs to be re-meshed using these new boundary nodes.

The mesh generation algorithm is to update mesh system after contacts occur. One of the good characteristics of triangular-element system is that it is very easy to be updated and reorganized. No matter what style of contacts occur, we only need to modify one node , add a new triangular element and remove the original element. For example, on Figure 5.4(1), when node A hits line BC, we add a new three-node element ADC, remove the original element ABC and modify the quadrilateral element from BEDC to ABED. Figure 5.4 shows three different types of contacts. The first type is contact between two solid elements. When the contact appears, the original triangular element void vanishes and a new solid element is created. The second type of contact exists among the void elements. When this occurs, two new elements are created. The third type of contact occurs among solid elements. After it occurs, the original quadrilateral element turn out to be a triangular element, and a new three-node element is generated.

The other analytic method is to create an element which is made of two four–node elements and one three-node element. The mesh type is utilized when one side of

the element hit by other ones. One of the advantages for the mesh generation method is we can update the mesh of the whole system without interfering other elements around the contact corner. The other pro is when some other contact happens to the other side of the original element, it is easy to generate some simple mesh types. Figure 5.7 shows the mesh generation for the situations in which the top, right and left sides are hit by other particles.

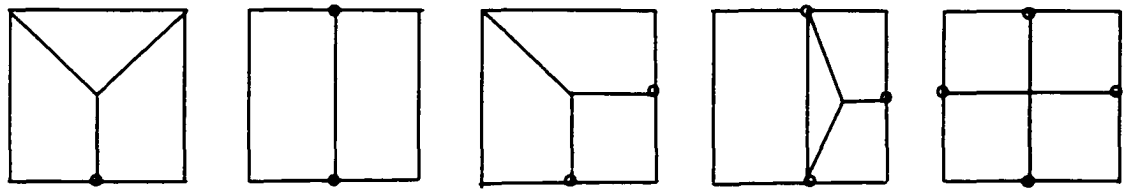

Figure 5.6: The analytic mesh generation of new mesh type when the element is hit (1) on the bottom side. (2) on the top and bottom sides. (3) on the bottom and right sides. (4) on the top, bottom and right sides. (5) on the four sides.

5.2.3 Concave Element Modification Algorithm

Another important issue in this research is to modify the concave element. The so-called concave element is defined as one of the angles of the four-side polygon element is larger than 180 degrees. Figure 5.7 shows what a concave element looks like. For most of static cases, it is difficult to map the element using the shape functions. Also, the Jacobian value is hard to be observed precisely.

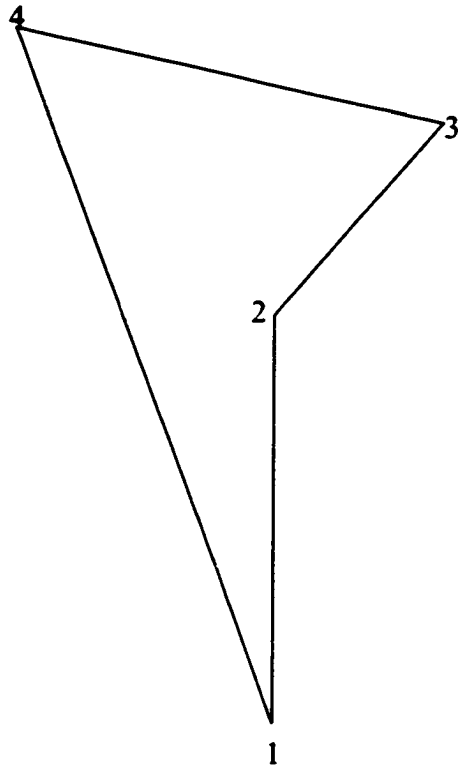

Figure 5.7: A concave four-node element.

The concave element modification algorithm is to modify the four-node concave element to appropriated form for finite element model. Figure 5.8 shows two different style of concave elements. For the first type of elements, the modification is similar to the mesh generation algorithm. We detect the contact, add a new element and remove the original element. For the second type of concave elements, we calculate cross product for four angles. If any of angle is larger than 180 degrees, the original four-node element ABCD is removed, and two triangular elements ABC and ACD are generated.

(1)

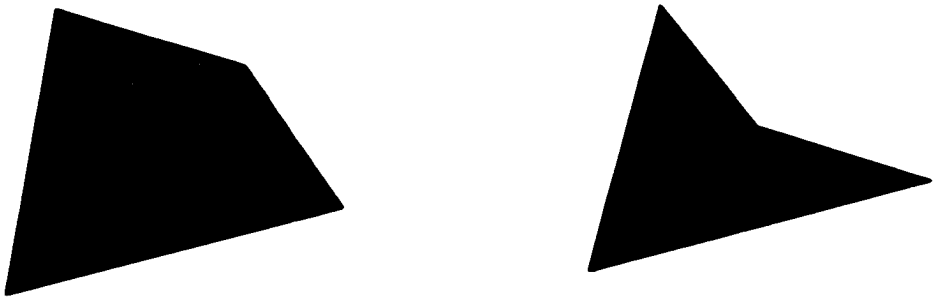

Convex corner of element tends to concave side. Formulation of new solid element.

(2)

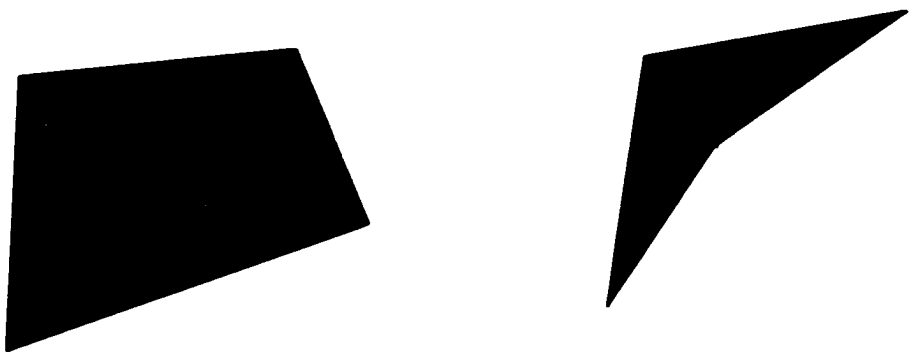

Convex corner of element tends to concave side. Formulation of new solid element.

Figure 5.8: Two types of concave elements.

5.2.4 Locking Prevention Algorithm

The use of the three-node element in the new element type is problematic because it might create locking problems. But, locking results from many triangle elements together adhere to the boundary. Figure 5.9 shows that one system is locked in which there are a bunch of triangular elements, and the other which has only a few three-node elements does not have any problem. According to our analysis, there is no possibility that a bunch of three-node elements collected near the boundary in our cases, so locking problem will not appear.

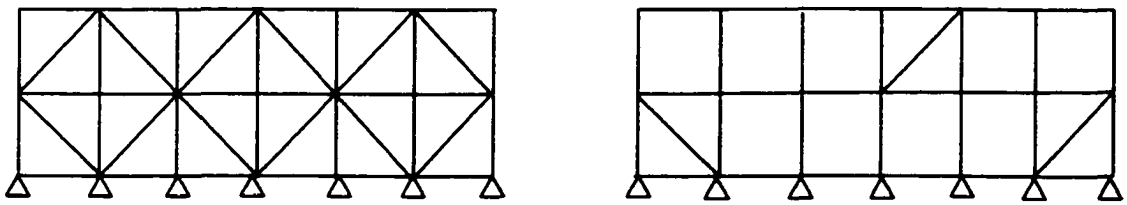

Figure 5.9: The system with more triangle elements is locked, but the system with few triangle elements is not.

The locking prevention algorithm is to control the number of adjacent solid triangular elements to the minimum. The algorithm is when the solid triangular element is generated, we search for the other adjacent solid three-node element, and combine them to a new four-node element. For example, on Figure 5.10(1), if we find triangular ABC and CBF connect to each other, we can create a four-node element ABFC. However, Figure 5.10(2) shows a special case in which three adjacent ABC DBA DEB can not combine together, because any of combinations is a concave type of element. For this special case, the algorithm needs to create two quadrilateral elements AFBC FDEB and a new triangular element ADF.

(1)

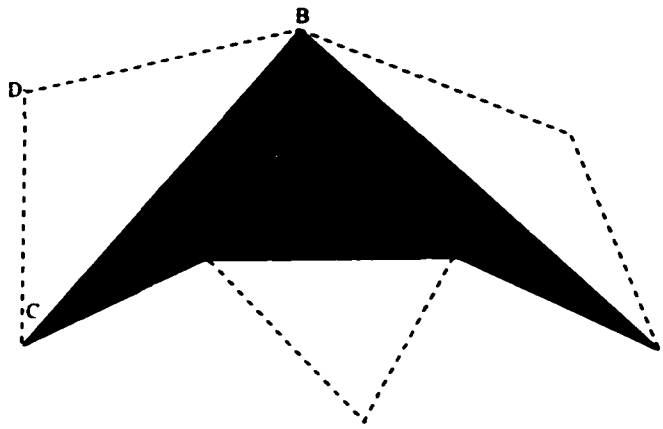

Formulation of three new elements.

(2)

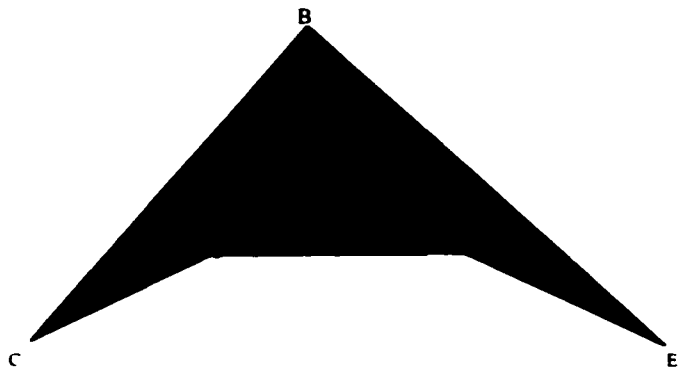

Formulation of two quadrilateral elements and one triangular element.

Figure 5.10: Modification of three adjacent triangular elements.

An analytic algorithm is developed to compare with the current mesh update algorithm. When two elements come in contact, the analytic algorithm generates a new type of element using a combination of two four-node elements and one three-node element. For example, on Figure 5.11, when node A hits line BC, elements AFDB ACEF

and FED are generated. However, this algorithm lacks of the function of contact detection, so we only use it as a case of comparison.

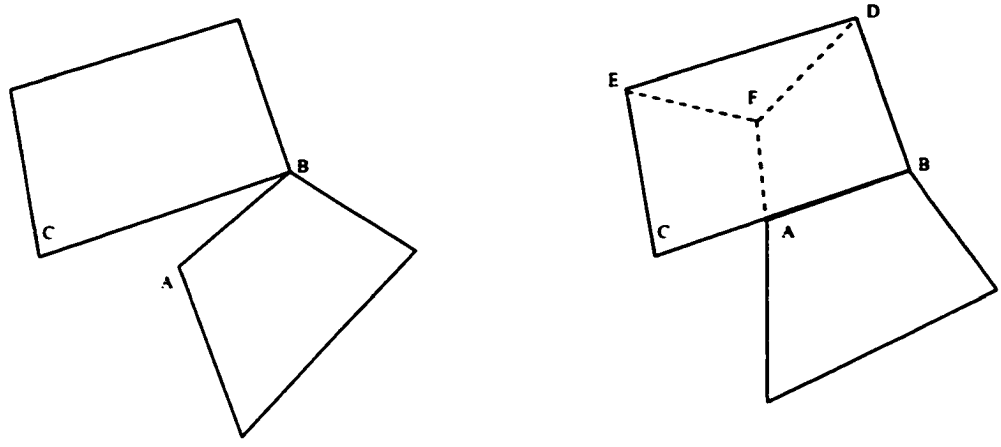

Figure 5.11: The analytic mesh generation algorithm

For multiple material cases, the modification of two adjacent triangular elements is different. Figure 5.12 shows that when triangular 132 and triangular 234 conect to each other, a new node 5 is created and the triangular 132 is modified to be rectangular 1352, and the triangular 234 is modified to be rectangular 2534. The method is used to adjust two adjacent three-node elements with different materials.

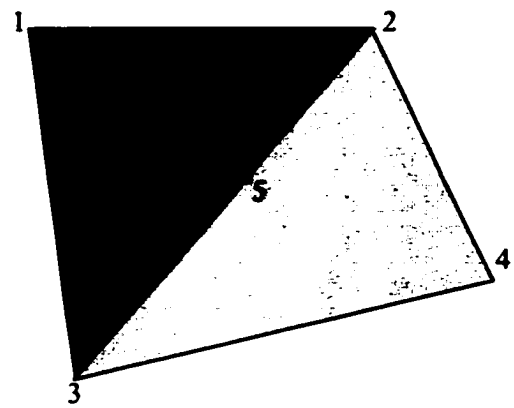

Figure 5.12: Modification of two adjacent triangular elements with different materials.

CHAPTER 6

COMPUTER SIMULATION

In this chapter, the numerical model and the new mesh method are verified by comparing results with some theoretical solutions and examining the area change. The penalty method and the mesh generation algorithm are used to make a numerical experiment for both single-material and multiple-material aggregate. A series of computer simulations of the isostatic and close die compaction for several systems of different size are observed. The objective is to take the original porosity from initial porosity turn to no porosity. Simulations of the whole process of compaction have demonstrated efficiency and accuracy of the mesh generation algorithm.

6.1 VERIFICATION

There are two divisions in this section. In the first division, the solutions from the finite element model have been compared with an analytic solution to verify its accuracy. They have been found in good agreement. In the second division, the area errors for several computer simulations of compactions have been computed. The little area deficiencies indicate that the numerical model is of high validity.

6.1.1 Juxtaposition with An Analytic Solution

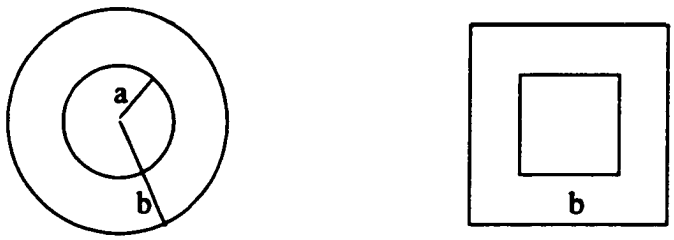

Figure 6.1: The analytic theoretical case and the finite element case.

Figure 6.1 shows the case of an analytic theoretical solution for a circular hollow disk and the one of the finite element model for a rectangular hollow disk. The theoretical solution of 2-dimensional visco-plastic circular disk is derived as following.

$$u = \frac{b}{E}[\frac{1}{2}\frac{b^2}{(a^2-b^2)} + \frac{3}{2}\frac{a^2}{(a^2-b^2)} + \frac{1}{2}]p$$

$$u = \frac{b}{2E}[\frac{-4a^2}{b^2-a^2}]p$$

Substituting $E=4\mu$,

$$u = \frac{pb}{8\mu}[\frac{4a^2}{b^2-a^2}]$$

$$p = 2\mu[\frac{b^2-a^2}{a^2}]\frac{u}{b}$$

According to the analytic formulation, the relation of bulk modulus and density is observed. Comparison of the analytic solution and the finite element solution for

rectangular disk is given in Figure 6.2. The result demonstrates that two methods have highly closeness especially when the density is from 0.5 to 0.9.

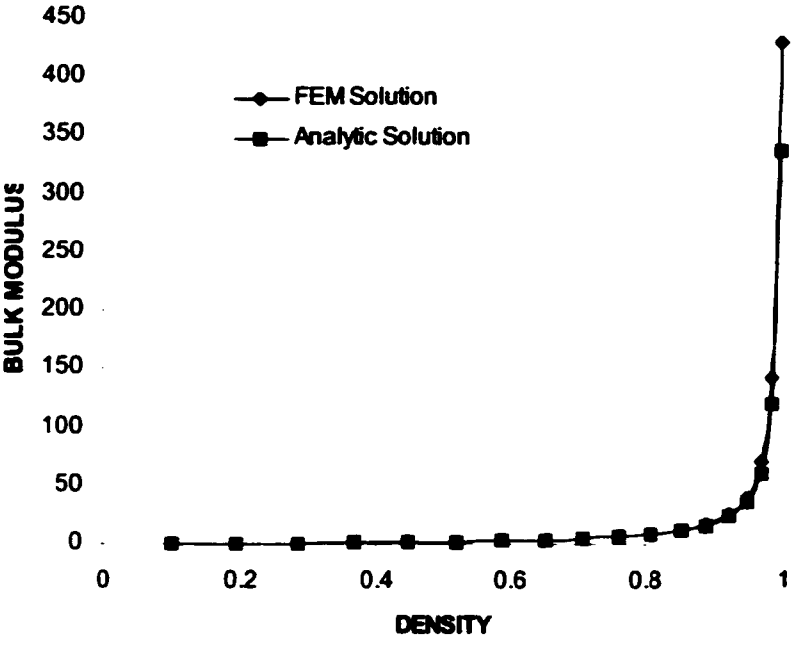

Figure 6.2: Comparison between the finite element solution and the analytic solution.

6.1.2 Area Errors

The total remaining area errors for these six numerical experiments are given in Table 6.1. It indicates that because all area errors are below 0.5%, generally the results of these simulations are highly accurate, and incompressibility can be nearly achieved.

Numerical experiment	Total area error(%)
Isostatic compaction for 10-element system	0.21
Close-die compaction fixed in x direction for 10-element system	0.04
Close-die compaction fixed in y direction for 10-element system	0.14
Isostatic compaction for 75-element system	0.27
Close-die compaction fixed in x direction for 75-element system	0.37
Close-die compaction fixed in x direction for 75-element system	0.23
Isostatic compaction for 296-element system	0.04
Close-die compaction fixed in x direction for 296-element system	0.08
Close-die compaction fixed in y direction for 296-element system	0.02
Isostatic compaction for 1076-element system	0.02
Close-die compaction fixed in x direction for 1076-element system	0.02

Table 6.1: Area errors of six numerical experiments.

6.2 SINGLE MATERIAL AGGREGATE

In this section, various single material aggregates with different numbers of elements, which range from ten to a thousand have been experimented and simulated. For comparison, the other simulation using analytic algorithm is introduced. There are four divisions in this section. In the first division, a computer simulation of two kinds of compactions for a 10-element granular system is presented. In the second division, a series of numerical simulations for a 75-element assembly are introduced. The other numerical simulation for a 296-element aggregate is demonstrated in the third division. Finally, another numerical experiment for a granular system containing 1076 elements is given in the fourth division.

6.2.1 Simulation for A 10-Element Assembly

Figure 6.3 shows the computer simulation of isostatic compaction of the 10-element granular system. Isostatic compaction is defined as compaction in which the four sides of the confining square boundary have the same velocity. The material properties are given as $C_{11}=C_{22}=2.0$, $C_{66}=2.0$. The time increment is taken as 0.05 second, with a total of 26 time steps. Figure 6.4 shows similar simulation using the analytic algorithm. There are several similarities between the two simulations from the different algorithms. For example, in both cases, the first contact happened in the 18^{th} time step, and the processing in both cases is ended in the 26^{th} time step. However, time consumed in running this analytic program is approximately ten times as long as running the previous one. That is one of the reasons that we only use the code as an analytic solution instead of formal results.

Two types of close-die compaction are studied. Close-die compaction is defined as compaction in which two sides of the confining boundary have been fixed and the other two sides have the same inward velocity or displacement. The material moduli are $C_{11}=C_{22}=2.0$, $C_{66}=2.0$. Both cases have a time increment is 0.05 second and a total of 46 time steps. Figure 6.5 shows computer simulation of close-die compaction fixed in the x direction.

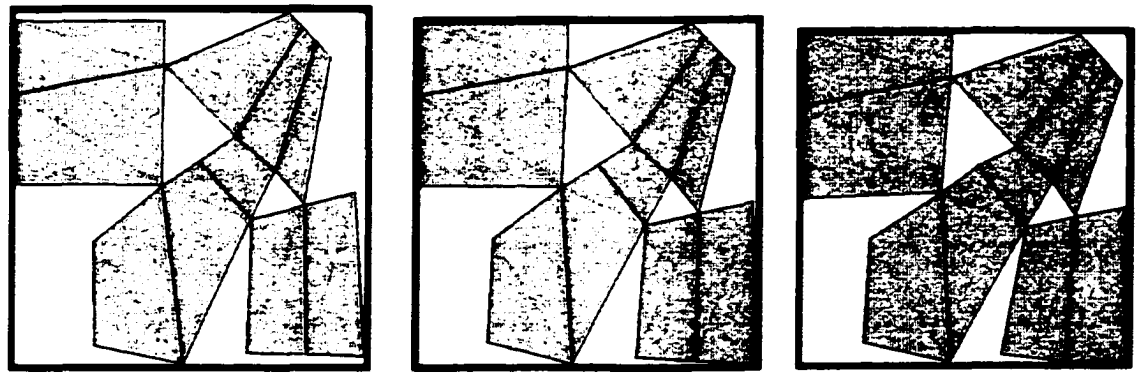

Time Step = 3 Time Step = 6 Time Step = 9

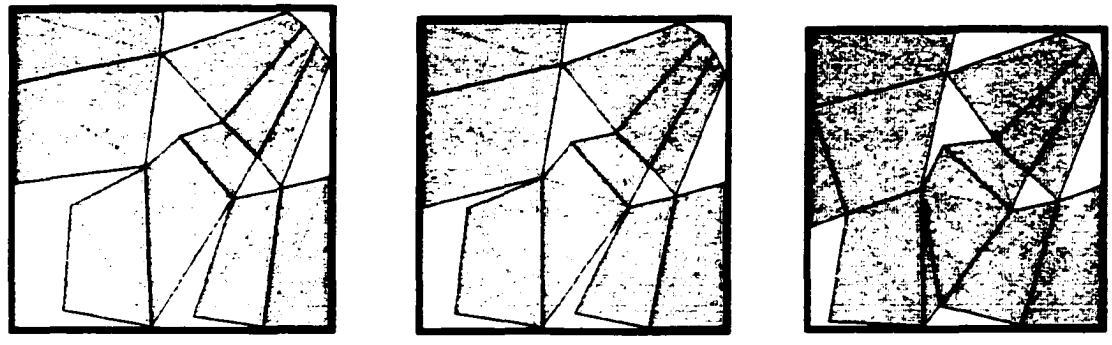

Time Step = 12 Time Step = 15 Time Step = 18

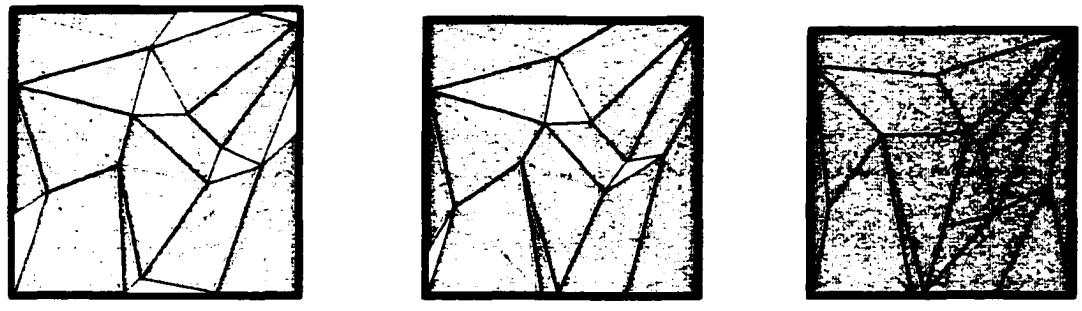

Time Step = 21 Time Step = 24 Time Step = 26

Figure 6.3: Computer simulation of isostatic compaction for the 10-element assembly.

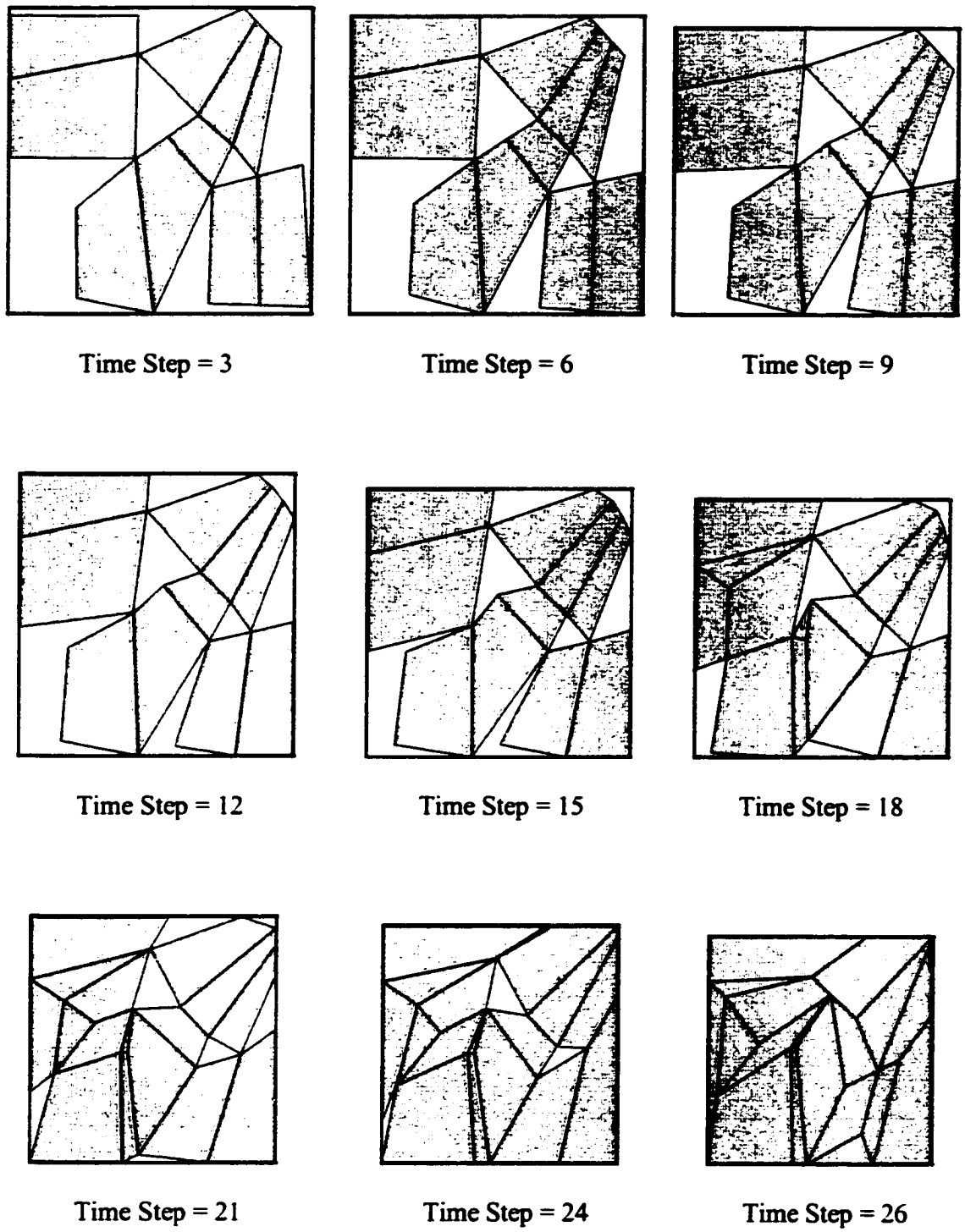

Figure 6.4: Similar simulation of isostatic compaction using the analytic algorithm.

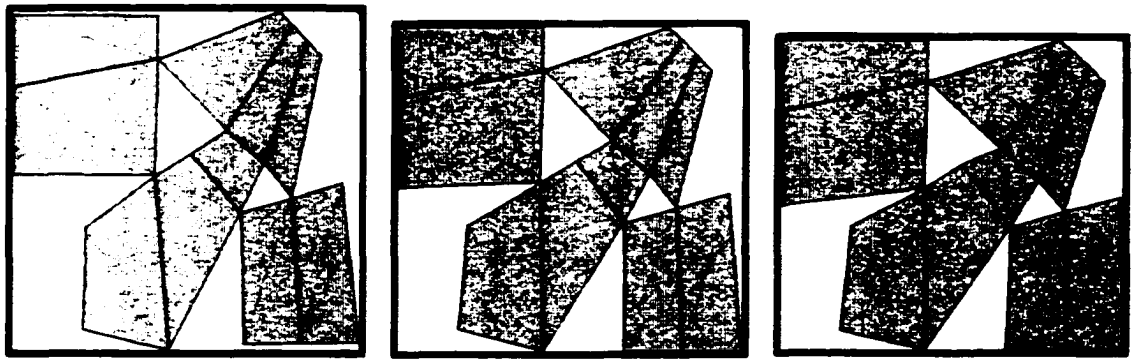

Time Step = 5 Time Step = 10 Time Step = 15

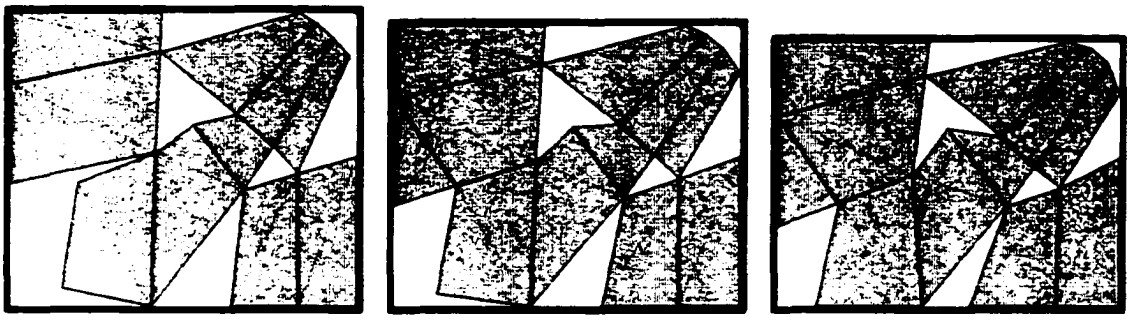

Time Step = 20 Time Step = 25 Time Step = 30

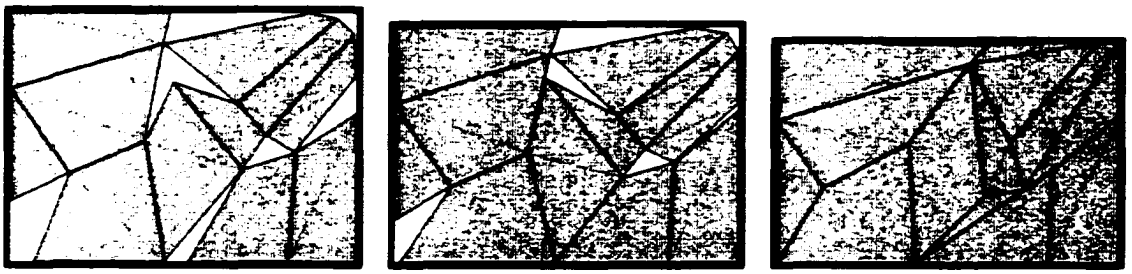

Time Step = 35 Time Step = 40 Time Step = 46

Figure 6.5: Computer simulation of close-die compaction fixed in x direction for the 10-element assembly.

6.2.2 Simulation for A 75-Element Assembly

Two computer simulations are presented in this division. The first one is for isostatic compaction of the 75-element granular system shown in Figure 6.6. The second one is for close-die compaction of the same system given in Figure 6.7. In both cases, the materical properties and time increment are the same as the previous cases. However, time consumed in running this cases is about 10 minutes. It makes a contrast with the previous experiment which only takes a few seconds. There are tens of contacts occurring during the entire process. Approximately 15 solid triangular elements are created in mesh generation. They are surrounded by quadrature elements, so the locking problem is eliminated.

In Figure 6.6, the first contact occurs at the fourth time step. The narrow long particle near the center of the system rotates clockwise around 60 degrees and hits the other particle. At the 12^{th} time step, the first concave quadrature element appears on the right lower corner. The second one and the third one is occurring at the 16^{th} time step. The first case of combination of two triangular elements to quadrature one appears on the right upper corner at the 20^{th} time step. The simulation is ended at the 33^{rd} time step.

The computer simulation of close-die compaction fixed in y direction for the 75-element assembly is given in Figure 6.7. The first contact occurs at the 6^{th} time step. Different from the previous case, the narrow long element near the center of the rectangle system rotates in a counter-clockwise direction and hit the left particle at the 24^{th} time step. The first concave quadrature element on the right lower corner is split into two pieces at the 30^{th} time step. Incompressibility is achieved at the 56^{th} time step. It has 23 more steps than the isostatic compaction.

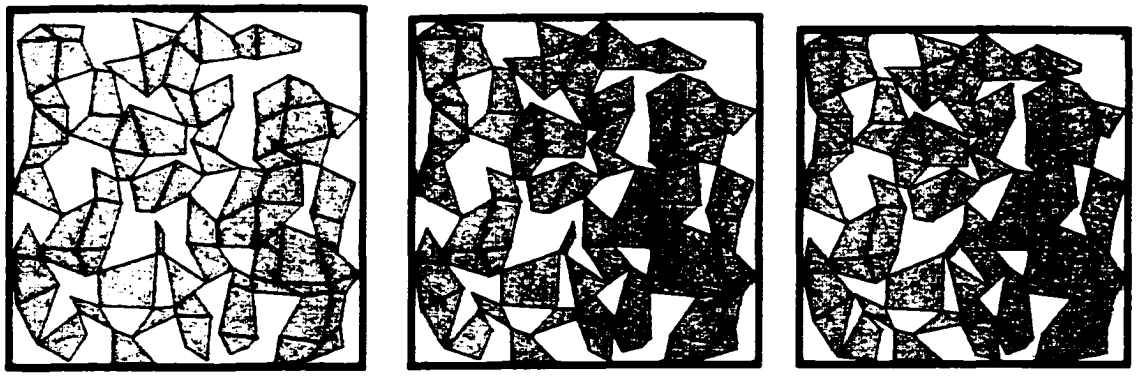

Time Step = 4 Time Step = 8 Time Step = 12

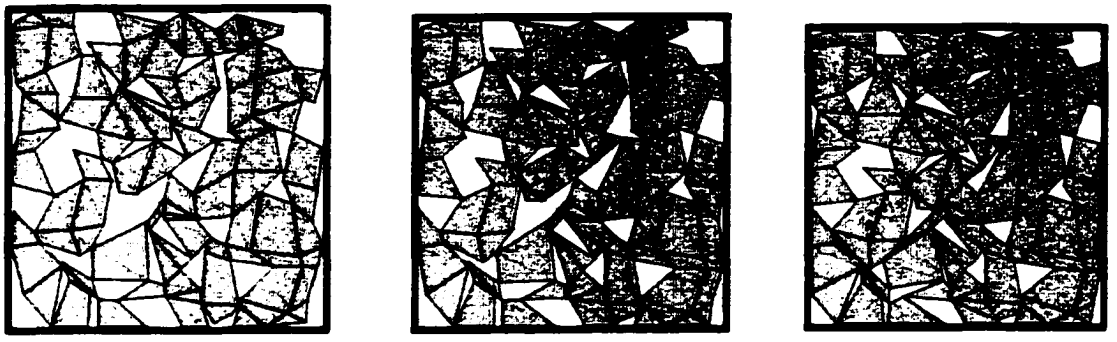

Time Step = 16 Time Step = 20 Time Step = 24

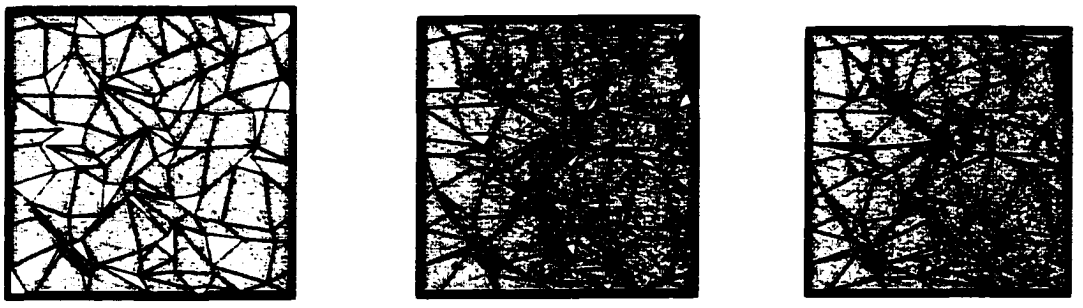

Time Step = 28 Time Step = 32 Time Step = 33

Figure 6.6: Computer simulation of isostatic compaction for the 75-element assembly.

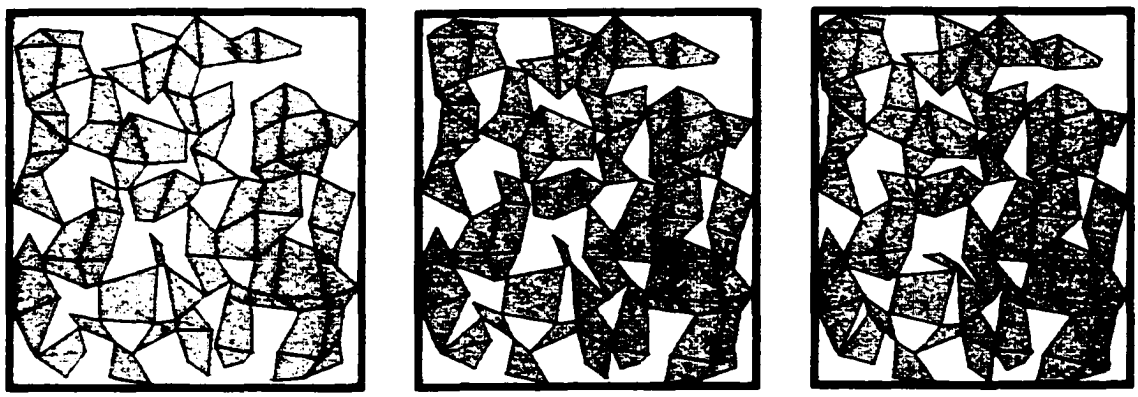

Time Step = 6 Time Step = 12 Time Step = 18

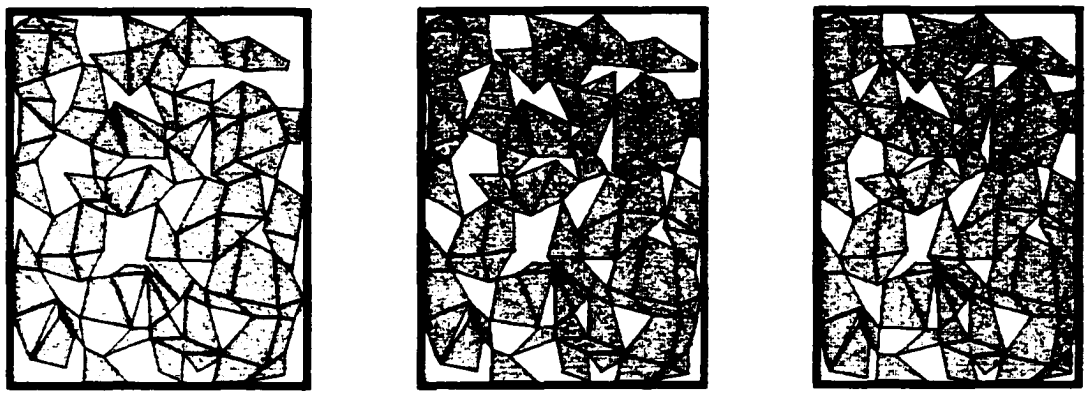

Time Step = 24 Time Step = 30 Time Step = 36

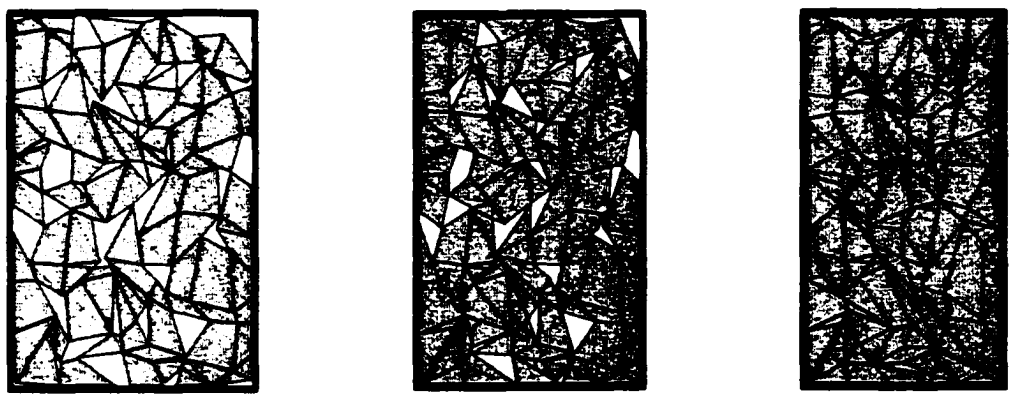

Time Step = 42 Time Step = 48 Time Step = 56

Figure 6.7: Computer simulation of close-die compaction fixed in *y* direction for the 75-element assembly.

6.2.3 Simulation for A 296-Element Assembly

The objective to make a simulation for a 296-element assembly is to test efficiency and precision for the discrete element model and the mesh generation algorithms. There are two experiments in this division. In Figure 6.8, the computer simulation of isostatic compaction for the 296-element assembly is presented. Figure 6.9 shows the compaction simulation of close-die compaction fixed in y direction for the 296-element assembly. The material properties and time increment are the same as the 75-element granular system discussed in the preceding section. It takes a couple of hours to run each test.

In Figure 6.8, there are nine diagrams which represent the granular system in nine different periods of time during compaction. No contact occurs at the first time step. The first contact appears on the right upper corner at the 4^{th} time step. The first concave gradrature element is occurring on the lower boundary at the 7^{th} time step. Some other contacts appear from the 12^{th} time step to the 18^{th} step. The simulation is ended at the 21^{st} step.

In Figure 6.9, similar to the foregoing figure, there are nine diagrams which represent the granular system in nine different periods of time during compaction. Approximately 50 contacts appears in the entire process. None of them occurs at the 4^{th} time step. In contrast with the preceding case, the first contact appears at the 8^{th} time step. The first three adjacent solid triangular elements is occurring at the 16^{th} time step. Incompressibility is achieved at the 38^{th} time step.

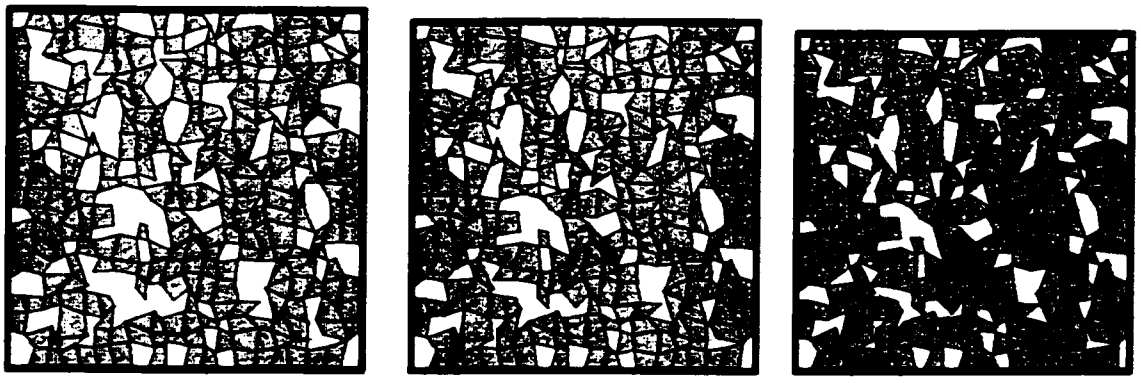

Time Step = 1 Time Step = 4 Time Step = 7

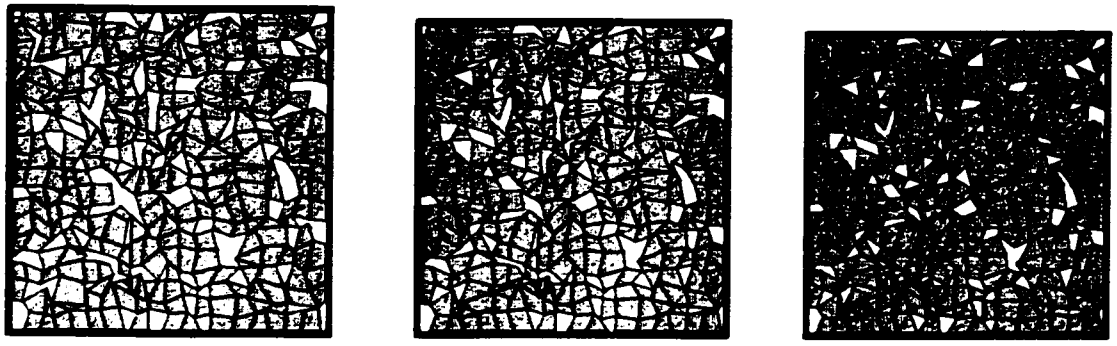

Time Step = 10 Time Step = 12 Time Step = 14

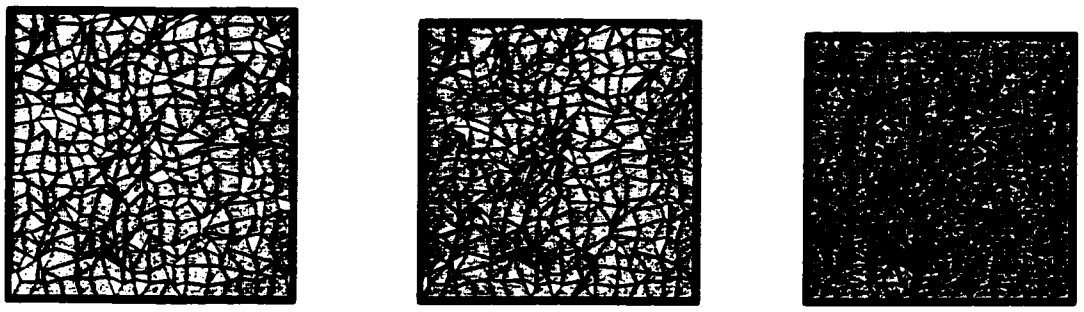

Time Step = 16 Time Step = 18 Time Step = 21

Figure 6.8: Computer simulation of isostatic compaction for the 296-element assembly.

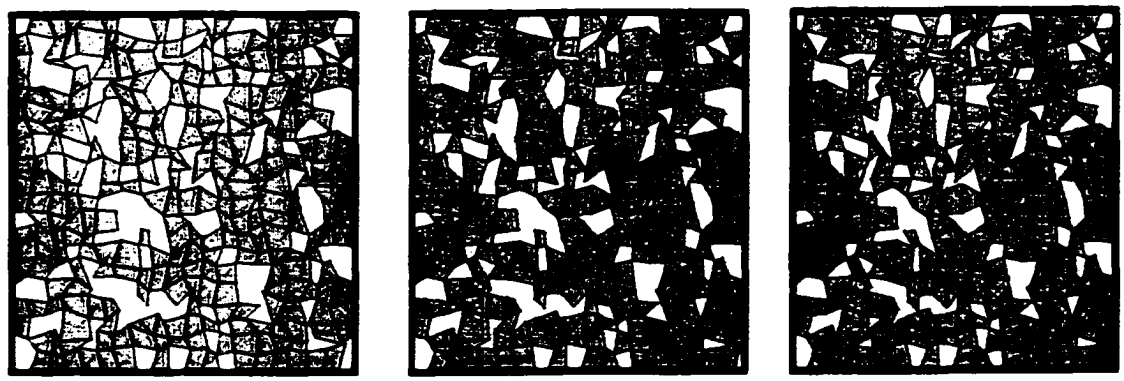

Time Step = 4 Time Step = 8 Time Step = 12

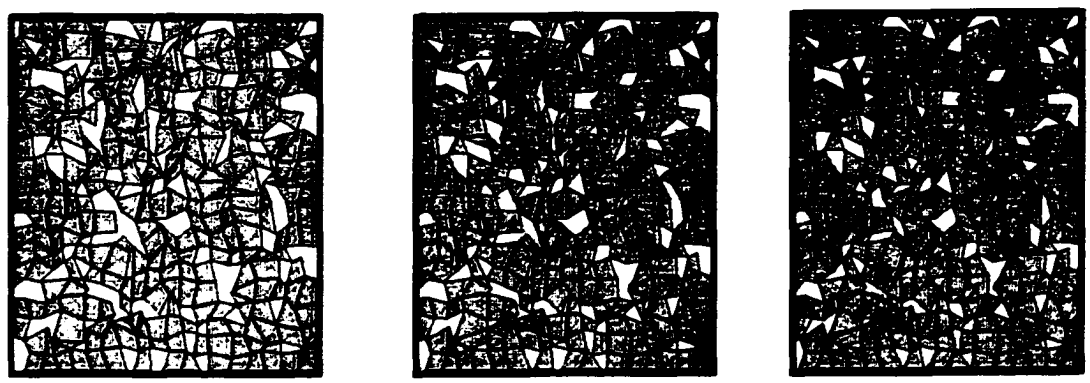

Time Step = 16 Time Step = 20 Time Step = 24

Time Step = 28 Time Step = 32 Time Step = 38

Figure 6.9: Computer simulation of close-die compaction fixed in *y* direction for the 296-element assembly.

6.2.4 Simulation for A 1076-Element Assembly

The purpose to make a simulation for a 1076-element assembly is, first of all, to find the limitation of the discrete element model and the mesh generation algorithms, secondly, to visualize the process of compaction for the granular system. There are two computer simulations in this division. Figure 6.10 shows the computer simulation of isostatic compaction for the 1076-element aggregate. In Figure 6.11, the compaction simulation of close-die compaction fixed in x direction for the same system. The initial void ratio is approximately 30 percent.

In Figure 6.10, there are nine diagrams which represent nine different periods of time of the isostatic compaction for the 1076-element assembly. Approximately 150 contacts appears during the entire process. No contact appears from the first time step to the third time step. Tens of contacts occurring from the 5^{th} time step to the 12^{th} tiem step. At the 15^{th} time step, all particles have been squeezed together. The simulation is finished at the 20^{th} time step.

Figure 6.11 shows nine diagrams of close-die compaction fixed in x direction for the 1076-element assembly. The first contact occurs at the 4^{th} time step. Some appears from the 8^{th} time step to the 12^{th} time step. Around 50 contacts occur from the 16^{th} time step to the 24^{th} time step. About 100 more appear at the final stage. Incompressibility is completed at the 35^{th} time step.

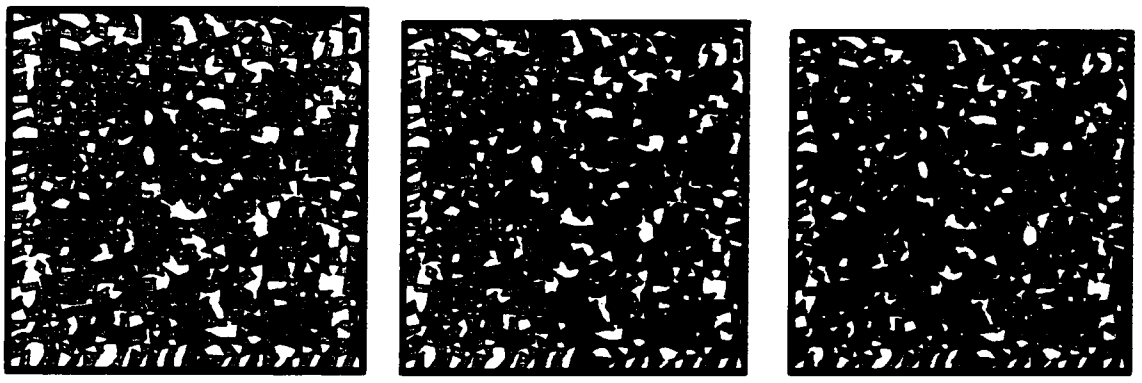

Time Step = 1 Time Step = 3 Time Step = 5

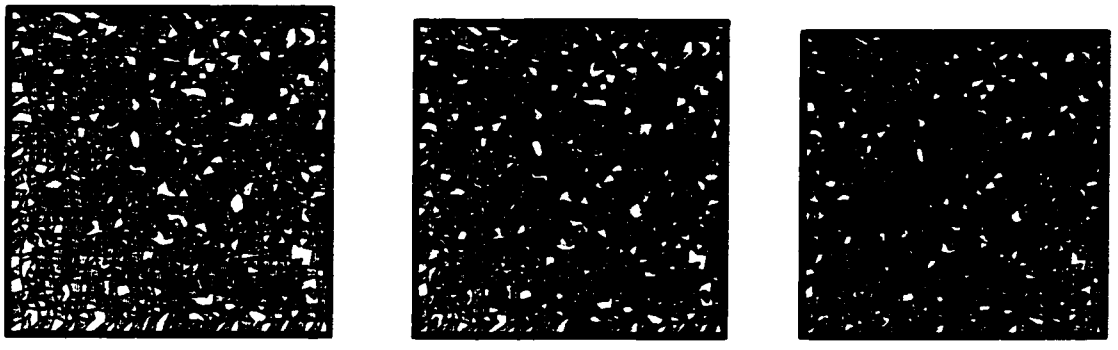

Time Step = 7 Time Step = 9 Time Step = 12

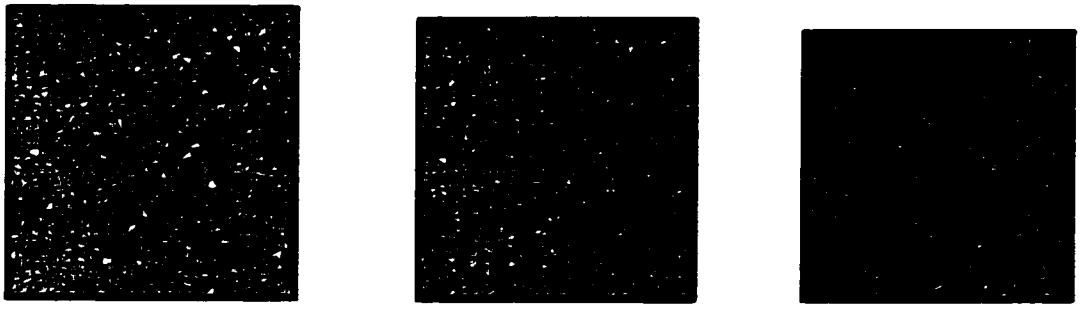

Time Step = 15 Time Step = 17 Time Step = 20

Figure 6.10: Computer simulation of isostatic compaction for the 1076-element assembly.

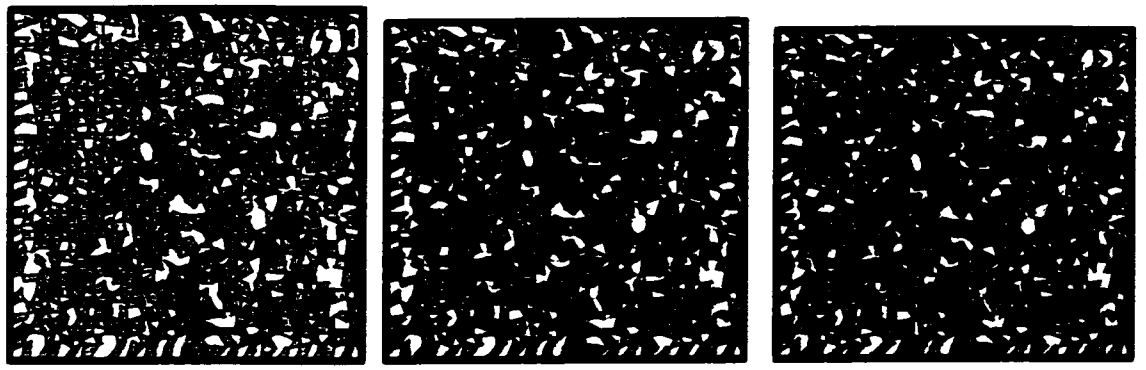

Time Step = 4 Time Step = 8 Time Step = 12

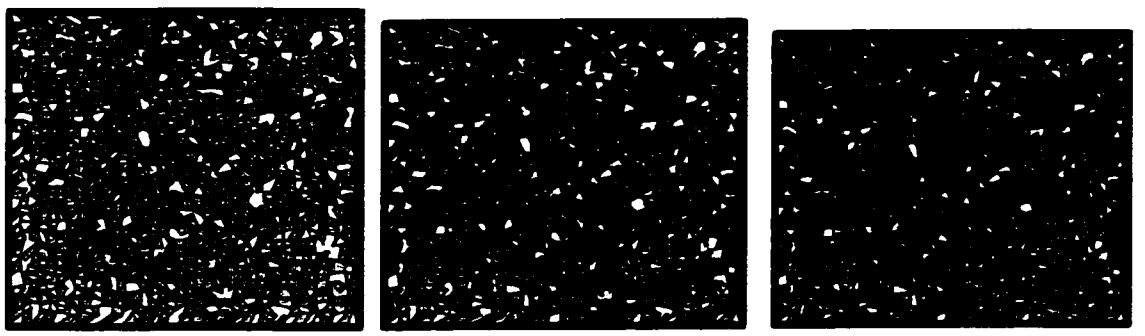

Time Step = 16 Time Step = 20 Time Step = 24

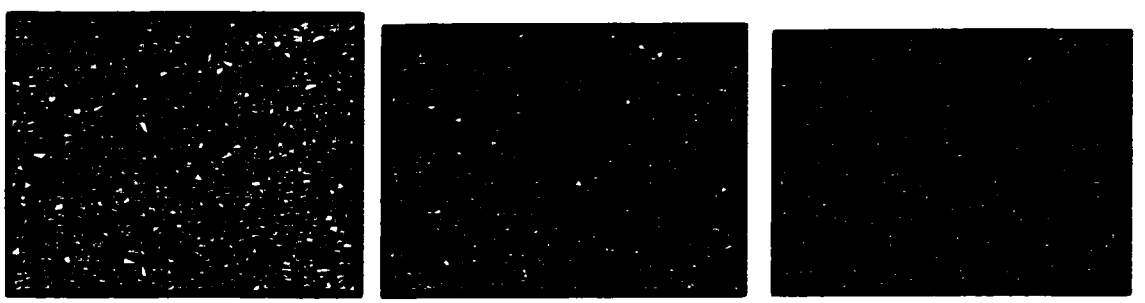

Time Step = 28 Time Step = 32 Time Step = 35

Figure 6.11: Computer simulation of close-die compaction fixed in x direction for the 1076-element assembly.

6.3 MULTIPLE MATERIAL AGGREGATE

A few computer simulations for two types of compactions of multiple material aggregates are given in this section. The section includes three divisions. One numerical simulation of a 10-element assembly is presented in the first division. In the second division, the other numerical experiment of a 75-element granular system is introduced. Finally, another computer simulation of a 296-element aggregate is demonstrated in the third division. In the figures given in the following division, the darker color of particle indicates it has stiffer material property and vice versa.

6.3.1 Simulation for A 10-Element Assembly

Figure 6.12 shows the computer simulation of isostatic compaction of the aggregate. The visco properties of three down-left elements are given as $C_{11}=C_{22}=2.0$, $C_{66}=2.0$. The ones of two down-right elements are $C_{11}=C_{22}=4.0$, $C_{66}=4.0$. The ones of two up-left elements are $C_{11}=C_{22}=6.0$, $C_{66}=6.0$. The ones of two up-right elements are $C_{11}=C_{22}=8.0$, $C_{66}=8.0$. Delta time is 0.05 second. There are totally 26 time steps. In the 18^{th} time step, the first contact happen and the system is re-meshed using the new mesh type. The processing is ended in the 26^{th} time step. Figure 6.13, 6,14 show computer simulations of close-die compaction fixed in the x, y directions respectively.

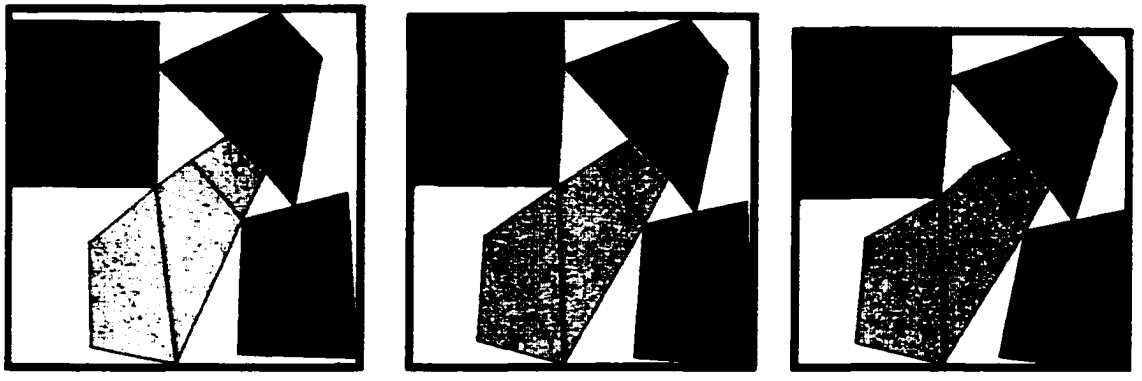

Time Step = 3 Time Step = 6 Time Step = 9

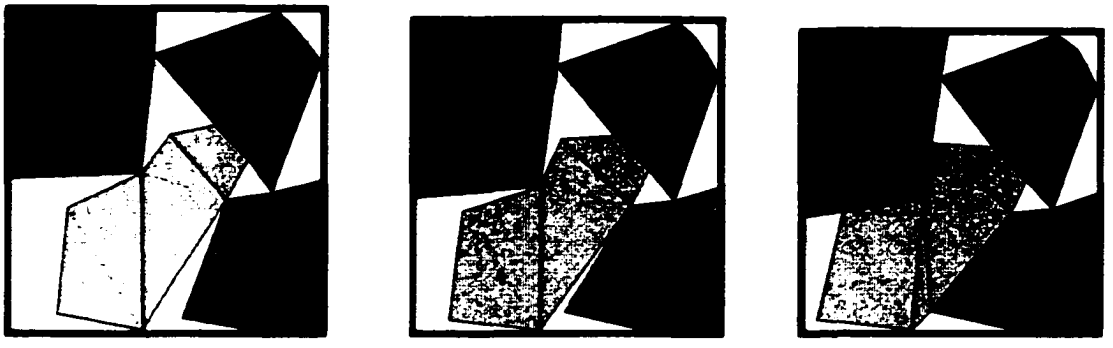

Time Step = 12 Time Step = 15 Time Step = 18

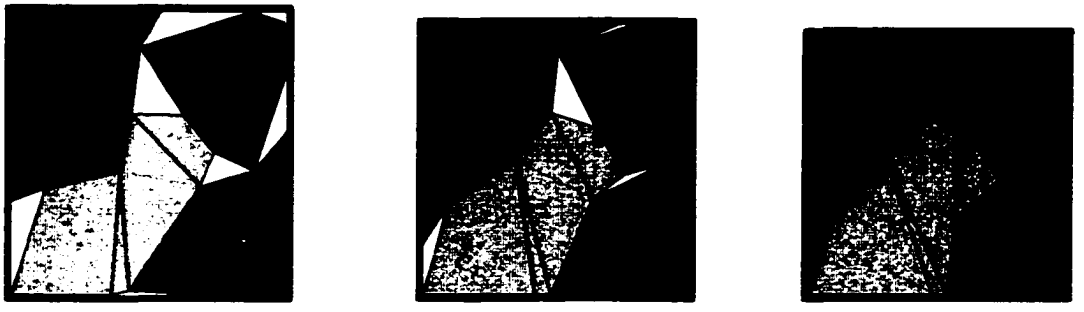

Time Step = 21 Time Step = 24 Time Step = 26

Figure 6.12: Computer simulation of isostatic compaction.

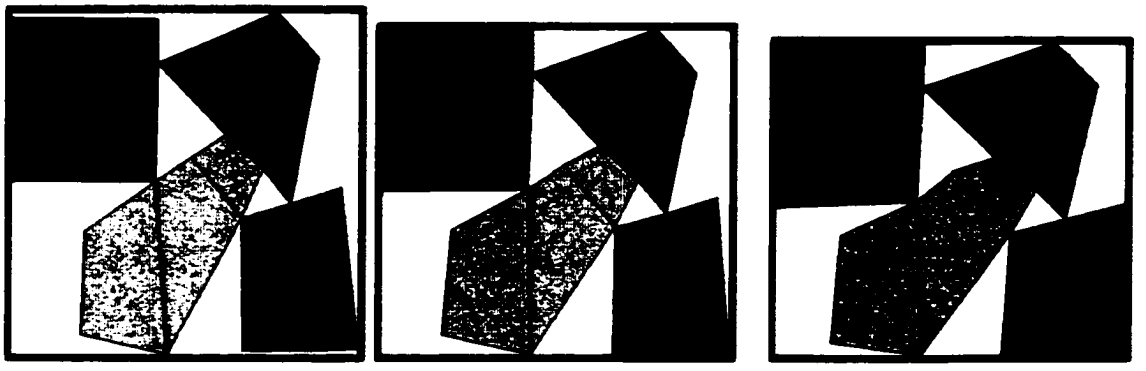

Time Step = 5 Time Step = 10 Time Step = 15

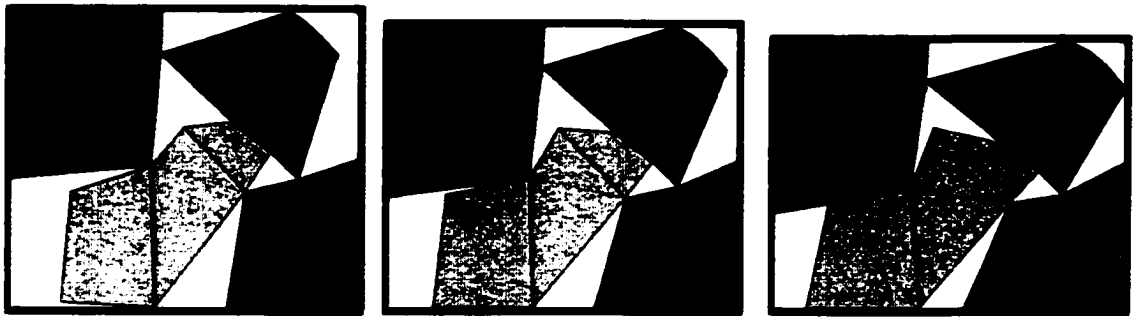

Time Step = 20 Time Step = 25 Time Step = 30

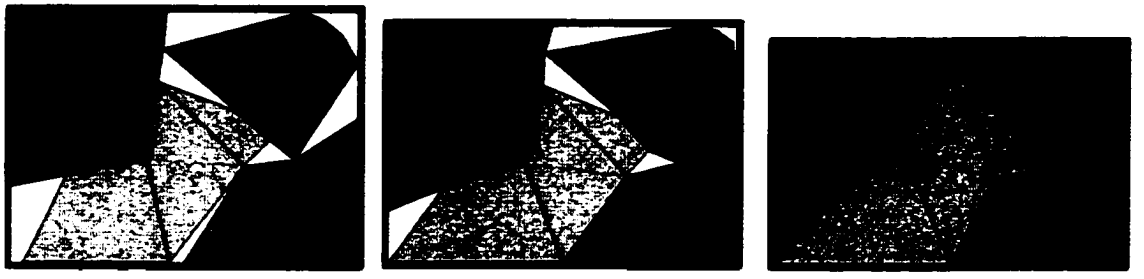

Time Step = 35 Time Step = 40 Time Step = 46

Figure 6.13: Computer simulation of close-die compaction fixed in x direction.

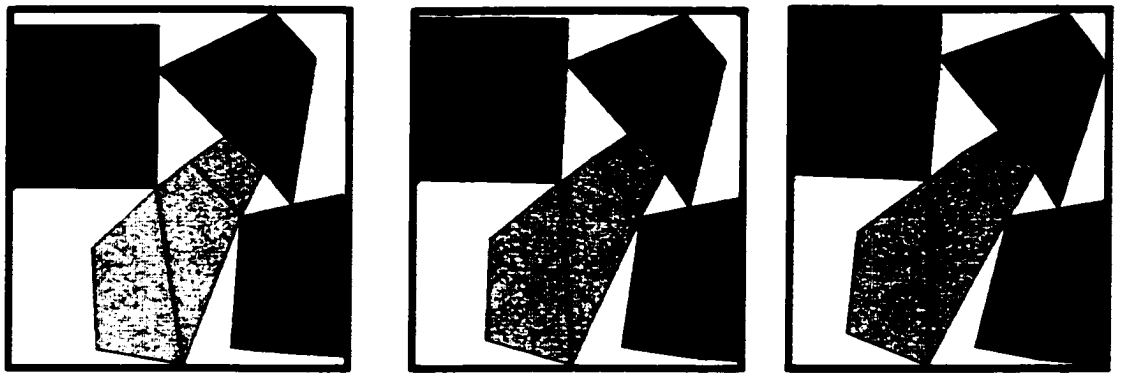

Time Step = 5 Time Step = 10 Time Step = 15

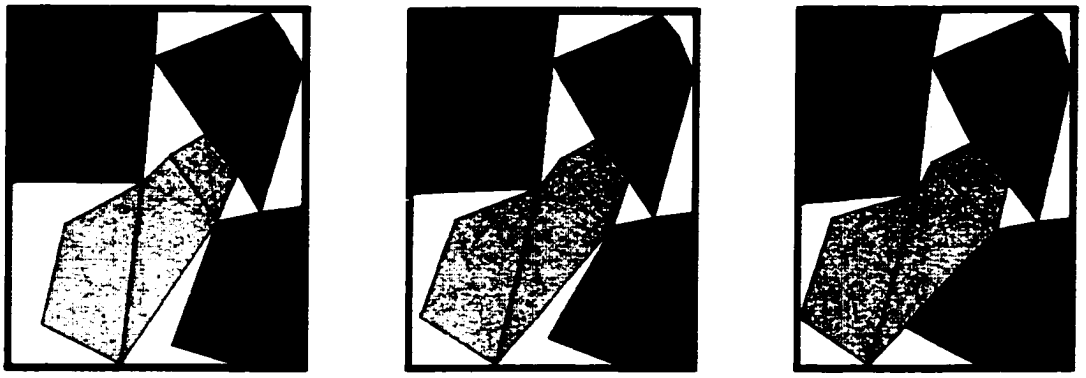

Time Step = 20 Time Step = 25 Time Step = 30

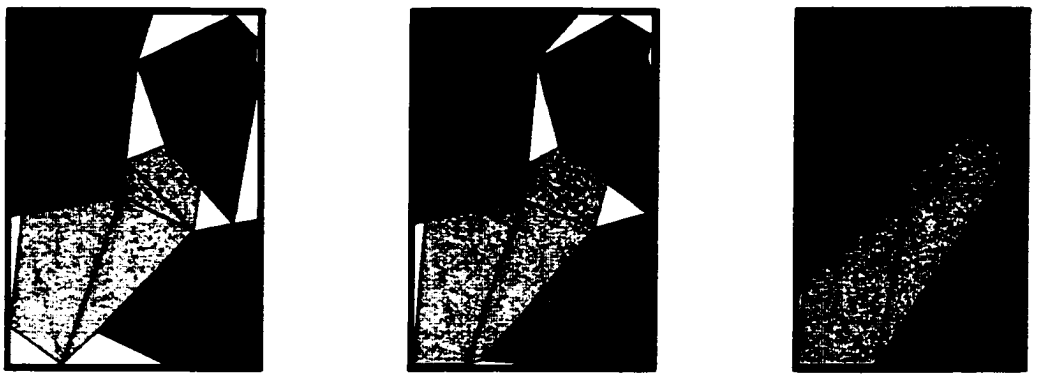

Time Step = 35 Time Step = 40 Time Step = 46

Figure 6.14: Computer simulation of close-die compaction fixed in y direction.

6.3.2 Simulation for A 75-Element Assembly

Three simulations for the granular system are presented in this division. First of all, the computer simulation of the isostatic compaction for the 75-element granular system containing several different materials is introduced. Then, the computer simulation of the close-die compaction fixed in x direction for the same system is demonstrated. At last, the computer simulation of the close-die compaction fixed in y direction is given. Time spent in running these simulation is about 10 to 20 minutes.

Figure 6.15 shows the computer simulation of isostatic compaction of the multiple-material aggregate. There are 4 different materials in the granular system. The visco properties are ranged from 2.0 to 8.0. The darker color indicates the particle has stiffer material property. The first contact appears at the 4^{th} time step. From the 8^{th} time step to the 12^{th} time step, the transition is similar to the simulation of the single material system. However, the first contact between 2 different material elements is occurring at the 16^{th} time step on the right upper corner. The specific mesh generation algorithm is launched. The simulation is completed at the 33^{rd} time step.

Figure 6.16 shows the compaction simulation of close-die compaction fixed in x direction. The first contact appears at the 6^{th} time step. The first contact between 2 solid triangular elements with 2 different materials is occurring at the 24^{th} time step on the right upper corner. The simulation is finished at the 56^{th} time step. Figure 6.17 shows the computer simulation of close-die compaction fixed in y direction. The first contact is occurring at the 12^{th} time step. The first contact between 2 solid triangular elements with 2 different materials appears near the right lower corner at the 18^{th} time step. Incompressibility is achieved at the 56^{th} time step.

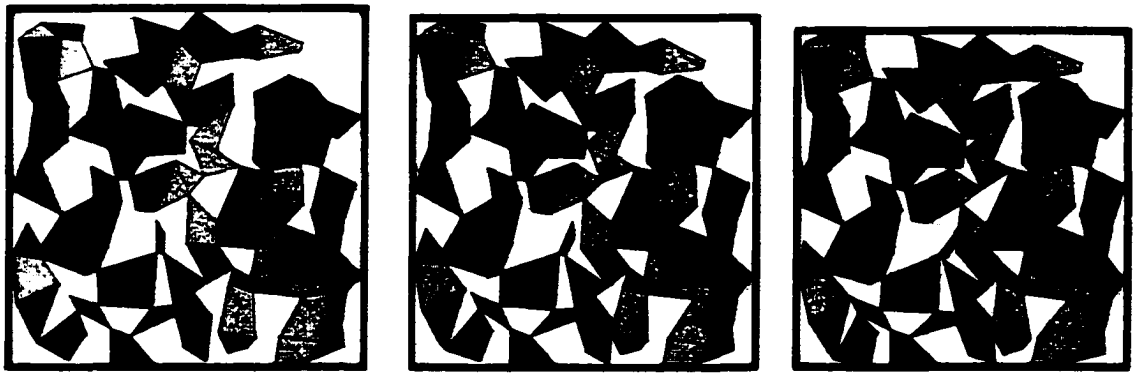

Time Step = 4 Time Step = 8 Time Step = 12

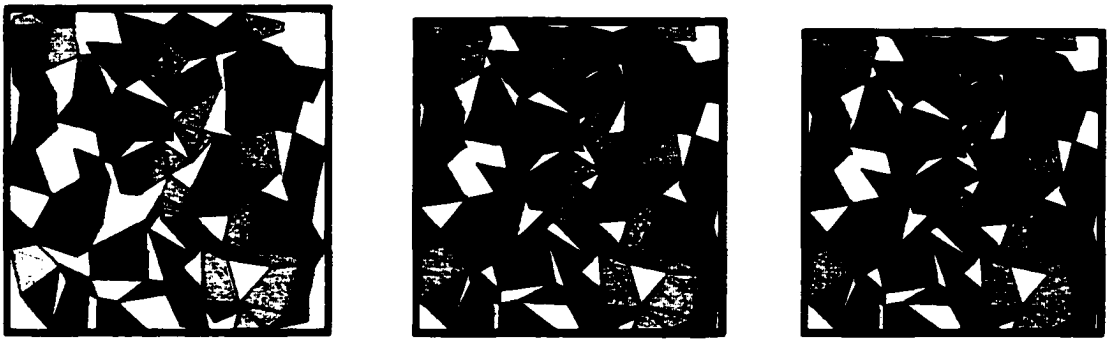

Time Step = 16 Time Step = 20 Time Step = 24

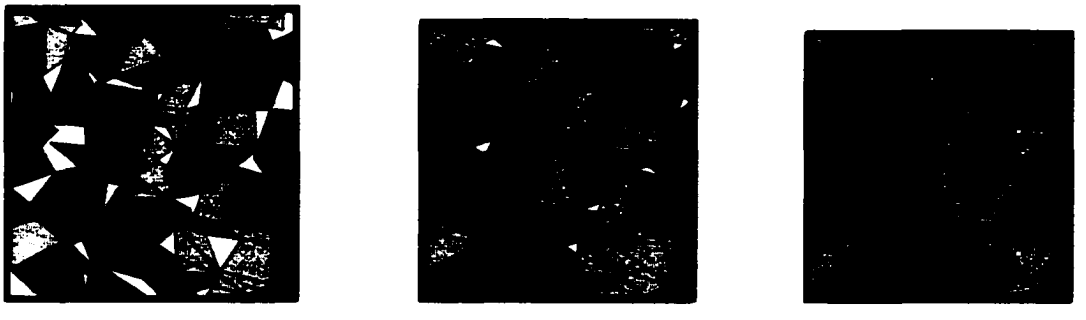

Time Step = 28 Time Step = 32 Time Step = 33

Figure 6.15: Computer simulation of isostatic compaction.

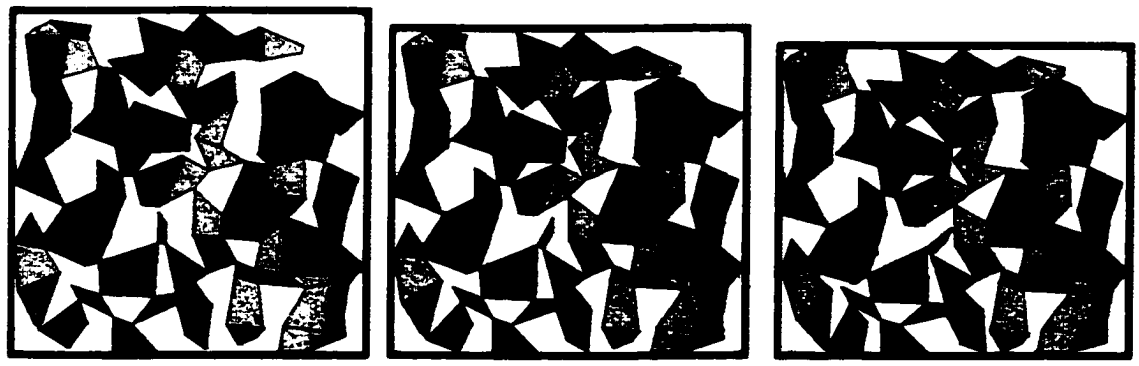

Time Step = 6 Time Step = 12 Time Step = 18

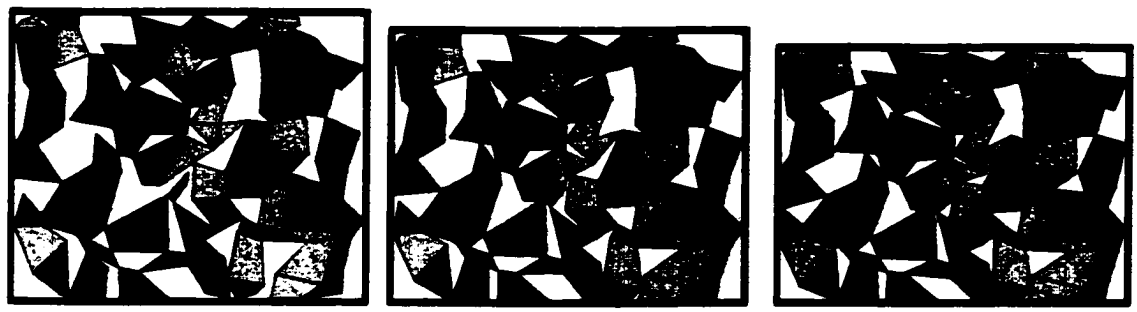

Time Step = 24 Time Step = 30 Time Step = 36

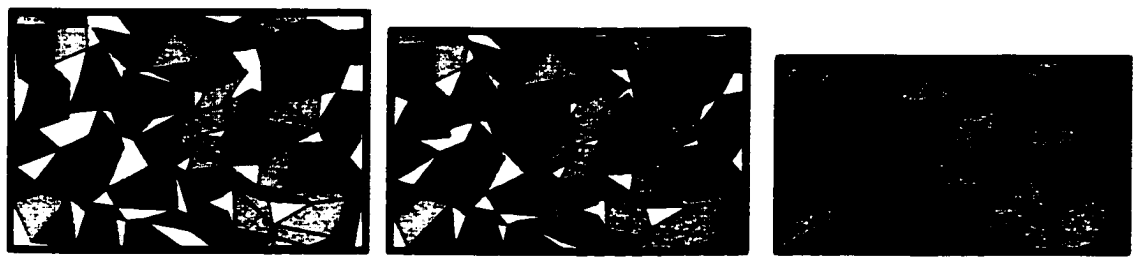

Time Step = 42 Time Step = 48 Time Step = 56

Figure 6.16: Computer simulation of close-die compaction fixed in x direction.

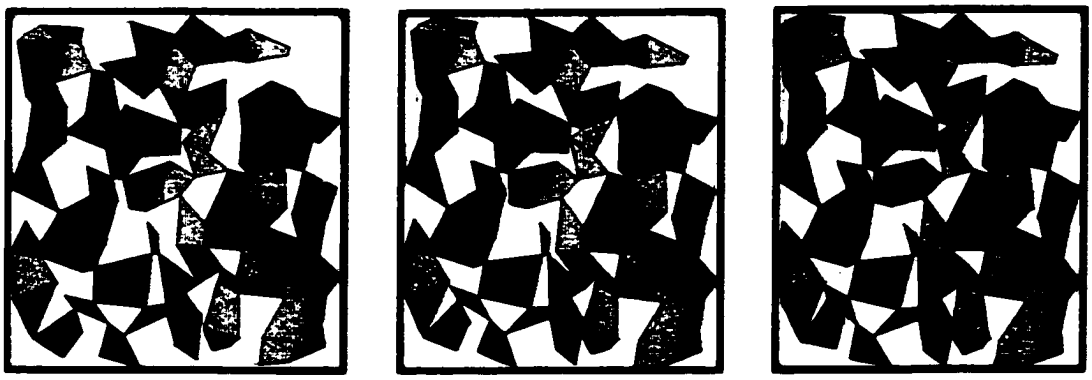

Time Step = 6 Time Step = 12 Time Step = 18

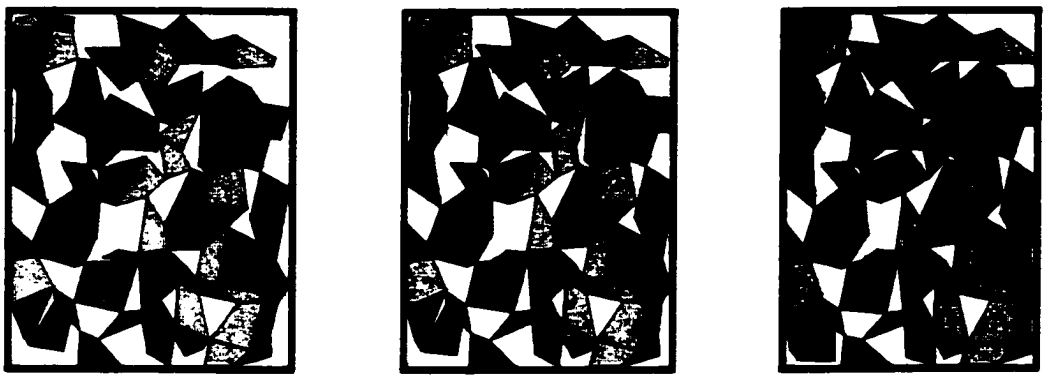

Time Step = 24 Time Step = 30 Time Step = 36

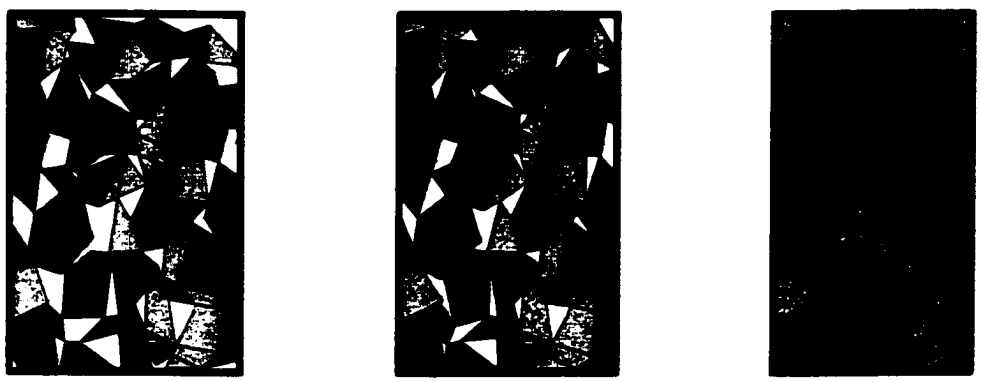

Time Step = 42 Time Step = 48 Time Step = 56

Figure 6.17: Computer simulation of close-die compaction fixed in y direction.

6.3.3 Simulation for A 296-Element Assembly

The goal of the simulation for the 296-element multiple-material assembly is to test if the discrete element model and the mesh generation algorithm work for this type of systems. There are three numerical simulation are made and introduced in this division Figure 6.18 demonstrates the computer simulation of isostatic compaction for the 296-element assembly with 4 different materials randomly distributed in the whole system. In Figure 6.19, the computer simulation of close-die compaction fixed in x direction is introduced. In Figure 6.20, the computer simulation of close-die compaction fixed in y direction is presented. It takes a couple of minutes to run each simulation. It is about the same as the single-material assembly of the same size.

In Figure 6.18, there are nine diagrams which represent the granular system in nine different periods of time. A few contacts from the first time step to the 7^{th} time step. The first case of contact between 2 triangular solid element with time different materials is occurring at the 14^{th} time step. The simulation is finished at the 21^{st} time step.

In Figure 6.19, the first contact appears at the 8^{th} time step. The first case of contact between 2 triangular solid elements with 2 different materials is occurring at the 24^{th} time step. Incompressibility is achieved at the 38^{th} step. Figure 6.20 introduces another case of close-die compaction in which the details are very similar to the foregoing case.

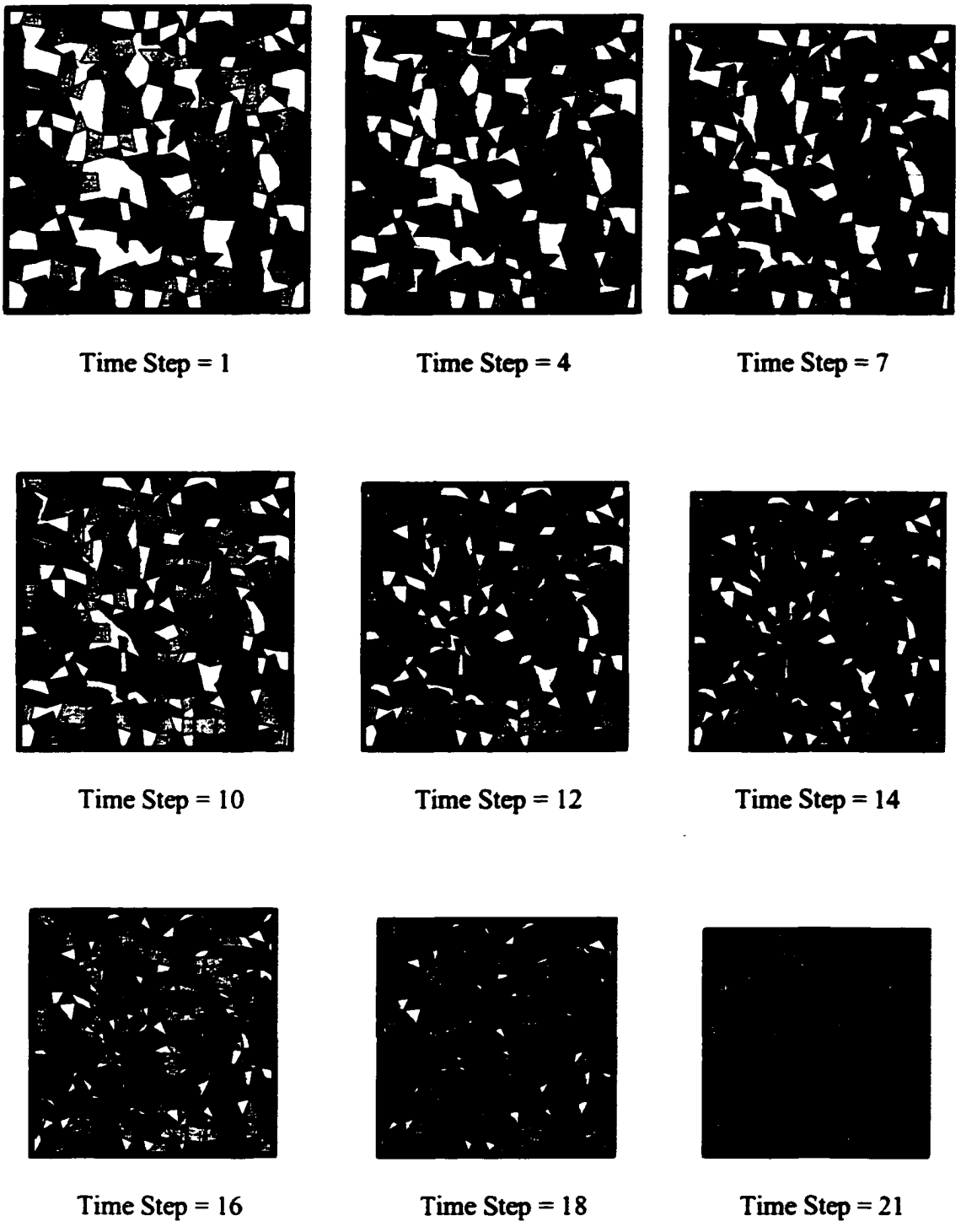

Figure 6.18: Computer simulation of isostatic compaction.

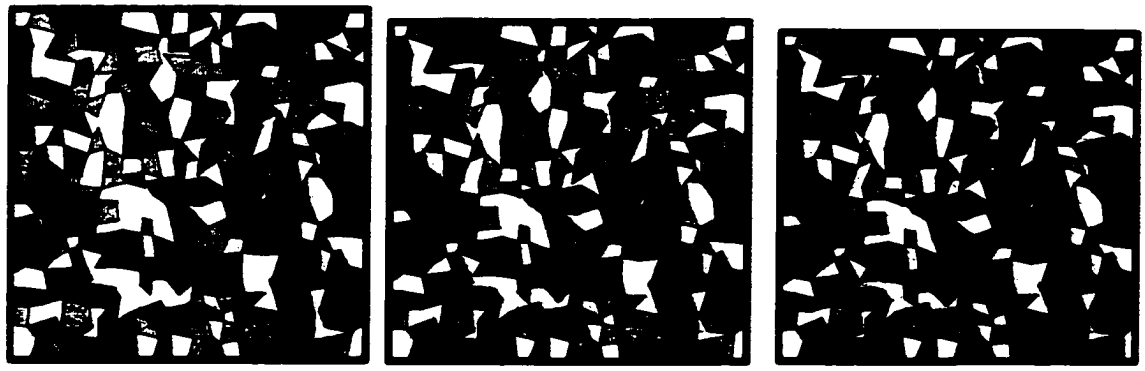

Time Step = 4 Time Step = 8 Time Step = 12

Time Step = 16 Time Step = 20 Time Step = 24

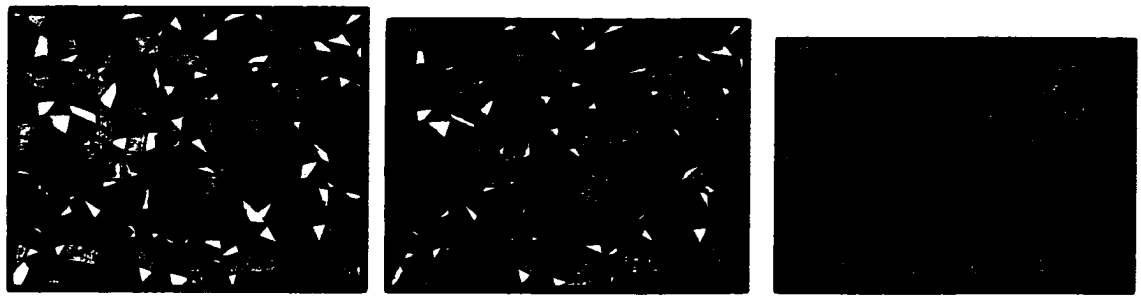

Time Step = 28 Time Step = 32 Time Step = 38

Figure 6.19: Computer simulation of close-die compaction fixed in x direction.

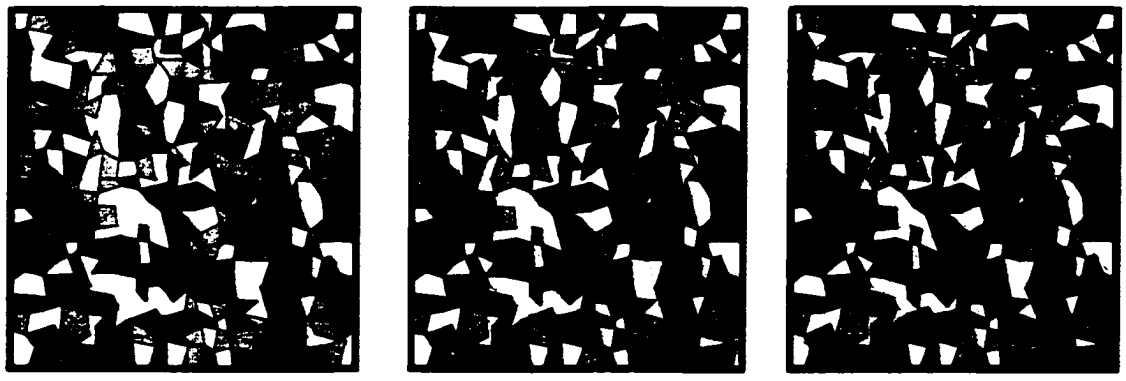

Time Step = 4 Time Step = 8 Time Step = 12

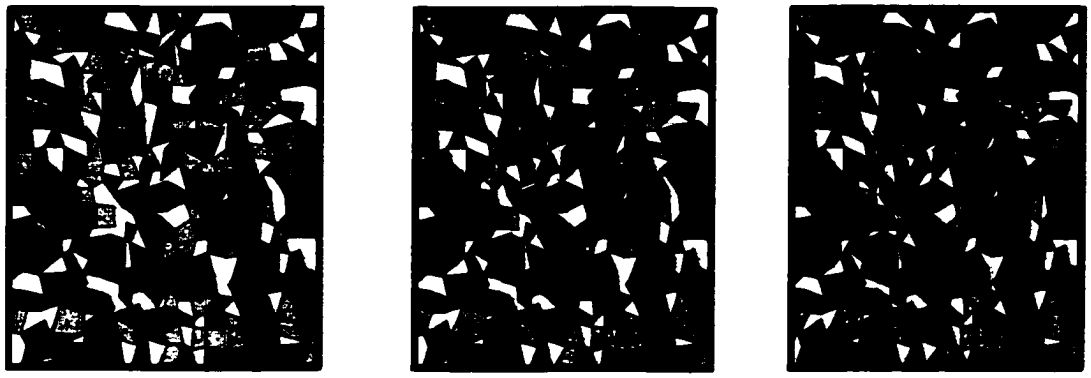

Time Step = 16 Time Step = 20 Time Step = 24

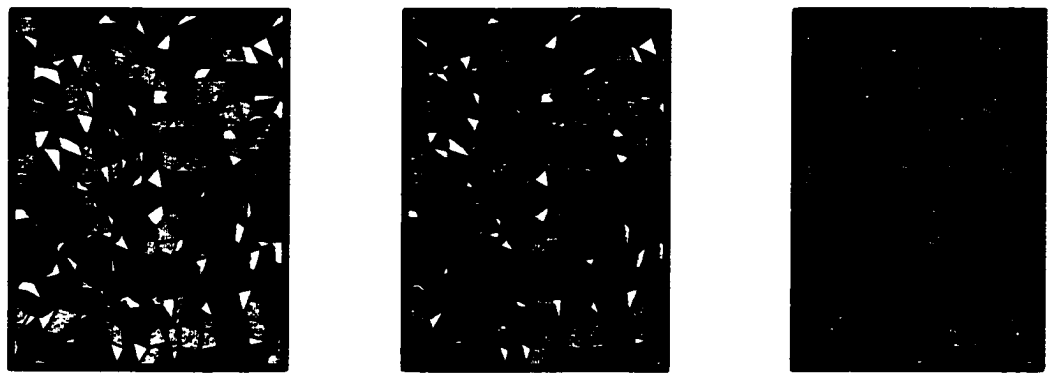

Time Step = 28 Time Step = 32 Time Step = 38

Figure 6.20: Computer simulation of close-die compaction fixed in y direction.

CHAPTER 7

CONCLUSIONS

The numerical model in which one element represents one particle is used at the initial stage of the research. It is found that the numerical error of the model is too large. Instead, the alternative model in which four elements represent one particle is suggested to use, because of its efficiency and accuracy. The model can be used to simulate the granular system containing more than 1000 particles and the result is very precise.

For viscoplastic material, when incompressibility is achieved, the stress goes to infinity. During compaction of the viscoplastic granular system, void ratio is an important parameter of overall aggregate response. A couple of numerical experiments have been made to demonstrate the fact.

In addition to void ratio, void position is the other suspicious factor which might have impact on the macroscopic behavior of the granular system. The result of the numerical experiment on void position has disprove that void position affect the global behavior too much. The overall aggregate response does not depend on void location.

Nearness of voids has been demonstrated to be the other parameter which has significant impact on the macroscopic behavior of the granular system. Small change of distance between voids creates considerable change of overall aggregate response.

Results of the numerical experiment on nearness of voids have proved that the granular system is very sensitive to distance between voids.

For the symmetric case, void size does not have any effect on the global behavior. The overall aggregate response is not dependent on void size at all. However, the macroscopic behavior of the viscoplastic granular system is dependent on geometry of voids. The assemblies with different shape of void got totally different response under compaction. It is demonstrated that void shape is another parameter which has significant impact on the global behavior of the whole system.

The numerical experiment on void pattern has been made to investigate the effect of void pattern. It has proved that void pattern has noticeable impact on the whole system.

The triangular mesh system gives mesh generation algorithms a fantastic opportunity due to its flexibility. Millions of contact situations might appear in granular systems with non-spherical particles. It is much more complicated than spherical particle systems in which the number of contact points between two particles is always one. In such a complex chaos, the triangular mesh system can combine every different mesh type to one single system. No other models can replace the triangular system and do the same job. A series of simulations have been made based on the algorithm.

In summary, the alternative discrete element method is presented in the current study. The mesh generation algorithms are established and used in several numerical experiments. Several significant factors which have considerable impact on global behavior of the whole aggregates are found.

APPENDIX A

LOCAL DENSITY ANALYSIS

Appendix A shows 30 cases of 1300-element granular systems and their local density analysis. These contour diagrams demonstrate random distribution of particles. It is hard to tell what big differences among these randomly scattered aggregates. It proves that these granular systems are very sensitive. They are affected by some variables.

Case 1

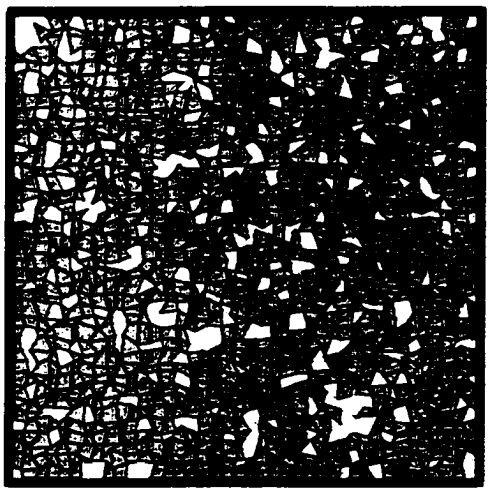

Case 2

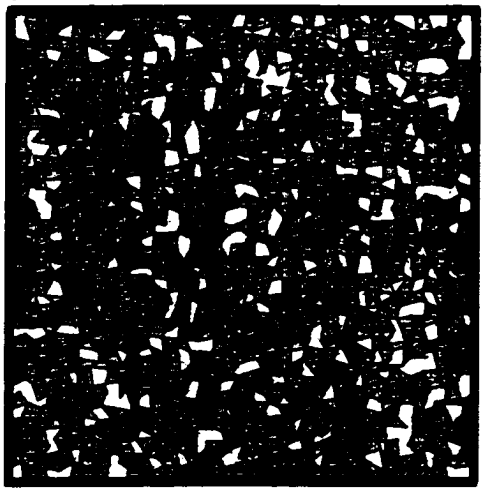

Case 3

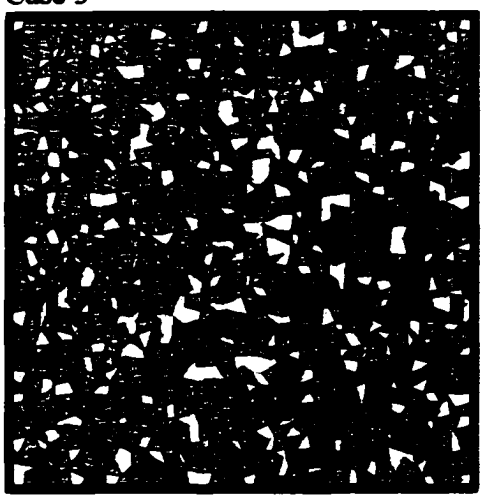

Case 4

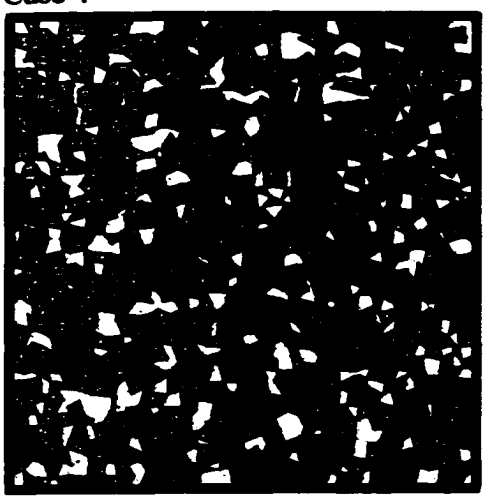

Case 5

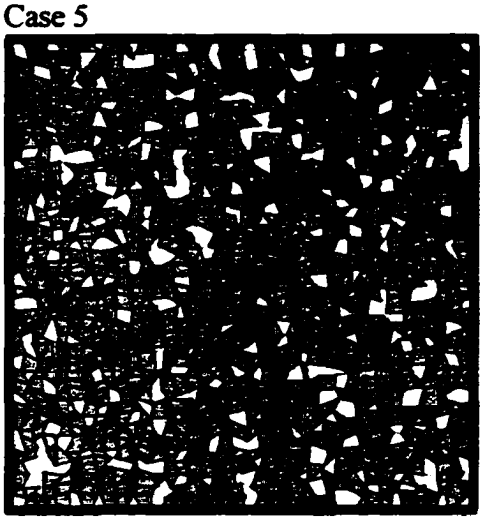

Case 6

Case 7

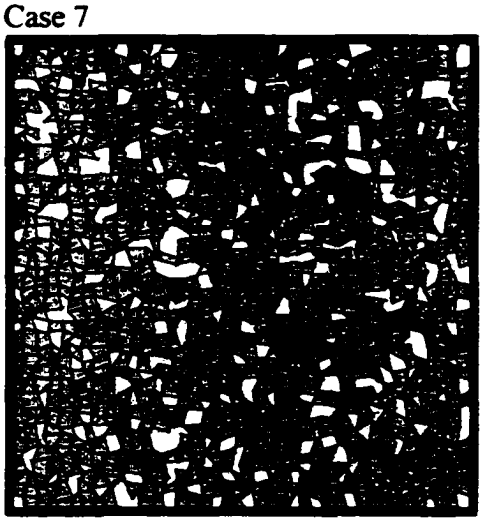

Case 8

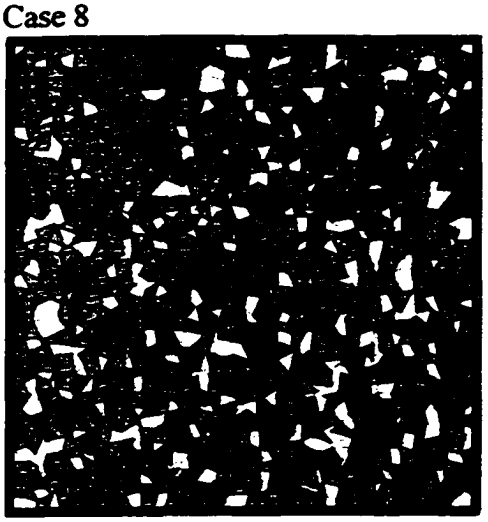

Case 9

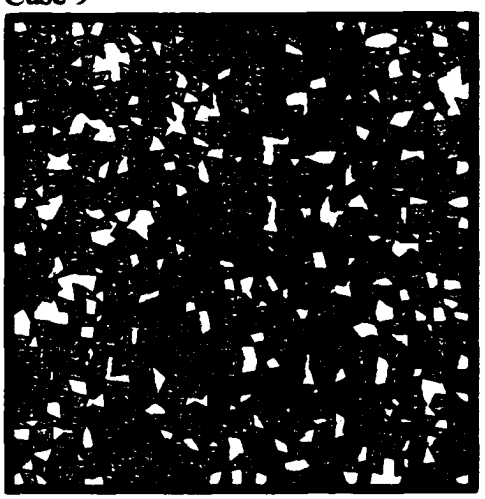

Case 10

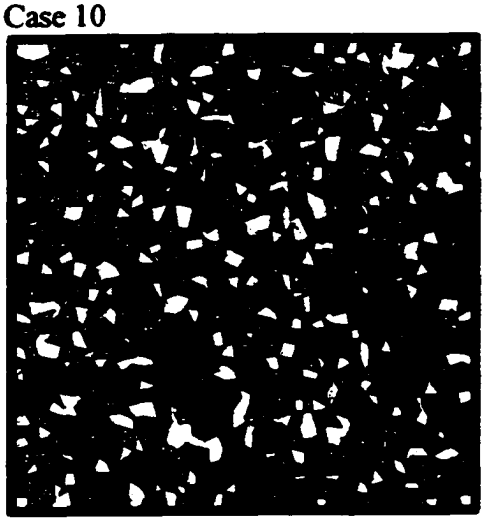

Case 11

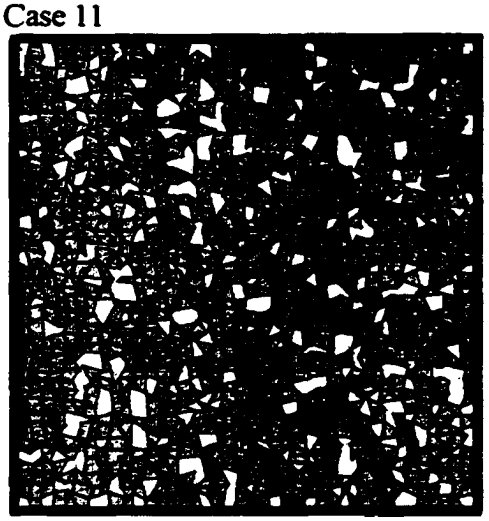

Case 12

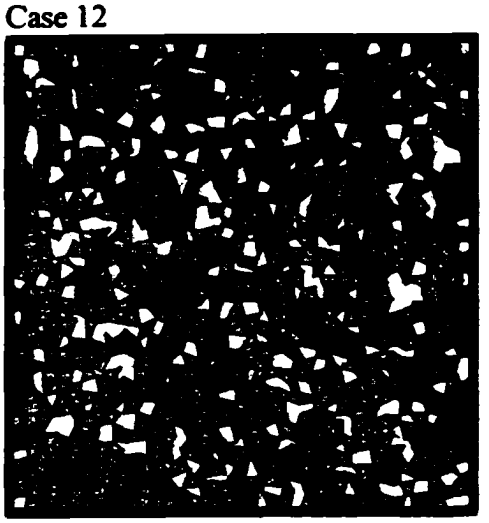

Case 13

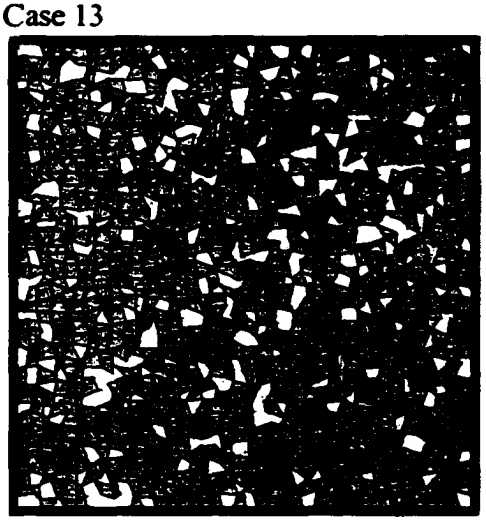

Case 14

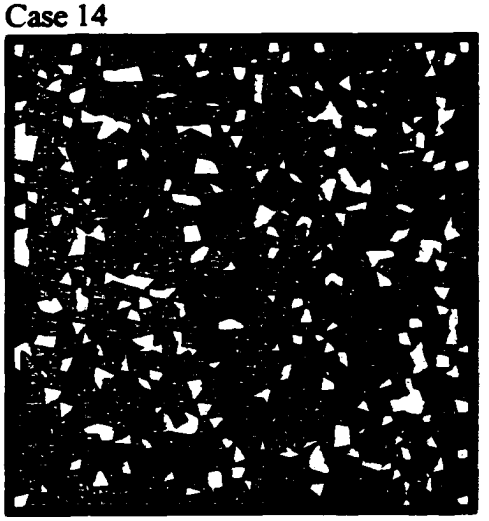

Case 15

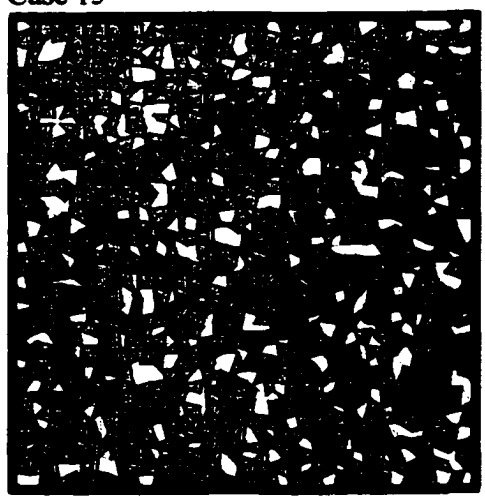

Case 16

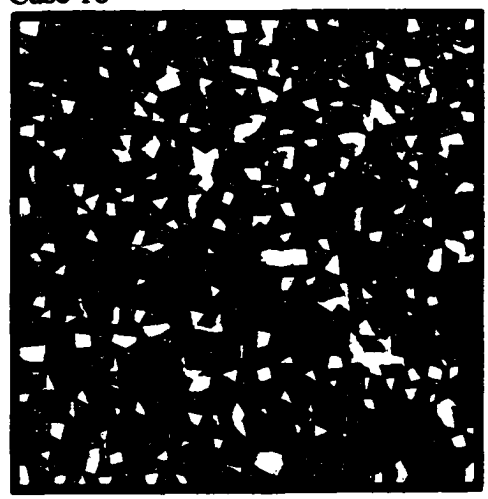

Case 17

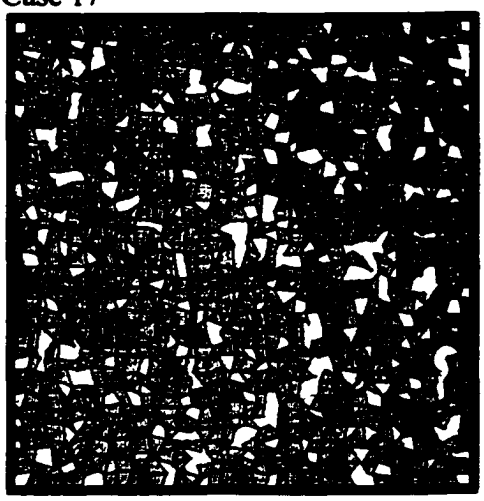

Case 18

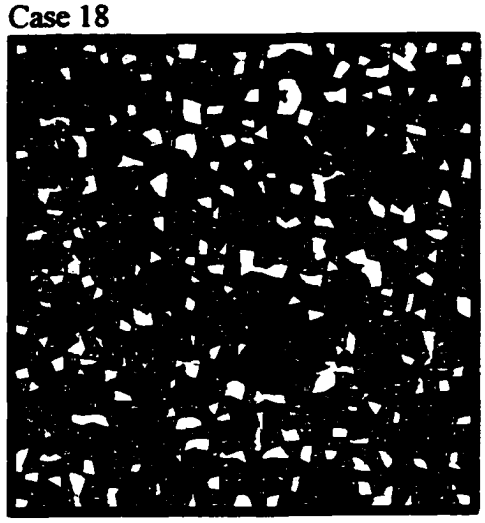

Case 19

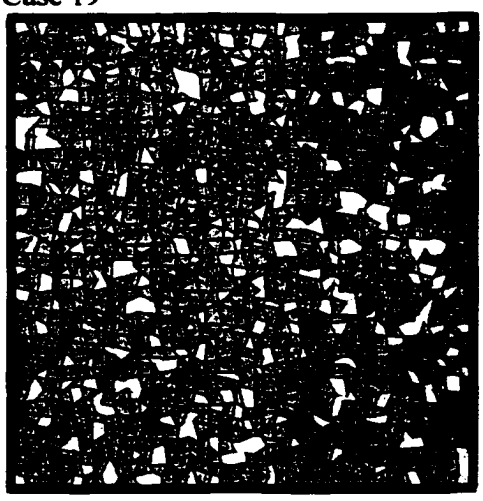

Case 20

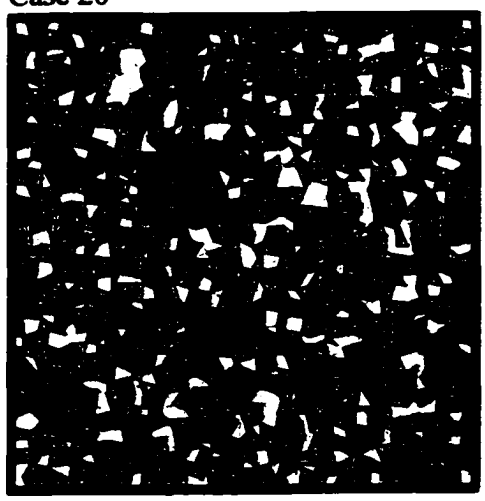

Case 21

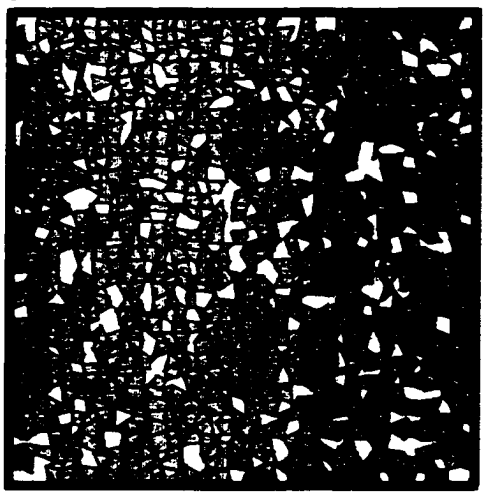

Case 22

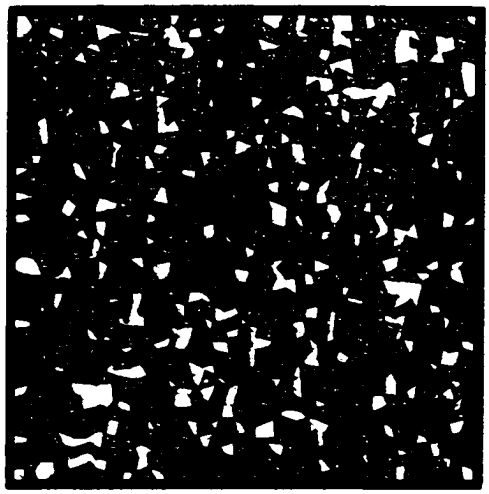

Case 23

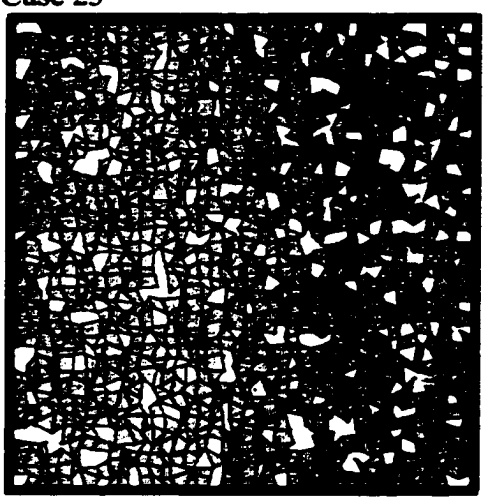

Case 24

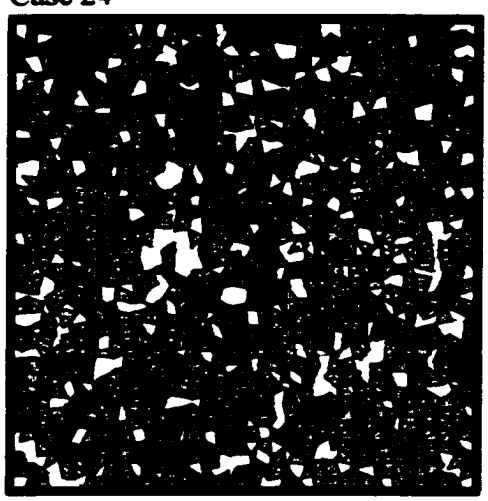

Case 25

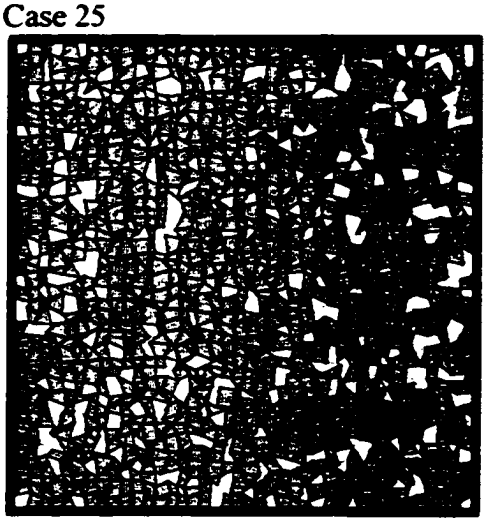

Case 26

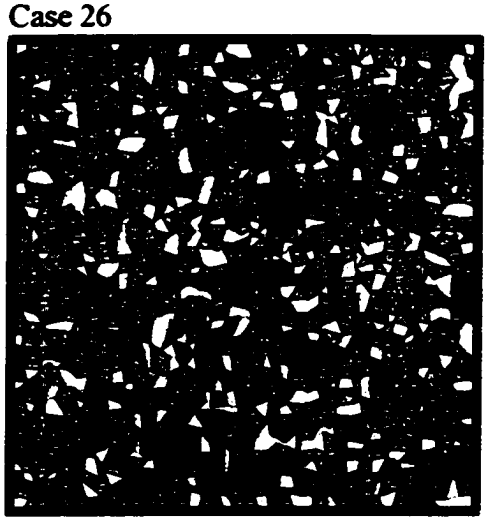

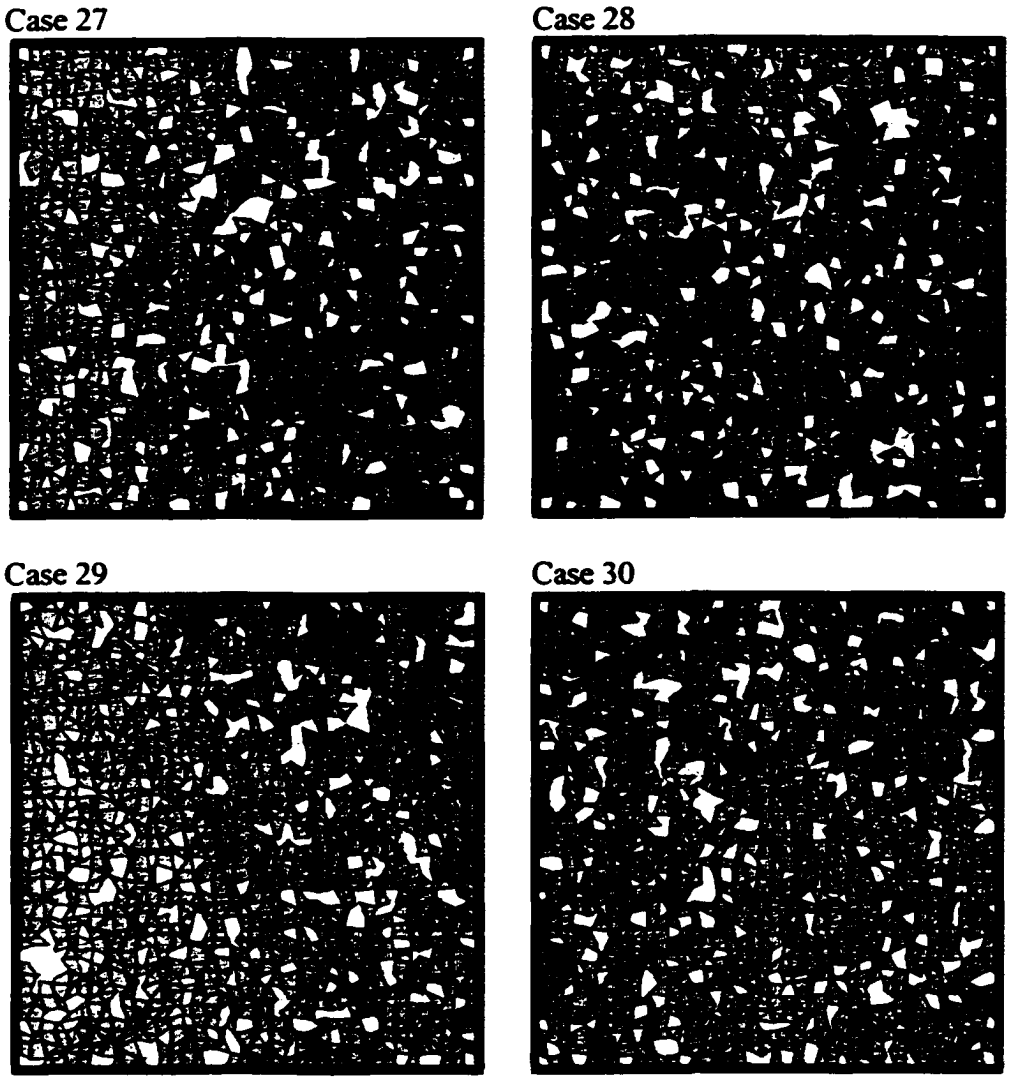

Figure A.1: The 30 cases of randomly distributed 1300-element granular systems

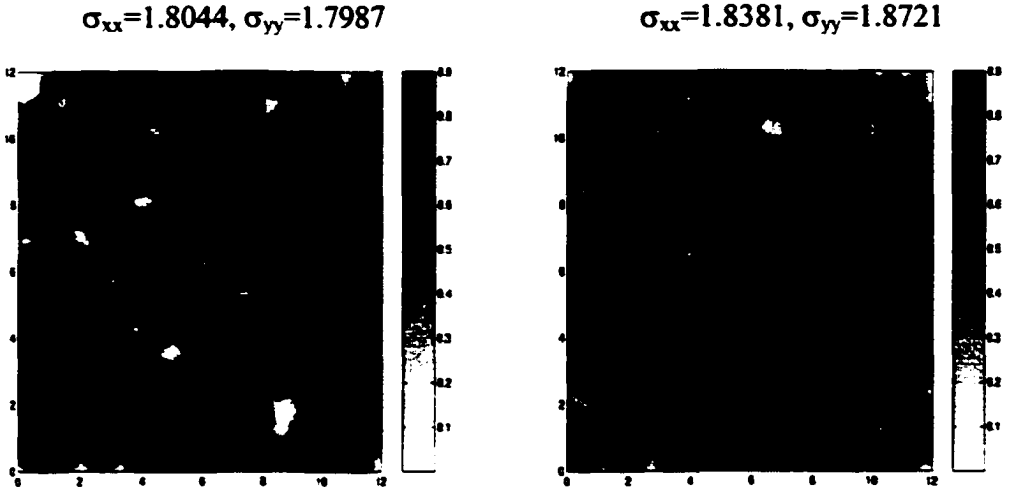

σ_{xx}=1.8418, σ_{yy}=1.8257

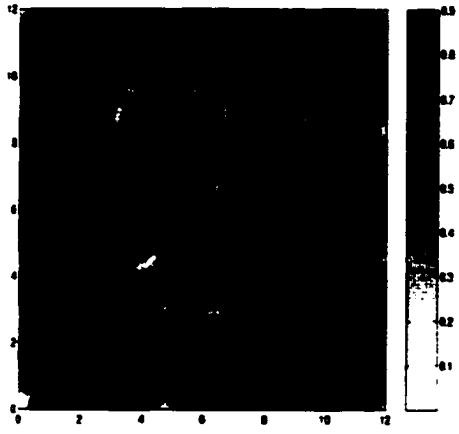

σ_{xx}=1.7525, σ_{yy}=1.6949

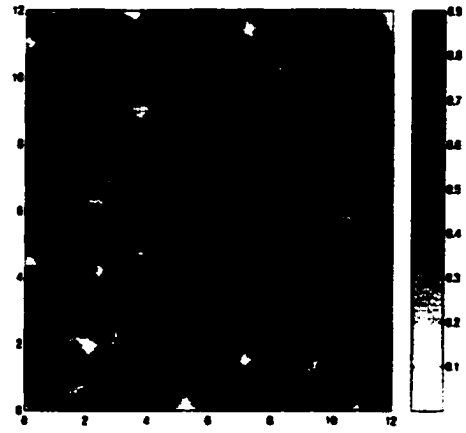

σ_{xx}=1.8437, σ_{yy}=1.8757

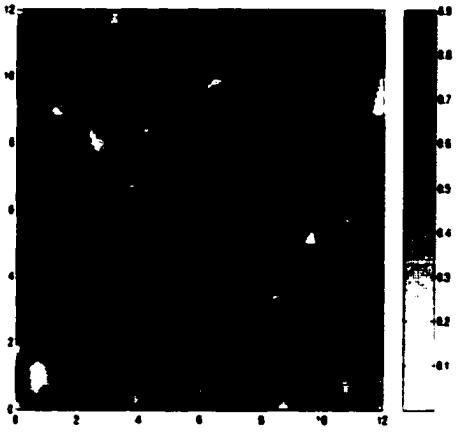

σ_{xx}=1.6281, σ_{yy}=1.6288

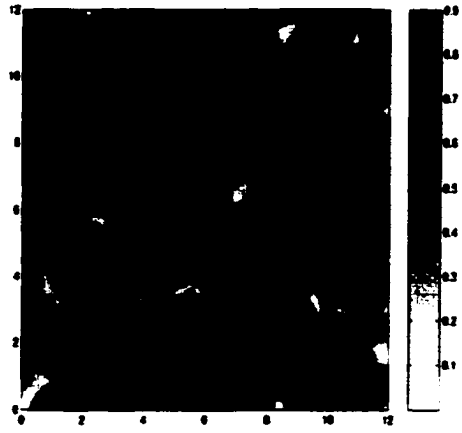

σ_{xx}=1.8672, σ_{yy}=1.8259

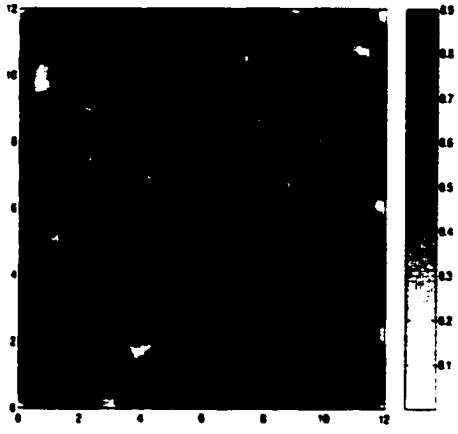

σ_{xx}=1.7236, σ_{yy}=1.7561

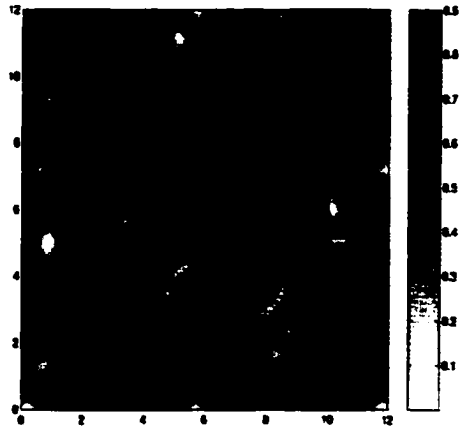

σ_{xx}=1.7433, σ_{yy}=1.7414

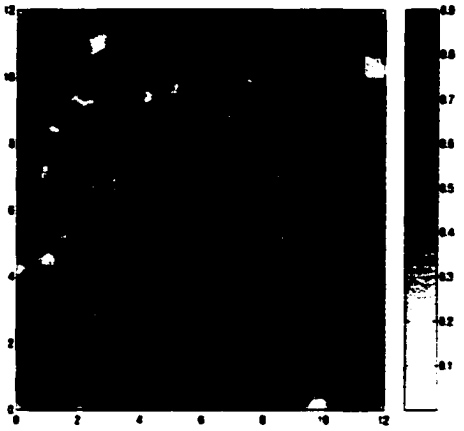

σ_{xx}=2.0090, σ_{yy}=1.9968

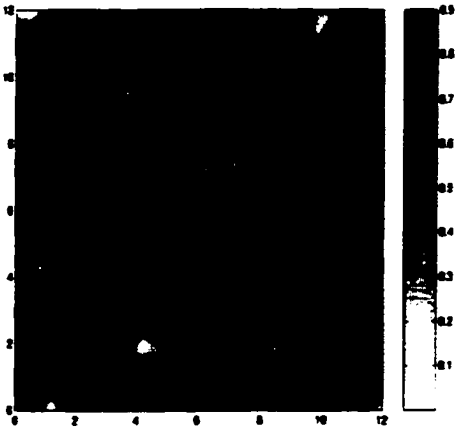

σ_{xx}=1.7528, σ_{yy}=1.7843

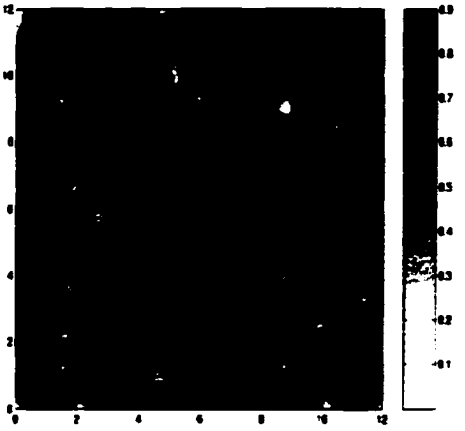

σ_{xx}=1.9771, σ_{yy}=1.9686

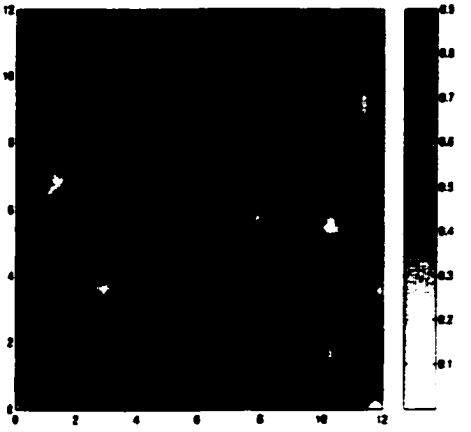

σ_{xx}=1.8191, σ_{yy}=1.7241

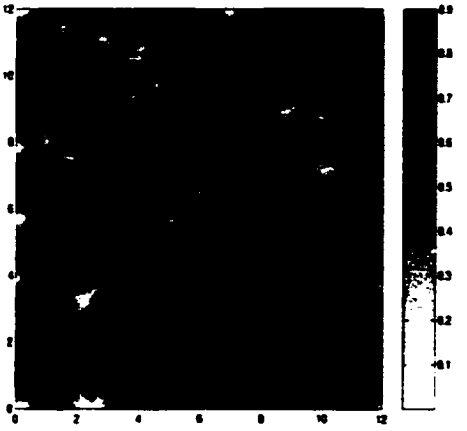

σ_{xx}=1.7960, σ_{yy}=1.7559

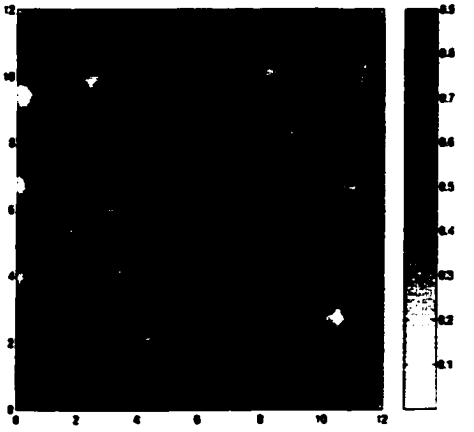

σ_{xx}=1.9691, σ_{yy}=1.9426

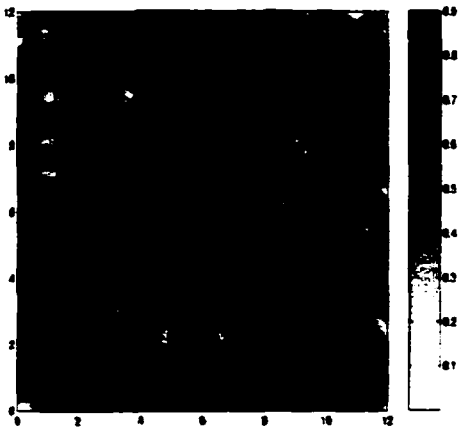

σ_{xx}=1.9449, σ_{yy}=1.9484

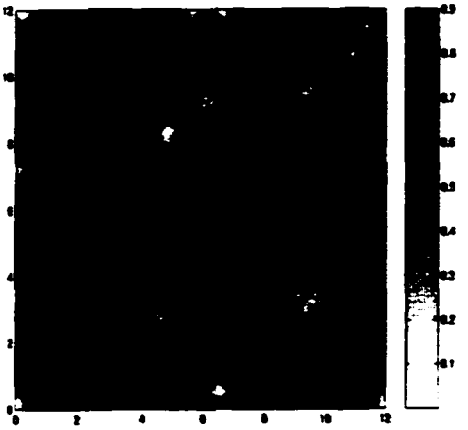

σ_{xx}=1.7475, σ_{yy}=1.8191

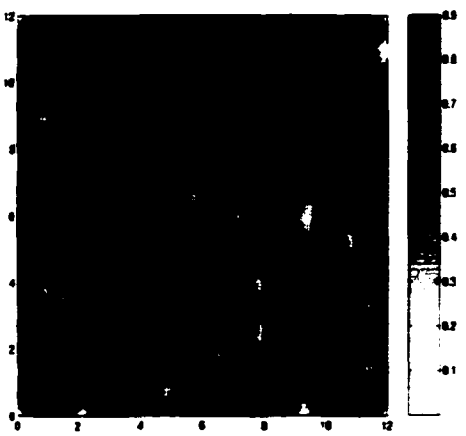

σ_{xx}=1.8436, σ_{yy}=1.8345

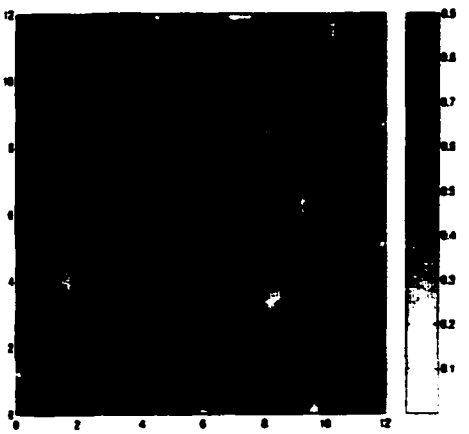

σ_{xx}=1.9822, σ_{yy}=1.9680

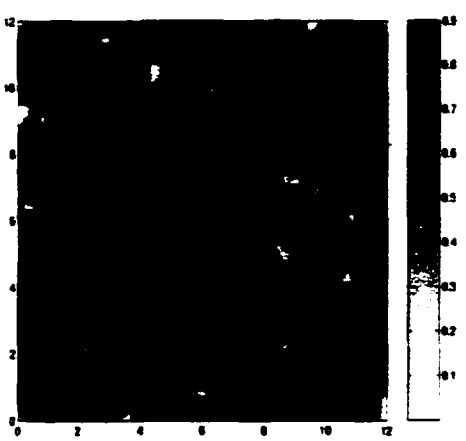

σ_{xx}=1.7475, σ_{yy}=1.7676

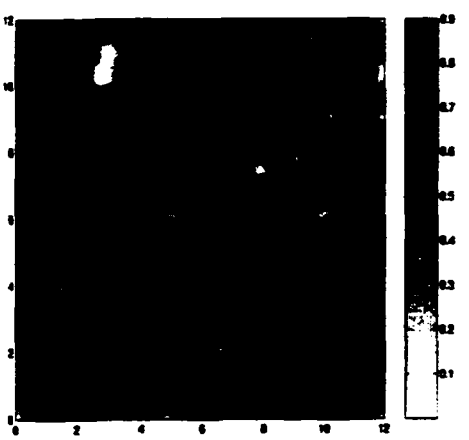

σ_{xx}=1.7819, σ_{yy}=1.7941

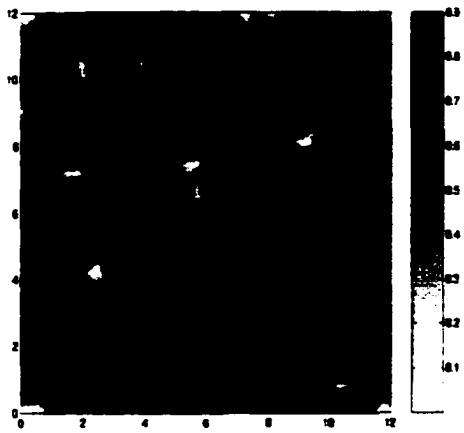

σ_{xx}=1.6792, σ_{yy}=1.7195

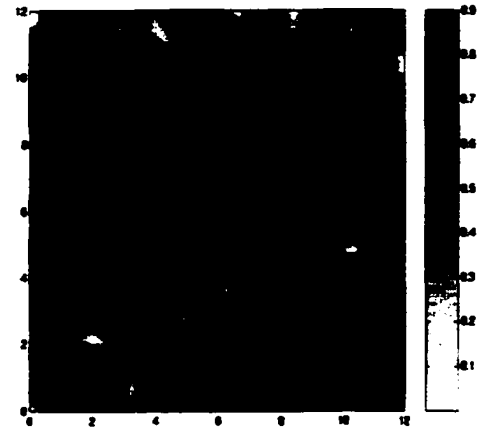

σ_{xx}=1.8209, σ_{yy}=1.7689

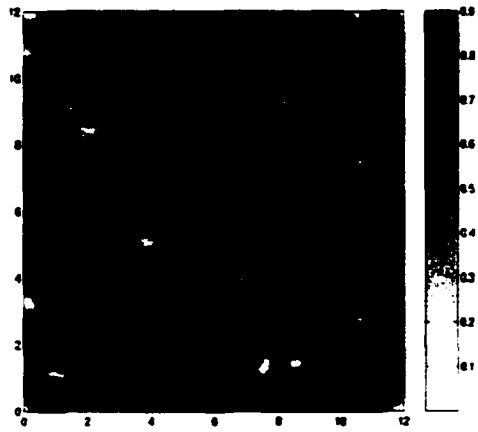

σ_{xx}=1.6273, σ_{yy}=1.6356

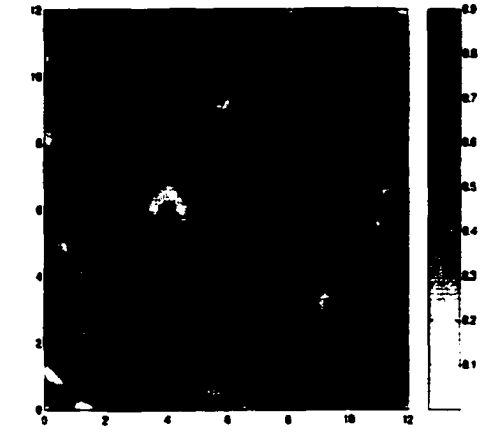

σ_{xx}=1.7882, σ_{yy}=1.7992

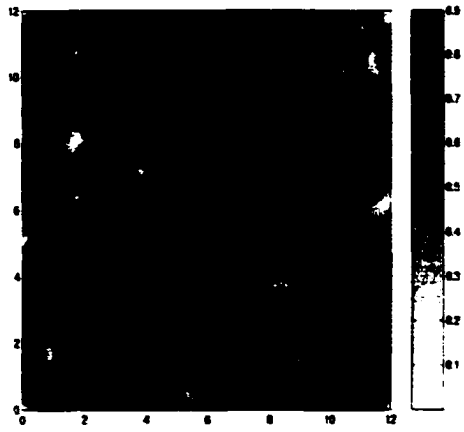

σ_{xx}=1.8200, σ_{yy}=1.8128

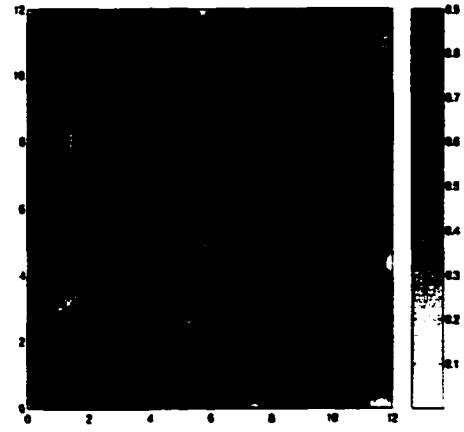

σ_{xx}=1.8463, σ_{yy}=1.8646

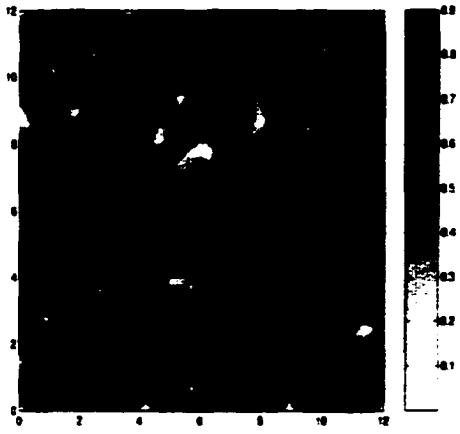

σ_{xx}=1.8796, σ_{yy}=1.8342

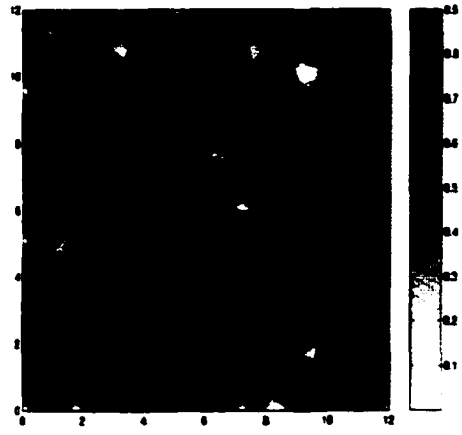

σ_{xx}=1.7272, σ_{yy}=1.6982

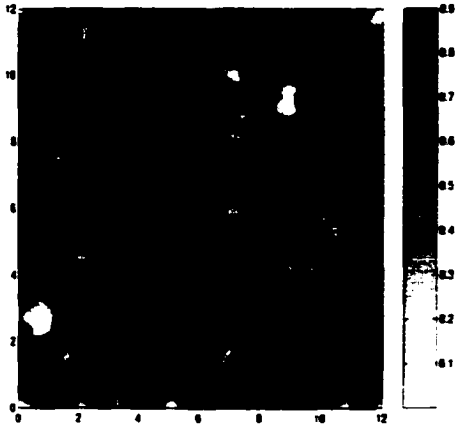

σ_{xx}=1.6917, σ_{yy}=1.7480

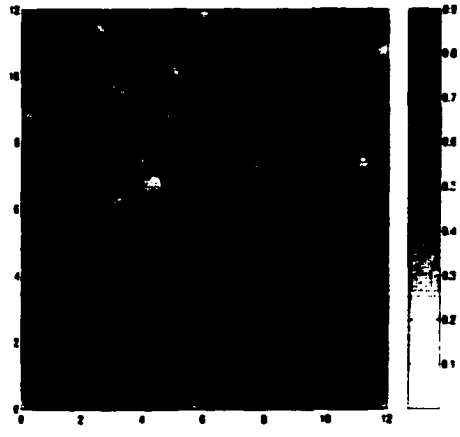

Figure A.2: The contour diagrams of local density for the 30 randomly distributed aggregates

REFERENCES

Akisanya, A.R., Cocks, A.C. and Fleck, N.A. (1997). The yield behavior of metal powders. Int. J. Mech. Sci., 39(12), 1315-1324.

Arzt, E. (1982). The influence of an increasing particle coordination on the densification of spherical powders. Acta allurgica, 30, 1883-1890.

Aurenhammer, F. (1991). Voronoi diagrams—a study of a fundamental geometric data structure. ACM Computer Surveys, 23, 345-405.

Bashir, Y.M. and Goddard, J.D., (1991). A novel simulation method for the quasi-static mechanics of granular assemblages. J. Rheol, 35(5), 849-885.

Bathurst, R.J. and Rothenburg, L. (1988). Micro-mechanical aspects of isotropic granular assemblies with linear contact interactions. J. Appl. Mech., 55, 17.

Bower, A.F., Fleck, N.A., Needleman, A. and Ogbonna, N., (1993). Indentation of a power law creeping solid. Proceedings of the Royal Society of London, A441, 97-124.

Buchholtz, V. and Poschel, T., (1994). Numerical investigations of the evolution of sandpiles, Physica A, 202, 390.

Chan, C.H. and Tuba, I.S. (1971). A finite element method for contact problems of solid bodies. Int. J. Mech. Sci., 13.

Christoffersen, J., Mechrabadi, M.M. and Nemat-Nasser, S., (1981). A micro-mechanical description of granular material behavior. Journal of Applied Mechanics, 48, 339-344.

Coppersmith, S.N., Liu, C.H., Narayan, O. and Witten, T.A., (1996). Model for force fluctuations in bead packs. Phys. Rev. E, 53(5), 4673-4685.

Cundall, P.A. and Strack, O.D.L., (1979). A discrete numerical model for granular assemblies. Geotechnique, 29(1), 47-65.

Dawson, P.R. and Thompson E.G. (1978). Finite element analysis of steady-state elasto-visco-plastic flow by the initial stress-rate method. International journal for numerical methods in engineering, 12, 47-57.

Dobry, R. and Ng, T.T., (1992). Discrete modeling of stress-strain behavior of granular media at small and large strains. Eng. Comput., 129-143.

Edwards, S.F. and Mounfield, C.C., (1996). A theoretical model for the stress distribution in granular matter. III: Forces in sandpiles. Physica A, 226, 25.

Fischmeister, H.F., Arzt, E. and Olsson, L.R., (1978). Particle deformation and sliding during compression of spherical powders: a study by quantitative metallurgy. Powder Metallurgy, 21, 179-187.

Fischmeister, H.F. and Arzt, E., (1983). Densification of powders by particle deformation. Powder Metallurgy, 26, 82-88.

Fleck, N.A., (1995). On the cold compaction of powders. Journal of the Mechanics and Physics of Solids, 43, 1409-1431.

Fleck, N.A., Kuhn, L.T. and McMeeking, R.M., (1992a). Yielding of metal powder bonded by isolated contacts. Journal of the Mechanics and Physica of Solids, 40, 1139-1162.

Fleck, N.A., Storakers, B. and McMeeking, R.M., (1997). The viscoplastic compaction of powders. IUTAM Symposium on Mechanics of Granular Flow and Powder Compaction, 15-17 July 1996, Cambridge, England, eds. N.A. Fleck and A.C.F. Cocks, Kluwer Academic Publishers, Amsterdam.

Francavilla, A. and Zienkiewicz O.C. (1975). A note on numerical computation of elastic problems. Int. J. Numer. Methods eng. 9, 913-924.

Goodman, R.E., Taylor, R.L. and Brekke, T.L. (1968). A model for the mechanics of jointed rock. J. Soil Mech. Found. Div., ASCE, 94(SM3), 637-659.

Gurson, A.L., (1997). Continuum theory of ductile rupture by void nucleation and growth: Part 1 Yield criteria and flow rules for porous ductile media. Trans. ASME J. Engng. Mats. And Technology, 99, 2-15.

Helle, A.S., Easterling, K.E. and Ashby, M.F., (1985). Hot-isostatic pressing diagrams: New developments. Acta Metallurgica, 33, 2163-2174.

Hemmingsson, J., Herrmann, H.J., and Roux, S. (1997). On stress networks in granular media. J. Phys. I, Vol. 7, 291-302.

Herrmann, H.J. and Luding, S., (1998). Modeling granular media with the computer. Continuum Mechanics and Thermodynamics, 10, 189-231.

Herrmann L.R. Finite element analysis of contact problems. J. Eng. Mech. Div., ASCE, 104(EM5), 1043-1057.

Hill, R., Storakers, B. and Zdunek, A.B. (1989). A theoretical study of the Brinell hardness test. Proceeding of the Royal Society of London, A436, 301-330.

Hong, D.C., (1993). Stress distribution of a hexagonally packed granular pile. Phys. Rev. E, 47(1), 760-762.

Issa, J.A. and Nelson, R.B., (1992). Numerical analysis of micromechanical behavior of granular materials. Eng. Comput., 9, 211-223.

Jaeger, H.M. and Nagel, S.R., (1992). Physics of the granular state. Science, 255, 1523.

Jaeger, H.M. and Nagel, S.R., (1996). The physics of granular materials. Physics Today, 49(4), 32-38.

Jagota, A., Dawson, P.R. and Jenkins, J.T., (1988). An anisotropic continuum model for the sintering and compaction of powder packings. Mech. Of Materials, 7, 255-269.

Jagota, A., Mikeska, K.R. and Bordia, R.K., (1990). Isotropic constitutive model for sintering particle packings. Journal of the American Ceramics Society, 73, 2266-2273.

Jagota, A. and Scherer, G.W., (1995). Viscosities and sintering rates of composite packing of spheres. J. American Ceramics Society, 78, 521-528.

Jokati, T. and Moriyama, R., (1979). On the bottom pressure distribution of the bulk materials piled with the angle of repose. Journal of the Society of Powder Technology, Japan, 16, 184-191.

Jullien, R. and Meakin, P., (1992). Three-dimensional model for particle-size segregation by shaking. Phys. Rev. Lett., 69(4), 640.

Kalker, J.J., Allaert H.J.C. and Mul J.D. (1981). The numerical calculation of contact problem in the theory of elasticity. Nonlinear Finite Element Analysis in Structural Mechanics, (Wunderlich et al, Eds.) Springer-Verlag.

Krishnasamy, J. and Jakiela, M.J., (1995). A method to resolve ambiguities in corner-corner interaction between polygons in the context of motion simulations. Eng. Comput., 12, 135-144.

Kuhn, H.A. and Downey, C.L., (1971). Deformation characteristics and plasticity theory of sintered powder materials. Int. J. Powder Metallurgy, 7(1), 15-25.

Kuhn, L.T. and McMeeking, R.M., (1992). Power law creep of powder bonded by isolated contacts. International Journal of Mechanical Sciences, 34, 563-573.

Larsson, L., Biwa, S. and Storakers, B., (1996). Analysis of cold and hot isostatic compaction of spherical particles. Acta Materialia, 44, 3655-3666.

Liao, C.L., Chang, T.P., Young, D.H. and Chang, C.S., (1997). Stress-strain relationship for granular materials based on the hypothesis of best fit. Int. J. Solids Structures, 34, 4087-4100.

Liffman, K., Chan, D.Y.C. and Hughes, B.D., (1992). Force distribution in a two dimensional snadpile. Powder Technol. 72, 255-267.

Liffman, K., Chan, D.Y.C. and Hughes, B.D., (1994). On the stress depression under a snadpile. Powder Technol., 78, 263-271.

Liu, C.H., Nagel, S.R., Schecter, D.A., Coppersmith, S.N., Majumdar, S., Narayan, O. and Witten, T.A., (1995). Force fluctuations in based packs. Science, 269, 513.

Luding, S., (1997). Stress distribution in static two dimensional granular model media in the absence of friction. Phys. Rev. E, 55(4), 4720-4729.

Mason, G., (1968). Radial distribution functions from small packings of spheres. Nature, 217, 733-735.

Matuttis, H.G., (1998). Simulations of the pressure distribution under a two dimensional heap of polygonal particles. Granular Matter, 1(2), 83-91.

McNamara, S. and Young, W.R., (1996). Dynamics of a freely evolving, two-dimensional granular medium. Phys. Rev. E, 53(5), 5089-5100.

Okamoto N. and Nakazawa M. (1979). Finite element incremental contact analysis with various frictional conditions. Int. J. Numer. Methods Eng., 14, 337-357.

Oron, G. and Herrmann, H.J., (1998). Exact calculation of force networks in granular media. Phys. Rev. E, 58(2), 2079-2089.

Potapov, A.V. and Campbell, C.S., (1998). A fast model for the simulation of non-round particles. Granular Matter, 1(1), 9-14.

Radjai, F., Jean, M., Moreau, J.J. and Roux, S., (1996). Force distribution in dense two-dimensional granular systems. Phys. Rev. Lett., 77(2), 274.

Reynolds, R., (1885). On the dilatancy of media composed of rigid particles in contact. Philos. Mag. Serv. 5, 50-20, 469.

Rosato, A.D., Strandburg, K.J., Prinz, F. and Swendsen, R.H., (1987). Why the brazil nuts are on top: size segregation of particular matter by shaking. Phys. Rev. Lett., 58(10), 1038.

Rosato, A.D., Strandburg, K.J., Prinz, F. and Swendsen, R.H.,(1987). Why the Brazil nuts are on top: size segregation of particular matter by shaking. Phys. Rev. Lett., 58(10), 1038.

Schumaker, L. L. (1987). Triangulation methods. In Topics in Multivariate Approximation, 219-232.

Scott, G.D., (1962). Radial distribution of the random close packing of equal spheres. Nature, 194, 956-957.

Shmazaki, Y. and Thompson E.G. (1981). Elasto visco-plastic flow with special attention to boundary conditions. International journal for numerical methods in engineering, 12, 97-112.

Sibson, R. Locally equiangular triangulations. (1978). Computer Journal, 21, 243-245.

Thompson, E.G. (1975). Average and complete incompressibility in the finite element method. International journal for numerical methods in engineering, 9, 925-932.

Thornton, C., (1997). Force transmission in granular media. KONA Powder and Particle, 15, 81-90.

Thornton, C. and Randall, C.W., (1988). Applications of theoretical contact mechanics to solid particles system simulation. In Micro-mechanics of granular media, Amsterdam. Elsevier.

Ting, J.M., (1992). A robust algorithm for ellipse-based discrete element modeling of granular materials. Computers and Geotechnics, 13, 175-186.

Ting, J.M., Corkum, B.T., Kauffman, C.R. and Greco, C., (1989). Discrete numerical model for soil mechanics. J. of Geotech. Eng., 115, 379.

Trollope, D.H. and Burman, B.C., (1980). Physical and numerical experiments with granular wedges. Geotechnique, 30(2), 137-157.

Turner, C.D. and Ashby, M.F., (1995a). The cold isostatic pressing of composite powders I. Experimental investigations using powders. To be published.

Walker, J., (1982). When different powders are shaken, they seem to have lives of their own. Sc. American, 247(3), 166.

Williams, J.R. and Pentland, A.P., (1992). Superquadrics and modal dynamics for discrete elements in interactive design. Eng. Comput., 9, 115-127.

Wilson, E.A. and Parsons, B. (1970). Finite element analysis of elastic contact problems using differential displacements. Int. J. Numer. Methods eng., 2, 387-395.

Wittmer, J.P., Claudin, P., Cates, M.E. and Bouchaud, J.P., (1996). An explanation for the central stress minimum in sand piles. Nature, 382, 336-338.

Wittmer, J.P., Cates, M.E. and Claudin, P., (1997). Stress propagation and arching in static snadpiles. J. Phys. I, 7, 39-80.

Wolf, D.E., (1996). Modeling and computer simulation of granular media. In Hoffmann, K.H., Schrelber, M. editors. Computational Physics, Springer, Heidelberg.

Yagawa, G., Yoshioka, A., Yoshimura, S. and Soneda, N. (1993). A parallel finite element method with supercomputer network. Computers and structures, 47, 407-418.

Yagawa, G. and Shioya, R. (1993). Parallel finite elements on a massively parallel computer with domain decomposition. Computer systems in engineering, 4, 495-503.

Yoshimura, S., Wada, Y. and Yagawa, G. (1999). Automatic mesh generation of quadrilateral elements using intelligent local approach. Computer methods in applied mechanics and eigineering, 179, 125-138.